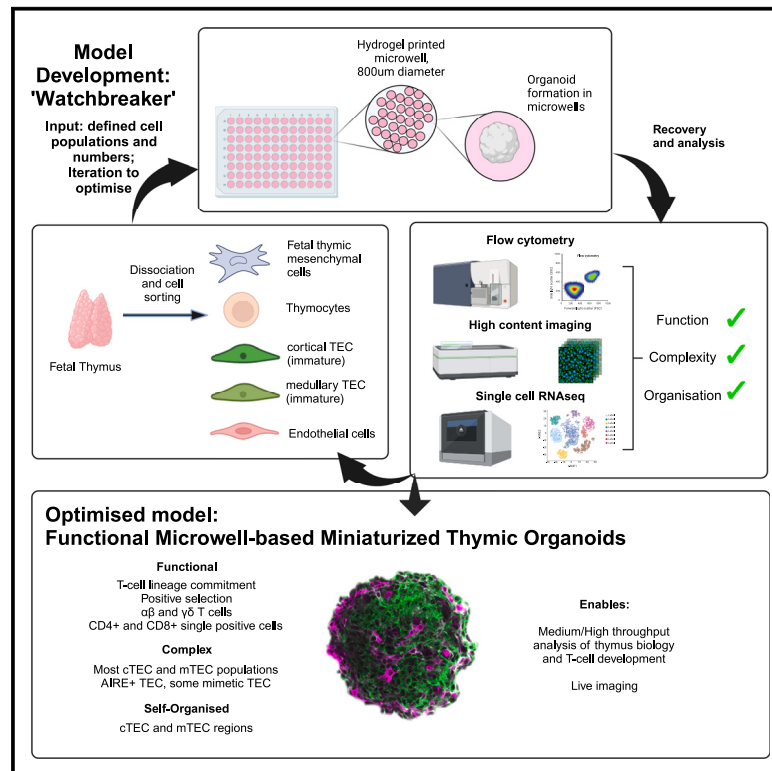


# Cell Reports

## Establishment of a microwell-array-based miniaturized thymic organoid model suitable for high-throughput applications

### Graphical abstract



### Authors

Viktoria Major, Sam Palmer, Paul Rouse, ..., Matthias P. Lütolf, Graham Anderson, C. Clare Blackburn

### Correspondence

c.blackburn@ed.ac.uk

### In brief

Major et al. present a microwell-array-based miniaturized thymus organoid (mTO) model. mTOs support T cell commitment and development, with organizational characteristics and key stromal cell complexity closely mirroring those of the native thymus. This *in vitro* model is adaptable to medium-/high-throughput applications and validated for exploration of thymus and T cell biology.

### Highlights

- Miniaturized thymic organoids (mTOs) were developed by iterative cellular input optimization
- mTOs exhibit near-native thymic epithelial cell complexity with some self-organization
- T cell commitment and  $\alpha\beta$  and  $\gamma\delta$  T cell development are supported
- This *in vitro* thymus model is medium/high throughput and live-imaging compatible



## Resource

# Establishment of a microwell-array-based miniaturized thymic organoid model suitable for high-throughput applications

Viktoria Major,<sup>1,2,10</sup> Sam Palmer,<sup>3,10</sup> Paul Rouse,<sup>1,2,6,10</sup> Jan Morys,<sup>1,2</sup> Timothy Henderson,<sup>1,2,7</sup> Tania Hübscher,<sup>4</sup> Joanna Sweetman,<sup>1,2,8</sup> Andrea Bacon,<sup>5</sup> Chengrui An,<sup>1,2</sup> Qiu Guiyun,<sup>1,2</sup> Yu Wang,<sup>1,2</sup> Andrea Corsinotti,<sup>1</sup> Justyna Cholewa-Waclaw,<sup>1</sup> S. Jon Chapman,<sup>3</sup> Matthias P. Lütolf,<sup>4,9</sup> Graham Anderson,<sup>5</sup> and C. Clare Blackburn<sup>1,2,11,\*</sup>

<sup>1</sup>Institute of Regeneration and Repair, Centre for Regenerative Medicine, University of Edinburgh, 5 Little France Drive, Edinburgh EH16 4UU, UK

<sup>2</sup>Institute for Stem Cell Research, School of Biological Sciences, University of Edinburgh, Edinburgh EH16 4UU, UK

<sup>3</sup>Mathematical Institute, University of Oxford, Woodstock Road, Oxford OX2 6GG, UK

<sup>4</sup>École Polytechnique Fédérale de Lausanne, EPFL SV IBI-SV UPLUT, AI 1208 (Bâtiment AI), Station 15, 1015 Lausanne, Switzerland

<sup>5</sup>Institute of Immunology and Immunotherapy, University of Birmingham, Birmingham B15 2TT, UK

<sup>6</sup>Present address: IMU Biosciences, 20 Water Street, London E14 5GX, UK

<sup>7</sup>Present address: Australian National University Medical School, The Canberra Hospital, Garran ACT 2605, Australia

<sup>8</sup>Present address: Resolution Therapeutics, SCRM Building, 5 Little France Drive, Edinburgh EH16 4UU, UK

<sup>9</sup>Present address: Roche Institute of Human Biology, Basel, Switzerland

<sup>10</sup>These authors contributed equally

<sup>11</sup>Lead contact

\*Correspondence: [c.blackburn@ed.ac.uk](mailto:c.blackburn@ed.ac.uk)

<https://doi.org/10.1016/j.celrep.2025.115579>

## SUMMARY

T cell development depends critically on the thymic stroma—in particular, the diverse array of functionally distinct thymic epithelial cell (TEC) types. However, a robust *in vitro* thymus model mimicking the native thymus and compatible with medium-/high-throughput analyses is currently lacking. Here, we demonstrate a high-density microwell-array-based miniaturized thymus organoid (mTO) model that supports T cell commitment and development, possesses key organizational characteristics of the native thymus, and is compatible with live imaging and medium-/high-throughput applications. We establish the minimum cellular input required for a functional mTO and show that mTO TEC phenotype and complexity closely mirror those of the native thymus. Finally, we use an mTO to probe the role of fetal thymic mesenchyme, revealing a requirement beyond maintenance of *Foxn1* in differentiation/maintenance of mature TEC sub-populations. Collectively, mTOs present an *in vitro* model of the native thymus adaptable to medium-/high-throughput applications and validated for exploration of thymus and thymus organoid biology.

## INTRODUCTION

The thymus is required for T cell development. Obligate dynamic interactions with thymic stromal cells regulate hematopoietic progenitor cell (HPC) colonization, commitment of HPCs to the T cell lineage, and subsequent progression through the T cell differentiation and selection pathways.<sup>1–4</sup> The thymic stroma comprises epithelial, mesenchymal, vascular, and hematopoietic components,<sup>5–7</sup> among which thymic epithelial cells (TECs) are critical for the organ's specialist functions.<sup>4</sup> The functionally distinct cortical (c) and medullary (m) TEC sub-lineages define the two main thymic compartments, with each containing several epithelial sub-types.<sup>8–13</sup> Broadly, cTECs regulate T cell lineage commitment, differentiation, and positive selection, while mTECs regulate central tolerance induction<sup>4,14–19</sup>; these distinct functions depend on unique, sub-lineage-specific gene expression programs.<sup>4,13,20,21</sup> TECs also

regulate the production of  $\gamma\delta$  T cells and non-conventional innate sub-sets, including invariant natural killer T cells (iNKTs).

The current strong interest in thymus biology and T cell development is underpinned by three main factors: (1) age-related thymic involution, which results in an age-related decline in new naive T cell output that contributes to the increased risk of cancer and infection with age and adversely affects recovery of immune function after cytotoxic therapies<sup>22–24</sup>; (2) immunodeficiencies caused by failure of thymus function or early life surgical thymectomy; and (3) the recent harnessing of T cells for successful cancer immunotherapies. Related to this, thymus transplants currently rely on neonatal thymus tissue, function only transiently, and are frequently associated with autoimmunity<sup>25</sup>; and neither clinically useful thymus regeneration nor the generation of bespoke T cell repertoires *in vitro* has yet been achieved.<sup>24</sup>

An *in vitro* experimental platform compatible with medium-/high-throughput mechanistic interrogation of physiological thymus



functions would enable progress in all the above areas. Existing models, however, each have substantive limitations. Fetal thymic organ culture (FTOC) and reaggregate FTOC (RFTOC)<sup>26</sup> largely recapitulate physiological function but are neither suitable for medium-/high-throughput approaches nor supportive of *in vitro* genetic manipulation of thymic stroma. Cell-line models, principally the Notch ligand-transduced mouse bone marrow-derived cell lines OP9-Delta-like 1 (OP9-DL1)/OP9-Delta-like 4 (OP9-DLL4) and MS5-DL1, partially support T cell development<sup>27–31</sup> but lack cTEC- and mTEC-specific molecular machineries required for physiological repertoire selection and cannot support studies investigating thymic stromal function. Additionally, although promising for further development, models based on direct reprogramming,<sup>32</sup> directed differentiation of mouse and human pluripotent stem cells (PSCs),<sup>33–36</sup> and cultured mouse and human TECs<sup>37–41</sup> largely remain poorly characterized relative to *ex vivo* TECs, RFTOC, and FTOC. Thus, improved models are required.

Recently, miniaturized organoids that mimic physiological function have been established for some other organs, prompting us to test whether this approach could be applied to the thymus. Here, we demonstrate that miniaturized thymic organoids (mTOs) able to mediate thymopoiesis can be established from *ex vivo* thymus tissue. We define the minimum cellular inputs required to generate functional mTOs and demonstrate the presence within these organoids of discrete cTEC and mTEC regions, including autoimmune regulator (AIRE)<sup>+</sup> mTECs. Via single-cell transcriptomics, we establish that most if not all normal intrathymic stromal cell types are present within mTOs and reveal likely pathways through which fetal thymic mesenchyme (FTM) impacts TEC development and function. This microphysiological thymic organoid system reduces variability and input cell numbers compared to other approaches, while retaining cTEC:mTEC compartmentalization and cellular diversity. Importantly, it is suitable for live/time-lapse imaging and medium-/high-throughput screening applications, representing a step change for interrogation of thymic stromal biology.

## RESULTS

The essential features of any functional thymic organoid are: (1) the ability to support T cell lineage commitment from HPCs; (2) the ability to support subsequent thymocyte differentiation to generate CD4<sup>+</sup> and CD8<sup>+</sup> T cells; (3) regions of cTECs that express DLL4 (HPC commitment to the T cell lineage<sup>42,43</sup>), C-X-C motif chemokine 12 (CXCL12;  $\beta$  selection of developing T cells<sup>44</sup>),  $\beta$ 5t (cTEC-specific proteasome sub-unit that generates the optimum peptide repertoire for positive selection of CD8<sup>+</sup> T-cells<sup>45</sup>), cathepsin L (cTEC-specific protease required for optimum positive selection of CD4<sup>+</sup> T cells<sup>46</sup>), and major histocompatibility complex (MHC) class I (MHCI) and MHC class II (MHCII) (positive selection of CD8<sup>+</sup> and CD4<sup>+</sup> T cells, respectively); and (4) expression by the TECs of cytokines needed to drive proliferation and differentiation of the developing T cells (e.g., FMS-related tyrosine kinase 3 ligand [Flt3L], CXCL12, and interleukin [IL]-7). An organoid containing these features should generate a repertoire of CD4<sup>+</sup> and CD8<sup>+</sup> T cells that have been positively selected on the peptide repertoires used

in physiological positive selection and so will be responsive to antigenic peptides in the correct affinity range. Establishment of mTOs that met criteria (1)–(4) above was the minimal goal of our study. The presence of medullary regions within thymic organoids, evidenced by the presence of TECs expressing cytokeratin 14 (K14), AIRE, FEZ family zinc finger (FEZF2), and a range of AIRE-dependent and AIRE-independent tissue-restricted antigens (TRAs), would promote central tolerance induction in the positively selected repertoire and would also be desirable for some applications.

### mTOs form in microwells and mediate thymopoiesis

To test whether thymic reagggregates could be established in microwell plates, we seeded defined numbers of dissociated fetal thymus cells from a range of developmental stages into single wells of Gri3D 96-well plates (SUN Biosciences), in which each well contains a U-bottomed microwell-printed polyethylene glycol (PEG)-based hydrogel insert (Figure 1A). Preliminary testing established that seeding cells from two thymic lobes (i.e., one embryo equivalent) per well, in which each well contained 31 800- $\mu$ m-diameter microwells, performed better than any of the other conditions tested (different input cell numbers and microwell diameters were tested; not shown).

We then analyzed the effect of developmental stage on reaggregate formation, choosing embryonic day 13.5 (E13.5), E14.5, and E15.5 fetal thymus cells as our input populations (these stages exhibit progressively increasing levels of TEC differentiation and complexity<sup>47–49</sup>). Dissociated-but-unsorted fetal thymus cells from each of the stages formed cellular aggregates in most if not all microwells by 24 h post-seeding and formed clear spheroid structures by 48 h. The spheroids persisted for at least 14 days in culture (the last time point analyzed; Figure 1B), at which time point double-negative (DN; CD8<sup>−</sup>CD4<sup>−</sup>), double-positive (DP; CD8<sup>+</sup>CD4<sup>+</sup>), CD4<sup>+</sup> single-positive (SP4), and CD8<sup>+</sup> single-positive (SP8) cells were present in all conditions. Thymocyte sub-set profiles were comparable to FTOC and standard RFTOC controls (Figures 1C and 1D; note that each standard RFTOC was formed from six thymic lobes; at E14.5 each lobe contains approximately  $1 \times 10^5$  total cells). E14.5 mTO performed very similar to FTOC and RFTOC in terms of proportions of DP, SP4, and SP8 present and were thus used for all further analyses.

### Defining the minimal cellular inputs for functional mTO formation

We next determined the minimal cellular inputs for establishment of functional mTO that met criteria (1)–(4) above, asking whether and in what proportion each of the major thymic stromal populations was required (Figure 2A). We called this experiment “Watch-breaker.” E14.5 thymi were microdissected, dissociated to single-cell suspensions, and separated into TECs, FTMs, and hematopoietic (CD45<sup>+</sup>; at E14.5 primarily DN1–3, see Figure S1) and endothelial cell (EC) populations by flow cytometric sorting. At E14.5, of the live cells, 60% were thymocytes, 30% TECs, 11% FTMs, and less than 1% ECs (Figure S1), with around 4% of TECs being UEA1<sup>+</sup> mTEC progenitors.<sup>48</sup>

We first tested the requirement for FTM and for altering the FTM:TEC ratio (Figures 2A and 2B), using three conditions: “Hi FTM,”  $1 \times 10^5$  TECs,  $5 \times 10^4$  DNs, and  $4 \times 10^4$  FTMs per

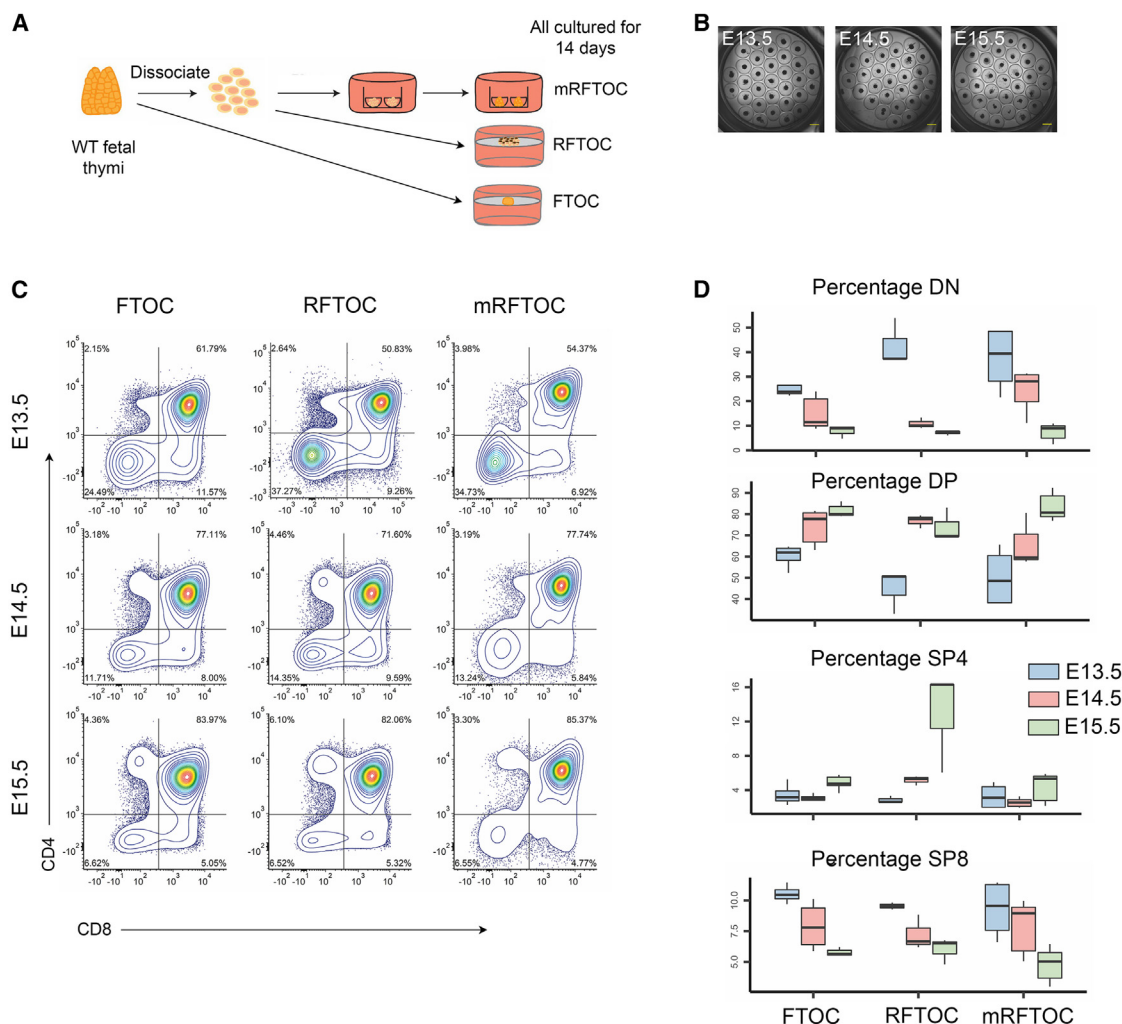


**Figure 1. Thymopoiesis in unsorted mTO culture, FTOC, and RFTOC**

(A) Schematic depicting creation of FTOC, RFTOC, and unsorted mTO.

(B) Bright-field image of E13.5 (left), E14.5 (middle), and E15.5 (right) unsorted mTO 7 days after seeding. Scale bars, 500  $\mu$ m.

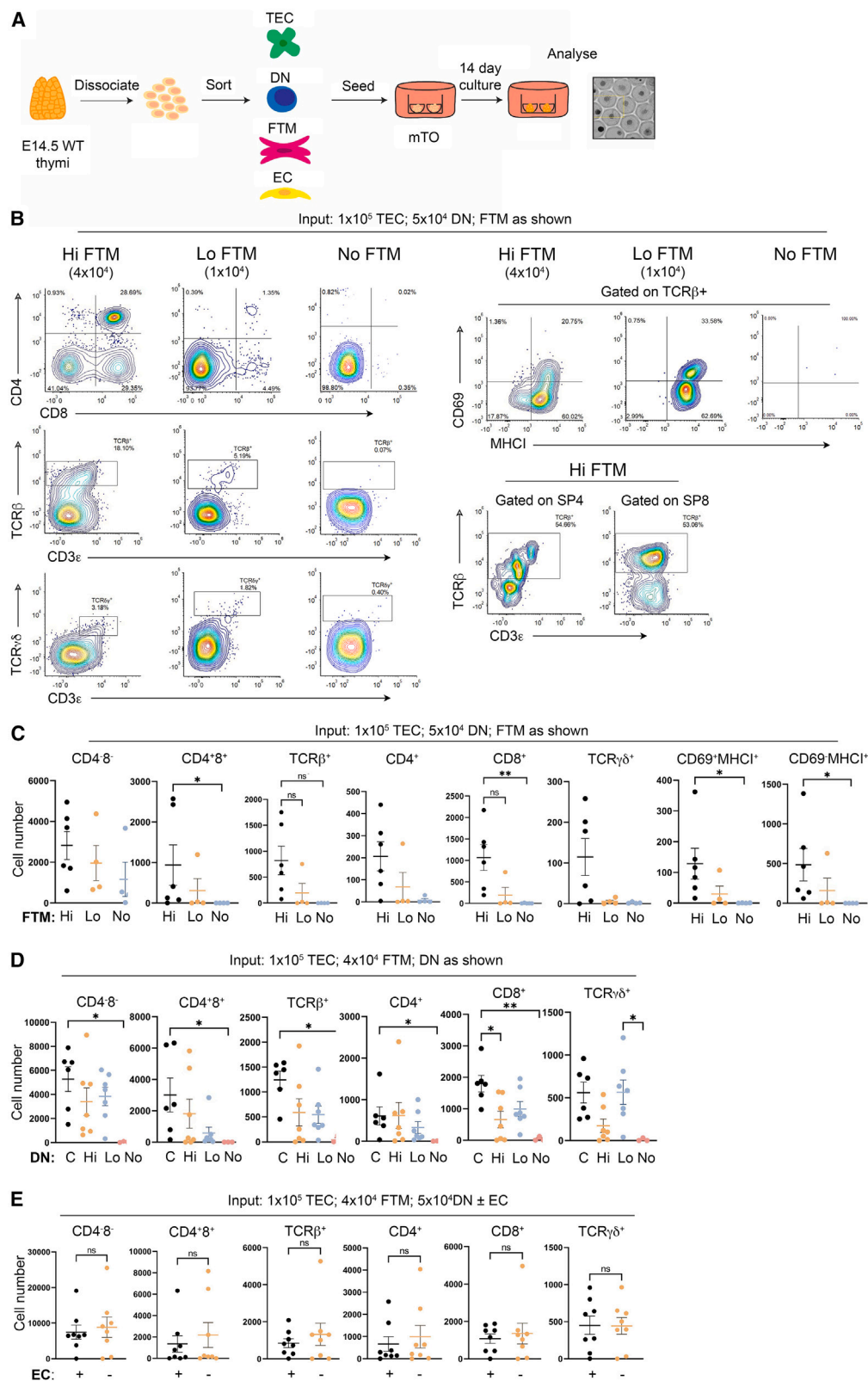
(C and D) Thymocyte sub-sets after 7 days of culture, with conditions and input tissue ages as shown. (C) Representative CD4 vs. CD8 plots for FTOC (left), RFTOC (center), and unsorted mTO (right) from the input ages shown. (D) Graphs show percentage of DN, DP, SP4, and SP8 thymocytes; statistical center indicated by the standard error of the mean (SEM). (C and D) Data shown are for live lineage-negative cells (lin = CD11b, CD11c, Gr-1, Nk1.1, B220, EpCAM, and Ter119).  $n = 3$  independent biological replicates for each experiment.

well (the physiological FTM:TEC ratio); “Lo FTM,”  $1 \times 10^5$  TECs,  $5 \times 10^4$  DNs, and  $1.5 \times 10^4$  FTM; and “no-FTM mTO,”  $1 \times 10^5$  TECs,  $5 \times 10^4$  DNs, and 0 FTM. ECs were not included. The Hi and Lo FTM conditions both sustained thymopoiesis, evidenced by the presence of DP, SP4, and SP8 populations after 14 days. TCR $\beta^{\text{hi}}$  SP4 and SP8 and TCR $\gamma\delta^+$  thymocytes were present in both Hi and Lo FTM conditions; the SP cells had undergone positive selection and subsequent maturation, evidenced by the presence of CD69 $^+$ MHCi $^+$  (M1) and CD69 $^-$ MHCi $^+$  (M2) populations (Figures 2B, 2C, and S2). In the absence of FTM, thymocyte development did not proceed beyond the DN stage (Figures 2B, 2C, and S2), with approximately 50% of DN cells adopting non-thymocyte lineages (CD45 $^+$ lin $^+$  cells, Figure S2). The Hi FTM condition resulted in greatly increased output cell

numbers compared to Lo FTM (see Figure 2C) and was thus adopted for all further experiments.

We then optimized the input thymocyte numbers, by generating mTOs in which TEC and FTM numbers were as for the Hi FTM condition ( $1 \times 10^5$  TECs and  $4 \times 10^4$  FTM), while DN thymocyte number was varied (“Hi DN,”  $2 \times 10^5$  DNs; “Control,”  $5 \times 10^4$  DNs (i.e., as in Hi FTM); “Lo DN,”  $1 \times 10^4$  DNs; and “No DN,” 0 DN cells). As expected, no thymocytes were recovered from the No DN condition. The Hi DN, Lo DN, and Control mTOs all sustained thymopoiesis and produced SP4 and SP8  $\alpha\beta$  and  $\gamma\delta$  T cells (Figure 2D). The Control (i.e., Hi FTM) condition produced the highest number of all thymocyte sub-sets (Figure 2D), with better maturation through the CD69 $^+$ MHCi $^+$  and CD69 $^-$ MHCi $^+$  stages (not shown), and also demonstrated less





(legend on next page)

variability across the individual replicates than the other conditions. We therefore used this condition for all further analysis. Notably, although the Hi DN condition represented the physiological E14.5 TEC:DN:FTM ratio, it performed worse than the Control (i.e., Hi FTM) condition, in which DNs were proportionally lower, in terms of output cell numbers.

We also tested whether the addition of thymic ECs to mTOs would affect functionality. No significant differences were found between the “With EC” and “Without EC” conditions tested ( $1 \times 10^5$  TECs,  $5 \times 10^4$  DNs,  $4 \times 10^4$  FTM, and  $\pm 1\text{--}2 \times 10^4$  ECs) (Figure 2E).

Finally, we tested whether increasing or decreasing the seeding cell number per well would affect mTO function and whether “pre-mixing” the different cell inputs affected mTO function compared to the sequential seeding approach used above. We established mTOs using the optimized Hi FTM ratios, but with the total cell numbers set at  $1.5\times$  or  $0.5\times$  the  $1\times$  Hi FTM control, and mTOs in which the seeding cells were either pre-mixed or seeded sequentially. The  $1\times$  Hi FTM and  $0.5\times$  Hi FTM conditions produced the highest numbers of cells per input CD45<sup>+</sup> cell for all thymocyte sub-sets tested, with the  $1\times$  Hi FTM condition performing better in terms of numbers of SP4 and SP8 produced (Figure S3). Therefore, this was retained as the optimized condition for further work. No significant differences were found for sequential seeding vs. pre-mixing, and therefore the pre-mixing protocol was adopted for subsequent experiments (Figure S4).

### mTOs support thymopoiesis from uncommitted hematopoietic progenitors

The above data used differentiation of DN thymocytes to read out mTO function. Since some of the E14.5 DN input cells were at or beyond the CD44<sup>+</sup>CD25<sup>+</sup> DN2 stage (i.e., had commenced T-lineage differentiation), we also tested whether mTOs could mediate T cell commitment. We isolated E14.5 fetal liver lymphoid-primed multipotent progenitors (LMPPs) and substituted these for the DN cells such that the input cell numbers were  $1 \times 10^5$  TECs,  $3.1 \times 10^3$  LMPPs, and  $4 \times 10^4$  FTM, with the control being  $1 \times 10^5$  TECs,  $5 \times 10^4$  DNs, and  $4 \times 10^4$  FTM (i.e., Hi FTM). mTOs supported robust thymopoiesis from LMPPs, albeit with delayed differentiation kinetics compared to DN cells, evidenced by the low proportion of TCR $\beta^{\text{hi}}$  cells in the LMPP condition at the time point assayed (Figures 3A and 3B). Indeed, the number of DP, SP4, SP8, and  $\gamma\delta$  thymocytes generated per input cell was higher for LMPPs

than for DNs (Figure 3B; input numbers of LMPPs were 16-fold lower than for the DNs).

### Kinetics of T cell development within mTOs

To analyze the kinetics of T cell development within mTOs, we also analyzed Hi FTM mTOs for thymocyte developmental progression and evidence of positive selection and SP maturation at a range of time points: days 7, 9, 11, and 14 of culture. A striking downward trend in DP numbers was evident as time in culture increased, from almost  $2 \times 10^4$  (day 7) to less than  $5 \times 10^3$  (day 14) (Figures 3C, 3D, and S5). The number of recovered SP4 and SP8 thymocytes also decreased, as did  $\gamma\delta$  T cell numbers (Figures 3C, 3D, and S5). Representative overview images showed more consistent mTO morphology at days 7, 9, and 11 compared to day 14 (not shown). Overall, the 7-day culture period yielded peak numbers of developing T cells and showed the lowest experiment-to-experiment variation, so it was adopted for further analyses (Figures 3D and S5; live CD45<sup>+</sup> cells recovered: 7-day endpoint,  $5.41 \times 10^4 \pm 2.38 \times 10^4$  vs. 14-day endpoint,  $9.2 \times 10^3 \pm 1.58 \times 10^3$ ).

Collectively, mTOs established from input E14.5 thymus cells can support thymopoiesis from both DN cells and LMPPs, with CD69 expression in DPs evidencing positive selection; formation of optimally functional mTOs requires FTM, but T cell development within mTOs does not require thymic ECs, and a 7-day culture period results in maximal cell numbers, while 12–14 days of culture yields more TCR $\beta^{\text{hi}}$  cells.

### Segregation of cortex-like and medulla-like regions in mTOs

We next assessed the organization and identity of stromal cells within mTOs (Figure 4). To analyze the distribution of TECs, we established mTOs from two reporter mouse strains, *Foxn1*<sup>GFP50</sup> and *Rank-Venus;Cxcl12dDsRed*.<sup>12,51,52</sup> Forkhead box N1 (FOXN1) is a master regulator of TEC differentiation required for the development of all mature TEC sub-populations,<sup>47</sup> while receptor activator of nuclear factor  $\kappa$  B (RANK) and CXCL12 mark mTECs and cTECs, respectively.

Live imaging of mTOs showed that GFP, reporting *Foxn1*, was expressed in mTOs throughout the 7-day culture period (the last time point analyzed; Figures 4A and 4B), in contrast to two-dimensional culture and submerged FTOT in which *Foxn1* is rapidly downregulated.<sup>53</sup> Counterstaining showed that *Foxn1* was expressed in most TECs, while transcriptome analysis confirmed that *Foxn1* expression was maintained and, thus, that the

**Figure 2. Establishment of the minimum cellular inputs for a functional mTO**

(A) Schematic of the experimental design.

(B and C) mTOs were generated with a constant number of TECs ( $1 \times 10^5$ ) and DNs ( $5 \times 10^4$ ) and varying numbers of FTM cells: “Hi FTM,”  $4 \times 10^4$  FTM per well (physiological FTM:TEC ratio); “Lo FTM,”  $1.5 \times 10^4$  FTM; and “no-FTM mTO,” 0 FTM. ECs were not included. (B) Representative plots showing thymocyte sub-set distribution after 14 days’ culture, for the markers and conditions shown. (C) Absolute numbers of recovered thymocytes from (B).

(D and E) mTOs were generated with a constant number of TECs ( $1 \times 10^5$ ) and FTM ( $4 \times 10^4$ ) and varying numbers of DN cells (D) or with and without thymic ECs (E). (D) Control,  $5 \times 10^4$  DNs; “Hi DN,”  $2 \times 10^5$  DNs; and “Lo DN,”  $1 \times 10^4$  DNs. (E) No EC control (–), 0 ECs, and ECs (+),  $1\text{--}2 \times 10^4$  ECs. Plots show the absolute numbers of recovered thymocytes for each sub-set with the statistical center indicated by the standard error of the mean (SEM).

(B and C)  $n = 5$ , (D)  $n = 8$ , and (E)  $n = 8$ , where  $n$  is an independent biological replicate performed on a separate day. Cell numbers shown are per single well of 96 wells. C, control. (B–E) Data shown are for live CD45<sup>+</sup> lineage-negative cells (lin = CD11b, CD11c, Gr-1, Nk1.1, B220, EpcAM, and Ter119); CD69<sup>+</sup>MHC1<sup>+</sup> and CD69<sup>+</sup>MHC1<sup>+</sup> data shown are after gating on TCR $\beta^+$  cells. Statistical analysis was by ordinary one-way ANOVA or Kruskal-Wallis rank test (C and D) or unpaired t test or Mann-Whitney rank test (E) based on the Shapiro-Wilk normality test. No  $p$  value indicates not significant ( $p > 0.05$ ); \* $p < 0.05$  and \*\* $p < 0.01$ . See also Figures S1–S4.

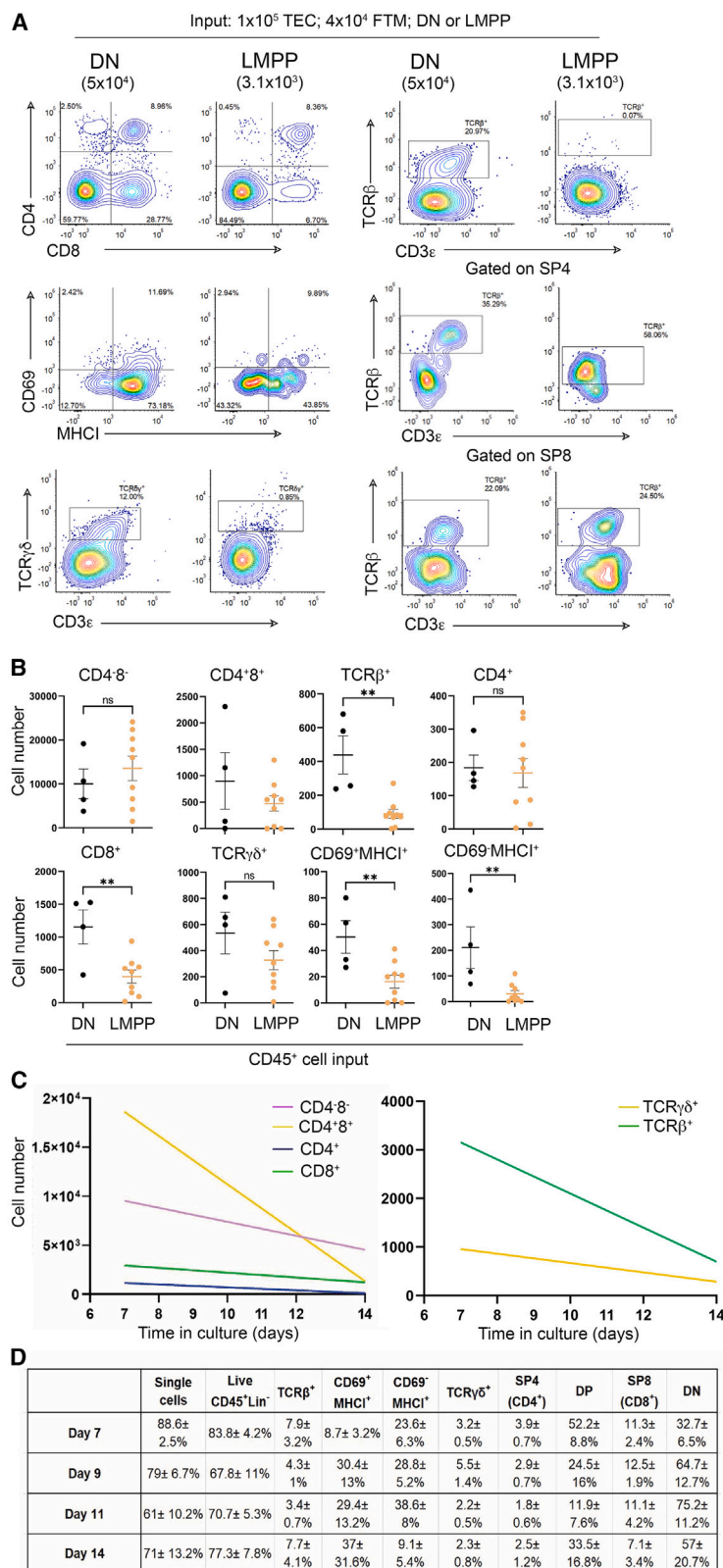


**Figure 3. Thymopoiesis from uncommitted hematopoietic progenitors**

(A and B) mTOs were established from E14.5 thymic cells under control conditions ( $1 \times 10^5$  TECs,  $5 \times 10^4$  DNs, and  $4 \times 10^4$  FTM) or with  $3.1 \times 10^3$  E14.5 fetal liver LMPPs instead of DNs. (A) Plots show representative flow cytometric analysis for the markers shown after 14 days' culture. (B) Absolute numbers of recovered thymocytes for each sub-set.

(C and D) mTOs established under control conditions ( $1 \times 10^5$  TECs,  $5 \times 10^4$  DNs, and  $4 \times 10^4$  FTM) were analyzed for thymocyte sub-set distribution at the time points shown. (C) Absolute cell numbers for the populations and time points shown. (D) Percentages for each population among all live lin<sup>-</sup> cells.

(A–D) Each data point represents the cells harvested from 1 well of 96. Graphs and table show mean ± SEM; statistical centers are indicated by the SEM.  $n = 4$  for each experiment, where  $n$  is an independent biological replicate performed on a separate day, with a total of nine technical replicates across  $n = 4$ . Statistical analysis was by unpaired t test or Mann-Whitney rank test based on the Shapiro-Wilk normality test. A linear regression model was used to plot thymocyte numbers over time (C). No  $p$  value indicates not significant ( $p > 0.05$ ); \* $p < 0.05$  and \*\* $p < 0.01$ . (A–D) Data shown are for live CD45<sup>+</sup> lineage-negative cells (lin = CD11b, CD11c, Gr-1, Nk1.1, B220, EpCAM, and Ter119); CD69<sup>+</sup>MHCII<sup>+</sup> and CD69<sup>-</sup>MHCII<sup>+</sup> data shown are after gating on TCRβ<sup>+</sup> cells. See also Figure S5.



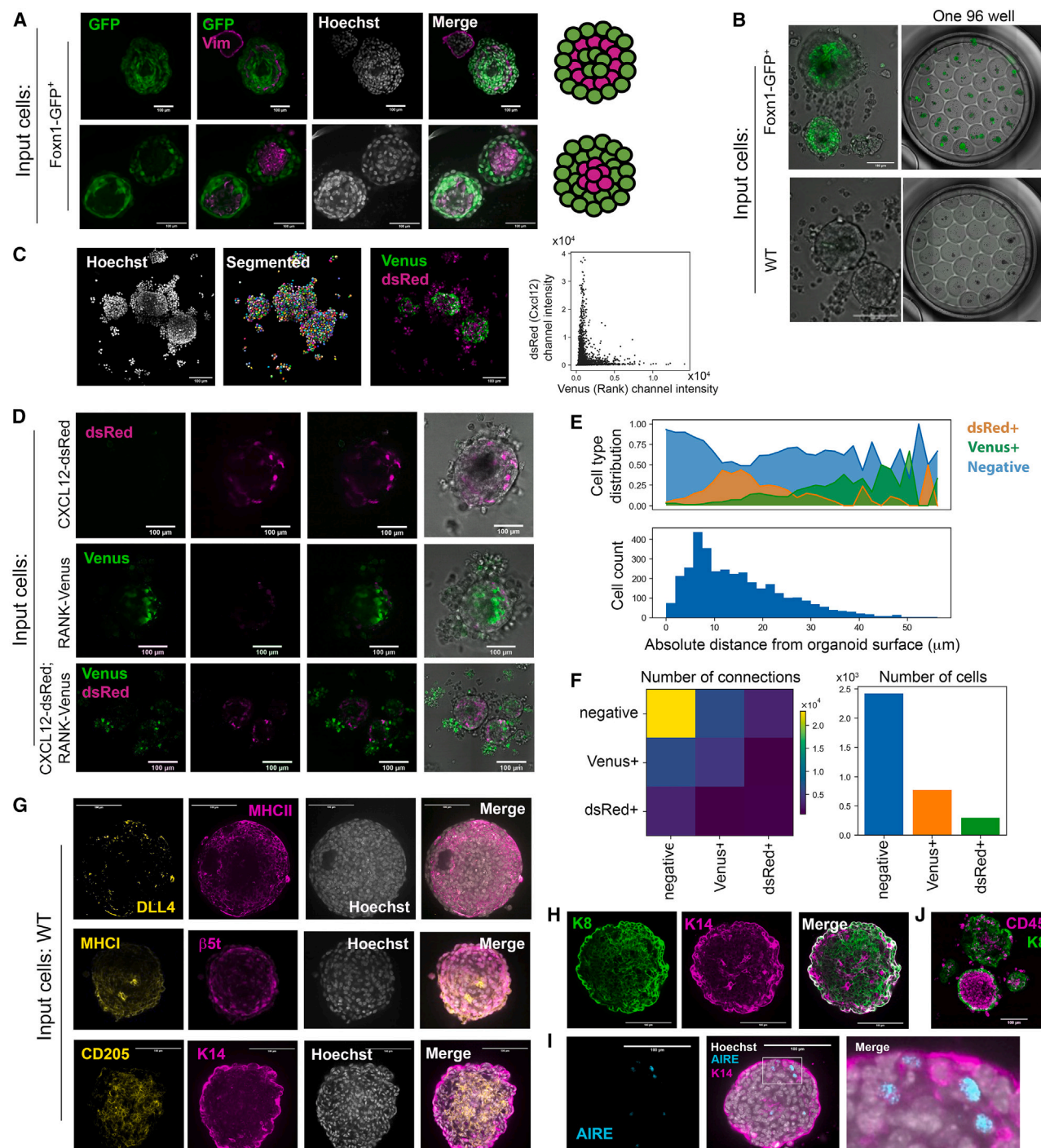


**Figure 4. cTEC and mTEC regions are segregated in mTOs**

Representative images of individual mTOs established from E14.5 wild type (WT), Foxn1<sup>GFP</sup>, Cxcl12-dsRED, Rank-Venus, or Cxcl12-dsRed;Rank-Venus thymi and cultured for 7 days. Images shown are single optical sections from the center of the mTOs, after live imaging at 40× using an Opera Phenix. Scale bars, 100 μm.

(A) Images are representative of Foxn1<sup>GFP</sup> mTOs, showing direct GFP fluorescence (green) and staining for vimentin (magenta) and nuclei (Hoechst, white). On the right is a schematic representation of the staining patterns observed.

(B–D) Images are representative of (B) Foxn1<sup>GFP</sup> showing direct GFP fluorescence (green) and (C and D) Cxcl12-dsRED, Rank-Venus, or Cxcl12-dsRed;Rank-Venus mTOs showing direct Venus (green) and dsRed (magenta) fluorescence and merged channels with bright field. The right side in (C) shows a fluorescence intensity plot for Venus and dsRed in each cell in the image shown on the left; cells were identified by segmentation.

(legend continued on next page)

persisting GFP signal reflected continued *Foxn1* transcription throughout the culture period (Figures 4A and 5). Counting of cells segmented on nuclear staining (Figure 4C) revealed that each mTO typically contained around 1000 cells.

Venus<sup>+</sup> mTEC and dsRed<sup>+</sup> cTEC present within the mTOs clustered separately (Figures 4C–4F), indicating that cTEC and mTEC regions had been established and were spatially segregated, while staining for cTEC and mTEC markers revealed DLL4,  $\beta$ 5t, CD205, K8, K14, AIRE, MHCI, and MHCII expression (Figures 4G–4I). Note that some Venus<sup>+</sup> cells were found just adjacent to mTOs (Figures 4C and 4D) and likely represent mesenchymal or CD45<sup>+</sup> cells. AIRE<sup>+</sup> mTECs were present in ~25% of mTOs, with one or two AIRE<sup>+</sup> cells typically detected per organoid by immunostaining after 7 days in culture; addition of RANKL to the culture medium increased both the percentage of mTOs containing AIRE<sup>+</sup> mTECs and the number of AIRE<sup>+</sup> mTECs per organoid by day 7 (Figure 4I and not shown).

FTM cells, identified by vimentin staining, were present in all mTOs (Figure 4A), where they preferentially associated with one another and exhibited two distinct distribution patterns: a single layer of cells separating two layers of TECs or a central cluster of cells surrounded by TECs (Figure 4A)—with the first form predominating (11/14 vs. 3/14 mTO scored). CD45<sup>+</sup> cells were typically found within mTOs, with a few free CD45<sup>+</sup> cells also present outside (Figure 4J; note that this image represents a day-14 mTO).

Overall, mTOs contain cTECs and mTECs expressing the expected sub-lineage-restricted functional markers and are segregated rather than interspersed within the mTO structure. Furthermore, mTOs are suitable for live and fixed whole-mount imaging applications, including time lapsing.

### Transcriptome analysis reveals that mTO TEC sub-population complexity is comparable to that in RFTOC, FTOC, and the native thymus

To further probe cellular complexity and phenotype, we performed single-cell RNA sequencing analysis (scRNA-seq). We set up nine Watch-breaker conditions for analysis (Figures 5A and S6): (1) FTOC, (2) submerged FTOC, (3) submerged RFTOC (unsorted cells), (4) RFTOC (unsorted cells), (5) RFTOC without murine embryonic fibroblasts (MEFs) (unsorted cells), (6) RFTOC in mTO proportions (sorted cells), (7) unsorted mTOs (i.e., mTOs made without MEFs from unsorted E14.5 thymic cells), (8) with-FTM mTO (i.e., Hi FTM mTO), and (9) no-FTM mTO (i.e., as for [8] but without FTM). This allowed us to control independently for the effects of submerging, presence/absence of MEFs, cell sorting, FTM, and varying input cell proportions. We were unable to recover any cells from condition (5) at the experimental endpoint (7 days).

Cells from all the remaining conditions were recovered and processed for flow cytometric analysis (CD45<sup>+</sup> cells) or scRNA-seq (CD45<sup>−</sup> cells) as shown (Figures 5A and S7; see STAR Methods for details). Analysis of the CD45<sup>+</sup> populations revealed poor thymocyte development in the sequenced mTO relative to the mean mTO performance, although all thymocyte populations analyzed were present (Figures S8 and S9; see also Figure 2), indicating that the sequenced mTO represented the lower end of the range of mTO outcomes. All other conditions performed as expected (Figures S8 and S9).

We sequenced the individual CD45-depleted cells from the eight conditions from which cells were recovered, using the 10x Chromium chip. Following initial quality control (STAR Methods), the resulting dataset comprised 4919 single-cell transcriptomes, with a median of 4512 unique genes per cell. Unsupervised clustering across all cells that passed quality control from all Watch-breaker conditions, using the Seurat package in R, revealed a number of TEC clusters and a separate cluster of mesenchymal cells, as expected, along with a small cluster of thymocytes (Figure 5B; see Figure S10 for plots including mesenchymal cells and thymocytes and all Watch-breaker conditions). TEC clusters were identified as shown in Figures 5C and S11, following the naming convention of Kernfeld et al., Magaletta et al., and Bornstein et al.<sup>54–56</sup> (see also Table S4): cluster “mTECI” represents cells also referred to as “intertypical TECs,”<sup>57</sup> “jTECs,”<sup>58</sup> and “pre-Aire mTECs”<sup>59</sup>; clusters mTECII and mTECIII are often called “mature mTECs” and “post-Aire mTECs,” respectively.<sup>57</sup> While cTECs are often split into three clusters—cTECI–III, with little difference between cTECI and cTECII<sup>54</sup>—we found two cTEC clusters, which we called cTECI and cTECIII, characterized by low and high expression of MHCII, respectively. The cTECIII cluster exhibited high expression of genes required in cTECs to support thymocyte development, such as *Dll4* and *Psm11*, as well as the “perinatal cTEC” marker *Cd83*.<sup>57</sup> In human TECs, a cell type called “mcTEC” or “PolyKRT TEC,” is marked by *Krt14* and *Krt15*.<sup>8,37</sup> While there is very little *Krt15* expression in the mouse thymus, *Krt14* expression is highest in mTECI cells (Figure 5C), suggesting mTECI is the mouse equivalent of mcTEC. The mTECI-proliferating cluster was very similar to mTECI but with high *Mki67* expression. Close correspondence between the cultured TECs and the *ex vivo* TECs was demonstrated by clustering the Watch-breaker datasets with those of Baran-Gale<sup>57</sup>; cells from the two datasets were interspersed in all TEC clusters (Figure 5D).

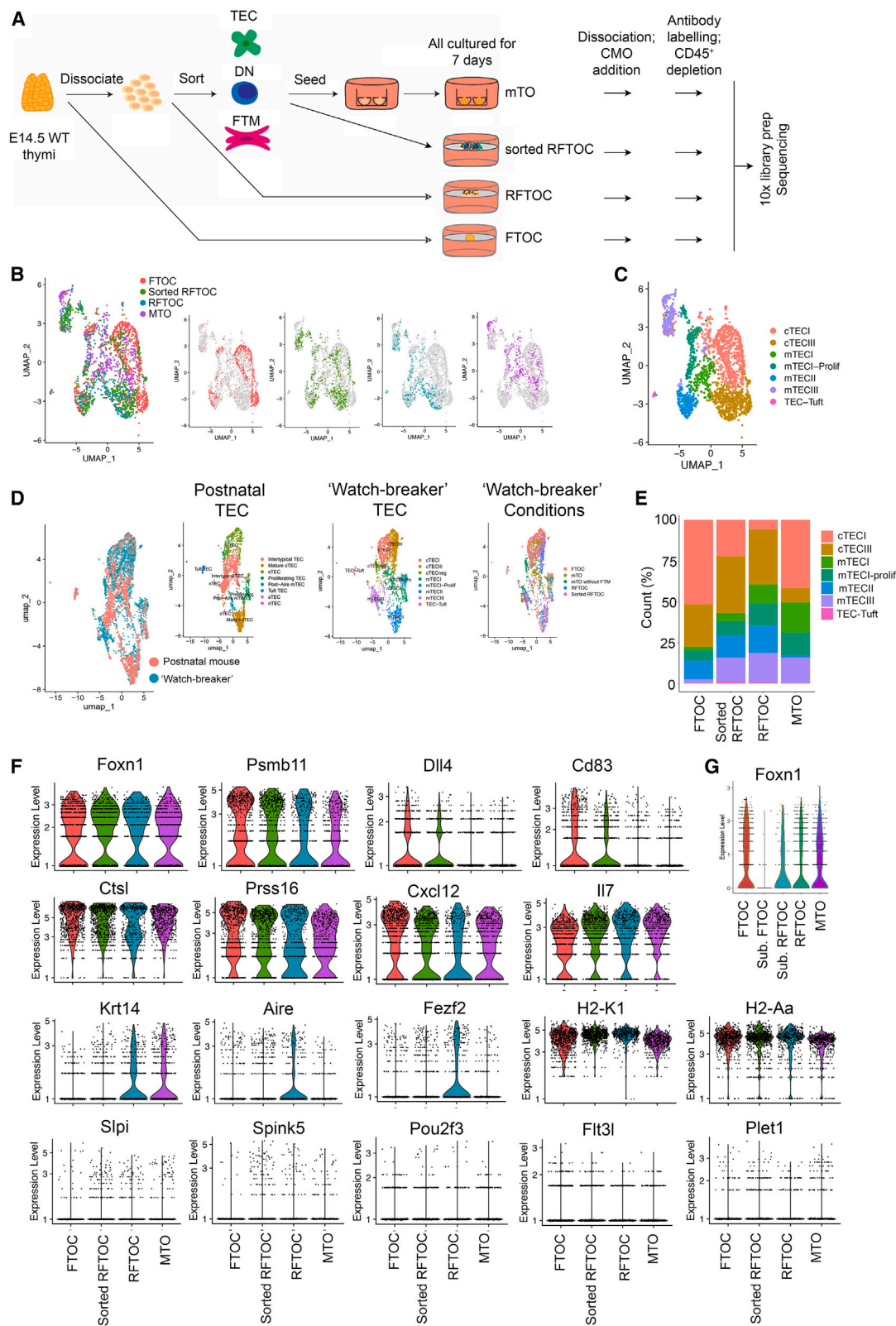
We first analyzed the FTOC, RFTOC, sorted RFTOC, and mTO conditions (Figures 5B, 5C, and 5E–5G). These conditions all contained cells in each of the TEC clusters identified, but differences in distribution across the conditions were observed,

(E and F) Plots show cell-type distribution against absolute distance from the organoid edge (E) and connections between cell types in the neighborhood network, after cell segmentation and analysis of the distribution of Venus<sup>+</sup>, dsRed<sup>+</sup>, and fluorescence-negative cells (F). (E) The y axis in the upper graph shows cell-type distribution expressed as a proportion of all cells within the given distance from the organoid surface. (E) shows data only for cells within organoids.

(G–J) WT mTOs showing  $\beta$ 5t, CD205, DLL4, K14, MHCI, and MHCII staining and merged channels with Hoechst (G); K8, K14, and AIRE staining and merged channels with Hoechst (H and I); and K8 and CD45 staining (J). (H and I) mTOs shown were cultured in the presence of RANKL. (G) The right side shows details from the middle image.

(A–D and G–J) Each mTO shown is from a different well. *n* = 3 independent biological replicates, each with several technical replicates, where *n* is an independent biological replicate performed on a separate day, except for the MHCI, MHCII,  $\beta$ 5t, and keratin staining, where *n* = 2. Hoechst reveals nuclei. (E and F) *n* = 4 organoids from two microwells (*n* = 1 and *n* = 3), with all organoids exhibiting similar structures. Cells within organoids were manually annotated.





(legend on next page)

including between FTOC and RFTOC (Figures 5B, 5C, and 5E). mTOs contained relatively few cTECIII and mTECII (although mTO cells were present in each of these clusters), but were well represented in all other clusters, including mTECIII and TEC-Tuft, and contained the highest proportion of mTECI-proliferating cells (Figures 5B–5E). The low number of mTO cells in the mTECII (mature mTEC) cluster was consistent with our immunohistochemical analysis and with the low numbers of DP thymocytes present in the sequenced mTOs (see Figures 5E, S8, and S9; DP thymocytes provide RANKL required for mTECII development<sup>60</sup>). However, mTO mTECII cells clustered with mTECII from FTOC and RFTOC (Figures S12A and S12B; Table S6) indicating they are phenotypically normal. Furthermore, some mTECIII expressed the hetero-post-AIRE TEC markers *Repetin* (*Rptn*), *polymeric immunoglobulin receptor* (*Pigr*), *serine peptidase inhibitor Kazal type 5* (*Spink5*), and *lymphocyte antigen 6D* (*Ly6d*),<sup>61</sup> while some mTECII expressed the ciliated TEC (CilTEC) markers *sperm-associated antigen 16* (*Spag16*) and *dynein axonemal heavy chain 12* (*Dnah12*)<sup>61</sup> (Figures S13 and S14). The hetero-post-AIRE TEC population included cells from mTO culture, FTOC, and RFTOC, while the five CilTECs identified were from FTOC and RFTOC but not mTO (Figures S13 and S14). From this, we conclude that mTOs contain at least some mimetic TEC sub-populations.

We next analyzed the expression of genes known to be important for TEC functionality, considering both differences in overall expression levels and differences in expression levels in specific TEC sub-sets. All four conditions maintained *Foxn1* expression throughout the culture period, with the overall level of *Foxn1* in mTOs at least equivalent to that in FTOC (Figure 5F; Table S5, 70% vs. 72% *Foxn1*<sup>+</sup> cells, adjusted  $p = 1$ ), consistent with reporter gene expression (Figure 4C). The four conditions also all expressed the cTEC markers *Dil4*, *Psb11* (encoding  $\beta 5t$ ), *Prss16* (encoding serine protease 16/thymus-specific serine protease [TSSP]), *Cxcl12*, and *Cd83* (Figure 5F), consistent with antibody staining (Figure 4E). None of these markers showed statistically significant expression in mTOs across all other conditions, although some condition-to-condition comparisons were statistically significant (e.g., for *Psb11*, the adjusted  $p$  value is  $<10^{-6}$  for mTO vs. FTOC but 1 for mTO vs. RFTOC, Table S5). This was also true for *Irf7*, *Kitl*, and *placenta-expressed transcript 1* (*Plet1*) and for the mTEC genes *Krt14*, *Fezf2*, *Spink5*, *secretory leukocyte peptidase inhibitor* (*Slpi*), and *POU class 2 homeobox 3* (*Pou2f3*) (Figure 5F; Table S5). *Aire* was significantly downregulated in mTOs vs. all other conditions; however, this reflected the poor representation of mTECII as within that population (which expresses *Aire*); *Aire* expression was not significantly

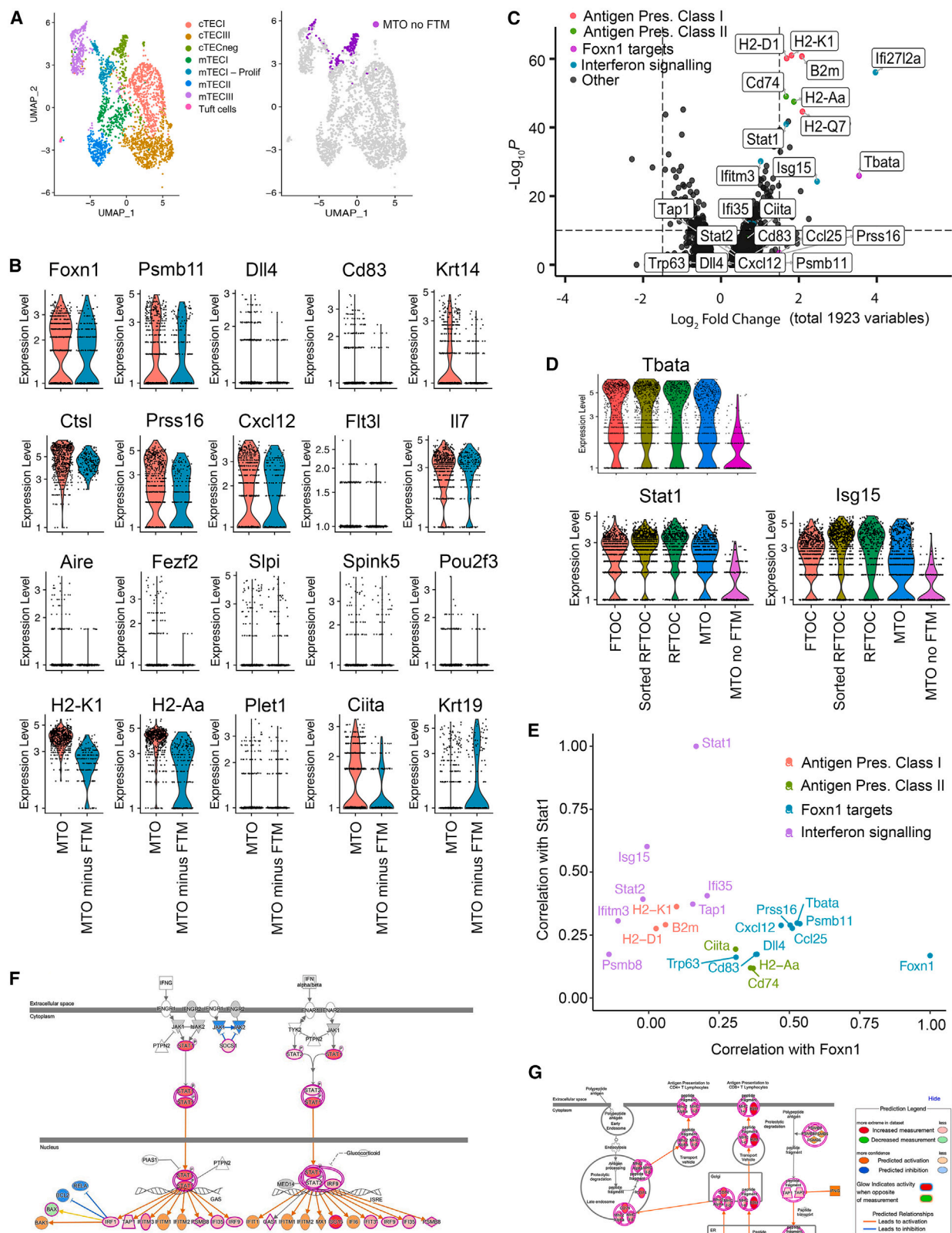
different between mTOs and FTOC (Figure S12B; Table S6). In contrast, *H2-K1* and *H2-Aa* (encoding MHCI and MHCII alleles) were also expressed in all conditions, but at slightly lower levels in mTO compared to each other condition (e.g., for *H2-K1* adjusted  $p < 0.05$  vs. FTOC,  $10^{-53}$  vs. RFTOC, and  $10^{-54}$  vs. sorted RFTOC, Figure 5F; Table S5); of note, this may reflect the low representation of mTECII in mTOs, since in mTECII the levels of *H2-K1* and *H2-Aa* were not significantly different for mTOs compared to all other conditions (Table S6). Overall, compared to all other conditions put together, the top downregulated genes in mTOs were *beta-2-microglobulin* (*B2m*), *H2-K1*, *interferon-induced protein with tetratricopeptide repeats 1* (*Ifit1*), *ubiquitin D* (*Ubd*), *bone marrow stromal cell antigen 2* (*Bst2*), *H2-D1*, and *histocompatibility 2, T region locus 23* (*H2-T23*) (Table S5, mTOvsAll3), while in mTECII only *stathmin 2* (*Stmn2*) was differentially expressed across all conditions (Figure S12B; Table S6).

Expanding our analysis to submerged conditions revealed that submerged FTOC expressed extremely low levels of *Foxn1*, as expected,<sup>53</sup> and submerged RFTOC also expressed much lower *Foxn1* levels than RFTOC cultured at the air-liquid interface (ALI) (Figure 5G). However, as noted above, *Foxn1* was not downregulated in mTOs (also a submerged condition) relative to ALI FTOC or RFTOC (Figure 5G, see also Figure 4A). Differences in cellular composition were also observed between FTOC, RFTOC, and their submerged counterparts (Figures S15A and S15B). Submerged FTOC and submerged RFTOC expressed lower levels of *Psb11*, *Dil4*, *Aire*, *Fezf2*, *Slpi*, and *Pou2f3* than their ALI counterparts (Figure S12B), while, as shown above (Figures 5F and S15C), mTOs expressed levels similar to those of ALI RFTOC and/or FTOC for all of these markers. Some differences were observed that might be attributable to cell dissociation. Most notably, *Dil4* and *Cd83* were downregulated and *Aire* and *Fezf2* upregulated in unsorted RFTOC vs. FTOC that were otherwise cultured under identical conditions (Figure 5F). However, although consistent between unsorted RFTOC and mTO, these changes were not seen in sorted RFTOC. Examination of hypoxia-induced genes (e.g., *hypoxia-inducible domain family member 1A* [*Higd1a*]) did not indicate a clear role for hypoxia in the differences observed (Figure S15D); indeed, hypoxia-induced genes were expressed more highly in FTOC than in other conditions. No clear effects of cell sorting were evident (Figure 5F; note that in the sorted RFTOC condition, the proportion of input cells is as for mTOs, rather than as in unsorted RFTOC).

Collectively, mTOs contain all major sub-types of TECs, and each sub-type expresses the expected range of markers at “normal” levels. Compared to FTOC and RFTOC, the most notable

#### Figure 5. mTOs contain all major TEC sub-types, determined by scRNA-seq

(A) Schematic representation of experimental design for 10x scRNA-seq data shown in (B)–(G). (B–G) Only data for TECs are shown. (B) UMAPs show combined data from the FTOC, RFTOC, sorted RFTOC, and mTO conditions (left) plus the contribution of individual conditions to the combined dataset. (C) Unsupervised clustering revealing TEC sub-sets among the combined dataset in (B). Cluster annotation follows the naming convention in Kernfeld et al.,<sup>54</sup> Magaletta et al.,<sup>55</sup> and Bornstein et al.<sup>56</sup> (D) Uniform manifold approximation and projections (UMAPs) showing dimensionality reduction of the “Watch-breaker” dataset combined with the post-natal TEC dataset from Baran-Gale et al.<sup>57</sup> Combined data are shown on the left, and the contributions of the Watch-breaker conditions and post-natal TECs to the combined dataset are shown on the middle and right, respectively. (E) Graph shows proportional representation of clusters for each Watch-breaker condition, as shown. (F and G) Violin plots showing expression of a selected panel of genes, as shown, in the Watch-breaker conditions shown. See also Figures S6–S14 and Tables S3, S5, and S6.



(legend on next page)



differences in mTOs are the relative paucity of *Aire*<sup>+</sup> mTECII and slightly lower expression of MHC genes and interferon (IFN) targets. Furthermore, our data reveal clear effects of submerging on gene expression in FTOC and RFTOC, but not in mTOs.

### Transcriptome analysis reveals activation of IFN and antigen presentation pathways by FTM

To gain insight into the mechanisms regulated by FTM in TECs we also compared with-FTM mTO with no-FTM mTO, revealing several key differences. First, dimensionality reduction showed that the vast majority of the no-FTM mTO cells formed a distinct cluster adjacent to the cTECI region (Figure 6A), which we named “cTECneg” due to the extremely low levels of both MHCI and MHCII (Figures 6A and 6B), with the remaining cells contributing to clusters mTECI, mTECI-Prolif, and mTECIII (Figure 6A). None of the other conditions contributed to the cTEC-neg cluster. Second, the no-FTM mTO condition expressed similar levels of *Foxn1* and *Ii7* compared to with-FTM mTO, FTOC, and RFTOC and only slightly lower levels of *Psm11*, *Cxcl12*, *Ctst*, *Prss16*, *Plet1*, *Slpi*, and *Spink5* than the other conditions. However, no-FTM mTO expressed markedly less MHCI (*H2-K1*), MHCII (*H2-Aa*), *Aire*, *Fezf2*, *Pouf2*, and *Krt14* than with-FTM mTO and almost no *Dll4* or *Cd83* (Figures 6B and 6C; Tables S7 and S8). Notably, *Prss16*, *Dll4*, *Cd83*, *thymus-*, *brain-*, and *testes-associated* (*Tbata*), *Psm11*, and *C-C motif chemokine ligand 25* (*Ccl25*) are all among the high-confidence FOXN1 target genes identified by chromatin immunoprecipitation sequencing (ChIP-seq),<sup>62</sup> and the differential expression of these genes in *Foxn1*<sup>+</sup> cells in the no-FTM mTO condition thus indicates that co-factors directly or indirectly regulated by FTM are required in addition to FOXN1 for their expression.

The top differentially expressed genes between the with-FTM mTO and the no-FTM mTO conditions were *B2m*, *H2-D1*, *H2-K1*, *H2-Aa*, *H2-Q7*, and *Cd74*, all members of the MHCI or MHCII antigen presentation pathways; the TEC regulator *Tbata*; and the IFN-stimulated genes (ISGs) *alpha-inducible protein 27-like 2a* (*Ifi272a*) and *interferon-stimulated gene 15* (*Isg15*), all of which were higher in the with-FTM mTO condition (Figures 6C and 6D). Pathway analysis also highlighted the downregulation of the IFN signaling and antigen processing and presentation pathways in the no-FTM mTO vs. mTO condition (Figures 6D–6G). *Signal transducer and activator of transcription 1* (*Stat1*), a key regulator of IFN signaling implicated in the regulation of antigen processing and presentation pathway components, including *class II major histocompatibility complex transactivator* (*Ciita*), *transporter associated with antigen processing 1* (*Tap1*), *Tap2*, and *proteasome subunit beta type-8* (*Psm8*), was among the most differentially expressed genes (Figures 6C–6E). Targets of

both type I and type II IFN signaling were also expressed more highly in the with-FTM mTO condition, including *IFN regulatory factor 1* (*Irf1*), *Irf9*, *Tap1*, *interferon-induced transmembrane protein 3* (*Ifitm3*), and *interferon-induced protein 35* (*Ipi35*), as were additional antigen presentation pathway components, including *Ciita* and *Tap1* (Figures 6C–6G; Tables S7 and S8).

Examination of cells in the TECs and mesenchymal clusters of the FTOC, RFTOC, and with-FTM mTO conditions revealed almost no interferon gamma (*ifng*) expression, some *ifnz* expression in cTECs (in all conditions except no-FTM mTO), and *Irfn1* and *Irfn2* expression in approximately 2% of mTECII, as reported elsewhere<sup>63,64</sup> (Figure S16; Table S6). This essentially rules out a direct effect of IFN signaling from FTM, leaving the possibilities that FTM is boosting IFN production in TECs themselves or in one or more intrathymic hematopoietic cell type. Of note is that MHC I expression in TECs has recently been shown to be independent of *interferon alpha/beta receptor 1* (*ifnar1*) and *interferon gamma receptor 1* (*ifngr1*), but dependent on *interferon lambda receptor 1* (*ifnlr1*), *Aire*, *Stat1*, and *NLR family CARD domain-containing 5* (*Nlr5*),<sup>65</sup> consistent with the hypothesis that IFN signaling is caused by type III IFNs from mTECII.

Related to this, we observed two sub-populations within the mTECIII cluster, with all no-FTM mTO mTECIII cells belonging to one sub-cluster (Figure 6A). This sub-cluster expressed high levels of *Krt19*, *Notch1*, *Claudin* (*Cldn*)3, *Cldn4*, *SRY-box transcription factor 9* (*Sox9*), and *Plet1*, markers of mTEC progenitors,<sup>66,67</sup> while both sub-clusters expressed the post-AIRE mTEC (mTECIII) markers *Slpi* and *Spink5*, which early mTEC progenitors do not. This raises the possibility that mTECIII contains an mTEC progenitor population as well as post-AIRE mTECs. In support of this, the algorithm CytoTRACE2<sup>68</sup> predicts the mTEC-progenitor-like sub-cluster of mTECIII to be less differentiated than the remaining sub-cluster (Figure S17).

## DISCUSSION

Taken together, the data presented demonstrate that functional mTOs can be generated from E14.5 fetal thymic cells in a micro-well format suitable for medium-throughput imaging and screening applications, including live imaging and time lapse. They establish the optimized cellular input requirements for these mTOs and show that they meet and surpass the minimal criteria for a functional thymic organoid. mTOs can support T cell lineage commitment and subsequent thymocyte differentiation to generate mature naive SP4 and SP8 T cells. They contain regions of cTECs and mTECs that express canonical sub-lineage-specific markers (cTECs, *DLL4*,<sup>42,43</sup> *CD205*, *CXCL12*,<sup>44</sup>  $\beta$ 5t,<sup>45</sup> and cathepsin L<sup>46</sup>; mTECs, *RANK*,<sup>69</sup> *K14*, and *AIRE*<sup>14</sup>; TEC markers,

### Figure 6. Effect of FTM on TEC populations and gene expression within mTOs

(A) UMAPs show combined data from the FTOC, RFTOC, sorted RFTOC, mTO, and no-FTM mTO conditions (left) plus the contribution of the no-FTM mTO condition to the combined dataset (right).

(B–G) Only data for TECs are shown. (B) Violin plots showing expression of a selected panel of genes, as shown, in the Watch-breaker conditions shown. (C) Volcano plot showing differential gene expression between the mTO and the no-FTM mTO conditions; on the x axis, positive numbers are upregulated in mTO vs. no-FTM mTO. (D) Violin plots showing expression of selected IFN pathway genes in the Watch-breaker conditions shown. (E) Plot shows correlation with *Foxn1* expression level and *Stat1* expression level of the differentially expressed genes highlighted in (C). (F and G) Schematics of Ingenuity pathway analysis of genes upregulated in mTO vs. no-FTM mTO for the IFN signaling and antigen processing and presentation pathways.

See also Figures S15–S17 and Tables S7, and S8.

MHCI and MHCII), Furthermore, global transcriptome analysis shows mTOs contain all major cTEC and mTEC sub-types, albeit with relative underrepresentation of mTECII compared to the early post-natal thymus—likely explained by the low numbers of DP thymocytes in the particular mTOs sequenced. Through use of the mTO system to probe the role of FTM in thymic organoids, our data also identify a necessary, likely at least partly indirect, role for FTM in supporting differentiation and/or maintenance of most TEC sub-sets from E14.5 input cells and identify IFN signaling as a candidate mechanism for driving this crosstalk. These findings collectively raise several important issues, as discussed below.

Our findings introduce mTOs as a platform for exploration of thymus biology, compatible with both live imaging and medium-throughput screening applications. In this system, each well of a 96-well plate contains at least 31 mTOs, enabling establishment of multiple replicates within each experimental condition while starting from a minimal number of input cells. Each mTO can be live imaged individually, allowing parallel analysis of organoid, TEC, and/or thymocyte behavior over time in response to experimental manipulations, including screening conditions.

mTOs meet the formal definition of an organoid, namely “self-organized three-dimensional structures which mimic the key functional, structural and biological complexity of an organ.... derived from ... stem cells or tissue-derived cells, including normal stem/progenitor cells ....”<sup>70</sup> They represent a step forward for analysis of thymic stromal biology and T cell development, as the only currently available near-physiological models (FTOC and RFTOC) require large cell numbers for their establishment, precluding parallel testing of multiple conditions. In contrast, mTOs are easier to establish, retain key physiological attributes of the fetal/perinatal thymus, and can easily be used for live and whole-mount imaging. As discussed below, our data already show the value of this platform for interrogating thymus biology (here, the role of FTM); beyond this, mTOs are amenable to further development for genetic manipulation and modeling and for high-throughput screening protocols.

mTOs can currently be produced in two formats—(1) based on dissociated but unsorted fetal TECs and (2) based on dissociated and sorted fetal TECs reassembled using optimized proportions. The former is already amenable to medium-throughput applications (e.g., to set up 96 wells, each containing 31 unsorted mTOs, would require approximately 15 timed matings), while the latter is currently suitable for smaller-scale screening applications, enabling parallel testing of a smaller number of wells, e.g., for image-based screening of multiple mTOs within a single well per condition (in our hands, for “optimized mTO,” 8 of 96 wells can be established per 10 timed matings). We expect this platform to develop rapidly, for instance, by incorporating *in vitro*-generated<sup>35,36</sup> or expanded<sup>37–39</sup> TECs.

In terms of “watch-breaking” and “watch-making,” we initially sought to determine which of the stromal cell types present in the native fetal thymus were required to generate functional mTOs. Iterative testing revealed the requirement for TECs and FTM, while omission of thymic ECs did not affect the capacity of mTOs to support thymopoiesis. From this, we conclude that, in terms of stromal inputs, the fetal thymus “watch” cannot easily be broken: not only are all elements, barring ECs, required to

elaborate a functional mTO, the requisite stromal elements must be in physiological proportion (TEC:FTM was 2.5:1) for optimal function. The reason for this physiological ratio remains to be determined, but it likely reflects the mechanisms through which FTM supports TECs and thymocytes,<sup>71–73</sup> including provision of extracellular matrix and of growth factors. The requirement for physiological proportionality, however, did not hold for thymocytes; optimal mTO outputs were achieved when the ratio of input TEC:DN cells was raised from 1:2 to 2:1, possibly reflecting a reduction in niche availability due to the cell dissociation and reaggregation process. In support of this, RFTOC generated with optimized mTO cell input proportions supported thymocyte development better than FTOC and unsorted RFTOC in terms of output numbers for most thymocyte populations analyzed.

Our finding that FTM is an essential mTO component was expected. The absence of FTM-derived fibroblast growth factor (FGF)7/10 leads to thymic hypoplasia,<sup>71</sup> and hypoplastic thymi develop upon transplantation of FTM-depleted fetal thymic lobes.<sup>74</sup> Furthermore, FTM is required in RFTOC to support early thymocyte development.<sup>72,73</sup> However, the effect observed herein was more severe than that in *in vivo* models lacking neural crest cell (NCC)-derived FTM. In *paired box gene 3* (*Pax3*<sup>−/−</sup>) mice (*Pax3*<sup>Spl/Spl</sup> and *Pax3*<sup>Cre/Cre</sup>), which almost completely lack NCC-FTM, an ectopic and hyperplastic thymus develops until at least E14.5,<sup>75</sup> while transplantation of E9.0 NCC-free third pharyngeal pouch endoderm (3PPE) results in the development of organized and functional thymi<sup>76</sup>—consistent with co-option of mesenchyme from the transplant site.<sup>77</sup> Our current findings indicate the near-complete failure of no-FTM mTO to support TEC development and/or maintenance and the complete failure to support thymocyte development. This was surprising, since the DN input cells for mTOs included CD44<sup>−</sup>CD25<sup>+</sup> (DN3) and CD44<sup>−</sup>CD25<sup>−</sup> (DN4) cells, while the requirement for FTM in RFTOC has been mapped to the CD44<sup>+</sup>CD25<sup>+</sup> (DN2) stage of thymocyte development, with later stages being FTM independent.<sup>72</sup> Furthermore, it did not result simply from failed reaggregation (see Figure S7).

Examination of the gene expression profile of no-FTM mTO cells revealed levels of *Foxn1* equivalent to those of with-FTM mTO cells (and all other conditions), ruling out loss of FOXN1 as the underpinning cause. Notably, despite this, the levels of some known direct FOXN1 transcriptional targets,<sup>62</sup> including *Dll4*, *Cd83*, and, less markedly, *Cxcl12*, *Psmb11*, *Ctstl*, and *Prss16*, were downregulated in no-FTM mTO. While this may reflect the absence of cell types that normally express these markers, it further suggests that co-factors required in addition to FOXN1 for normal expression of these genes are limiting in cTEC-neg and mTECIII cells and/or that accessibility of these loci is TEC-sub-type specific.

Analysis of gene expression in with-FTM mTO vs. no-FTM mTO conditions revealed the marked downregulation of type I IFN-regulated genes, including *Stat1*, MHC I (*H2-K1*), MHC II (*H2-Aa*), and multiple members of the class I and class II antigen processing and presentation pathways, suggesting that lack of FTM-regulated IFN signaling might explain the failure of no-FTM mTO. However, while receptors for all IFNs (*Ifnar1*, *Ifnar2*, *Ifngr1*, *Ifngr2*, and *Ifnlr1*) were broadly expressed across all Watch-breaker conditions, essentially no IFNs were observed



in FTM, and in TECs, only *Ifnz* (which was expressed by a few cTECs in FTOC, RFTOC, and mTOs) and *Ifnb1*, *Ifnl2*, and *Ifnl3* (which were expressed in ~2% of mTECII in all conditions with mTECII), as expected,<sup>64</sup> were observed.

IFN expression in the thymus is thought to be restricted to AIRE<sup>+</sup> mTECs (mTECII),<sup>64,65</sup> with *Aire*-, *Ifnlr1*-, *Stat1*-, and *Nlrp5*-dependent expression of type III IFNs regulating MHCI expression.<sup>65</sup> Although IFN $\alpha$  has been reported in human thymic plasmacytoid dendritic cells (pDC),<sup>78</sup> as well as IFN $\gamma$  in thymic iNKT cells and eosinophils,<sup>79</sup> the expression of MHCI in the TECs was dependent on only the type III IFN receptor *Ifnlr1* and not *Ifnar1* or *Ifngr1*.<sup>65</sup> Similarly, *Ifnlr1* was shown to play a bigger role than *Ifnar1* or *Ifngr1* in the maturation of thymic DC1s, macrophages, B cells, and T<sub>reg</sub> cells.<sup>64</sup> In no-FTM mTO, the IFN-regulated gene signature was strongly downregulated in all cell types. This suggests IFN signaling may play an earlier, previously undefined role, in TEC development. Alternatively, it may simply reflect the absence of mTECII. Since FTM has been shown to regulate proliferation of fetal TECs,<sup>74</sup> and differentiation of stem/progenitor cells is proliferation dependent in at least some other lineages,<sup>80,81</sup> it is also possible that the absence of FTM leads to a lack of TEC proliferation, resulting in the absence of more differentiated TEC phenotypes. However, inspection of cell-cycle regulators revealed no obvious deficit in no-FTM mTO cells (not shown). On balance, we favor a role for IFN signaling pathway in TEC differentiation and/or maintenance.

The inability of no-FTM mTO to support thymopoiesis could in part be explained by the very low levels of *Dll4* expression in this condition. This was puzzling, as *Dll4* is a known direct transcriptional target of FOXN1,<sup>62</sup> yet *Foxn1* levels were near normal in no-FTM mTO. Vascular endothelial growth factor (VEGF) is known to act via FOXC1 to regulate *Dll4* expression in ECs.<sup>82</sup> *Foxc1* was expressed in some TECs across all conditions analyzed; thus, the observed downregulation of *Vegf* in the no-FTM mTO condition provides a possible explanation for the loss of *Dll4*.

Thymic organoids have enormous therapeutic potential, both for generating positively and/or negatively selected T cells and for acting as model systems for understanding thymic involution and regeneration. Three-dimensional cell-line-based cultures, called artificial thymic organoids (ATOs) have already been used to generate chimeric antigen receptor (CAR) T cells<sup>83</sup> and mature T cells from bone marrow organoid-derived hematopoietic cells.<sup>84</sup> As ATOs lack TEC-specific functions required for beta, positive selection, and tolerance induction, deployment of *bona fide* thymic organoids such as mTOs should substantially improve these systems. The establishment of a medium-/high-throughput thymic organoid system, described here, will also aid in the development of serum- and feeder-free thymic organoids, as well as treatments aimed at regenerating thymic tissue. Furthermore, thymic organoids have the potential to be patient specific, e.g., if derived from patient PSCs, allowing for patient-specific T cell receptor (TCR) repertoire selection: we expect the mTO system to be readily adaptable to human fetal thymus and PSC-derived TEC inputs.

### Limitations of the study

The data presented herein report the full findings of the study; no data were excluded. The main limitation of this method is exper-

iment-to-experiment variability, also a feature of other *in vitro* thymus models, including RFTOC.<sup>85</sup> We wish to note two points regarding the variation in the current data. Each figure represents an individual experiment addressing a specific question. Experiments performed early in the mTO development process typically had lower yields and higher within-experiment variability than those performed once the operator was experienced—this was at least partly because we were able to iteratively improve the experimental technique, e.g., by minimizing the time from dissection to plating, improving the plating technique, and introducing improvements such as cell pre-mixing. We expect that other researchers will also experience decreased variability as operator experience increases. We note that this issue affected the scRNA-seq data presented, and in future analyses we would build a quality control step in for the mTO (e.g., flow cytometric analysis of CD4 vs. CD8) before proceeding to sample processing. Second, as is evident in some of the imaging figures, individual mTOs with different cellular compositions can be present within 1 of 96 wells and, indeed, within one microwell. This structure-to-structure variability is also a feature of RFTOC and of other organoids. While we expect to better understand and in the future minimize variation through further work, one of the strengths of the mTO system is that these differences are averaged across a microwell so that the overall variability is comparable from experiment to experiment.

### RESOURCE AVAILABILITY

#### Lead contact

Requests for further information and resources should be directed to and will be fulfilled by the lead contact, Clare Blackburn ([c.blackburn@ed.ac.uk](mailto:c.blackburn@ed.ac.uk)).

#### Materials availability

This study did not generate new unique reagents.

#### Data and code availability

- Data: scRNA-seq data have been deposited at NCBI SRA and are publicly available as of the date of publication. Accession numbers are listed in the [key resources table](#).
- Codes: The codes for the analyses shown in [Figures 4, 5, and 6](#) and related [supplemental information](#) have been deposited in Zenodo and are publicly available as of the date of publication. DOIs are listed in the [key resources table](#).
- Other items: Any additional information required to reanalyze the data reported in this paper is available from the [lead contact](#) upon request

### ACKNOWLEDGMENTS

We thank C. Cryer and F. Rossi (IRR, University of Edinburgh) for cell sorting, M. Vermeren (IRR, University of Edinburgh) for imaging, and the BVS staff for animal care. The research leading to these results received funding from the School of Biological Sciences, University of Edinburgh (T. Henderson and C.A.); the UKRI-Biotechnology and Biological Sciences Research Council through an industrial CASE studentship (award no. BB/M016412/1; C.C.B. and P.R.) and an EASTBIO DTP studentship (Q.G.) and through a UKRI-BBSRC/NC3Rs grant (award no. NC/X002470/1; C.C.B. and V.M.); the Darwin Trust (J.M.); the European Union Seventh Framework Programme (FP7/2007–2013) collaborative project ThymiStem under grant agreement no. 602587 (P.R., T. Henderson, and C.C.B.); the UKRI-Medical Research Council through a DTP in Precision Medicine studentship (award no. MR/N013166/1) (J.S.); and Wellcome Trust collaborative award 211944/Z/18/Z (V.M., P.R., T. Henderson, Y.W., S.P., T. Hübscher, S.J.C., G.A., M.P.L., and C.C.B.). G.A. is supported by

a UKRI-MRC Programme grant (MR/T029765/1). The graphical abstract was created in BioRender. Blackburn, C. (2025) <https://BioRender.com/k56g336>.

## AUTHOR CONTRIBUTIONS

V.M., P.R., T. Henderson, S.P., and J.M.: conception and design, collection and assembly of data, data analysis and interpretation, and manuscript writing. T. Hübscher: conception and design and collection and assembly of data. J.S., C.A., A.C., J.C.-W., Q.G., Y.W.: collection and assembly of data. S.J.C. and M.P.L.: conception and design. A.B.: provision of study materials. G.A.: conception and design, provision of study materials, and data analysis and interpretation. C.C.B.: conception and design, financial support, provision of study materials, data analysis and interpretation, manuscript writing, and final approval of the manuscript.

## DECLARATION OF INTERESTS

The authors declare no competing interests.

## STAR★METHODS

Detailed methods are provided in the online version of this paper and include the following:

- KEY RESOURCES TABLE
- EXPERIMENTAL MODEL AND STUDY PARTICIPANT DETAILS
- METHOD DETAILS
  - Thymus dissociation
  - Tissue culture
  - Generation of mTO
  - FTOC and RFTOC
  - Flow cytometry
  - Immunohistochemistry
  - Antibodies
  - Image analysis
  - Single cell RNA-seq
- QUANTIFICATION AND STATISTICAL ANALYSIS
  - Statistics and experimental design

## SUPPLEMENTAL INFORMATION

Supplemental information can be found online at <https://doi.org/10.1016/j.celrep.2025.115579>.

Received: September 24, 2024

Revised: December 20, 2024

Accepted: March 27, 2025

Published: April 16, 2025

## REFERENCES

1. Boyd, R.L., Tucek, C.L., Godfrey, D.I., Izon, D.J., Wilson, T.J., Davidson, N.J., Bean, A.G., Ladyman, H.M., Ritter, M.A., and Hugo, P. (1993). The thymic microenvironment. *Immunol. Today Off.* 14, 445–459.
2. Ritter, M.A., and Boyd, R.L. (1993). Development in the thymus: it takes two to tango. *Immunol. Today* 14, 462–469. [https://doi.org/10.1016/0167-5699\(93\)90250-O](https://doi.org/10.1016/0167-5699(93)90250-O).
3. Miller, J. (1961). Immunological function of the thymus. *Lancet* 278, 748–749.
4. Abramson, J., and Anderson, G. (2017). Thymic Epithelial Cells. *Annu. Rev. Immunol.* 35, 85–118. <https://doi.org/10.1146/annurev-immunol-051116-052320>.
5. Manley, N.R., Richie, E.R., Blackburn, C.C., Condie, B.G., and Sage, J. (2011). Structure and function of the thymic microenvironment. *Front. Biosci.* 16, 2461–2477.
6. Klein, L., Kyewski, B., Allen, P.M., and Hogquist, K.A. (2014). Positive and negative selection of the T cell repertoire: what thymocytes see (and don't see). *Nat. Rev. Immunol.* 14, 377–391. <https://doi.org/10.1038/nri3667>.
7. Anderson, G., and Takahama, Y. (2012). Thymic epithelial cells: working class heroes for T cell development and repertoire selection. *Trends Immunol.* 33, 256–263. <https://doi.org/10.1016/j.it.2012.03.005>.
8. Yayon, N., Kedlian, V.R., Boehme, L., Suo, C., Wachter, B.T., Beuschel, R.T., Amsalem, O., Polanski, K., Koplev, S., Tuck, E., et al. (2024). A spatial human thymus cell atlas mapped to a continuous tissue axis. *Nature* 635, 708–718. <https://doi.org/10.1038/s41586-024-07944-6>.
9. Michelson, D.A., Hase, K., Kaisho, T., Benoist, C., and Mathis, D. (2022). Thymic epithelial cells co-opt lineage-defining transcription factors to eliminate autoreactive T cells. *Cell* 185, 2542–2558.e18. <https://doi.org/10.1016/j.cell.2022.05.018>.
10. Michelson, D.A., and Mathis, D. (2022). Thymic mimetic cells: tolerogenic masqueraders. *Trends Immunol.* 43, 782–791. <https://doi.org/10.1016/j.it.2022.07.010>.
11. James, K.D., Cosway, E.J., Parnell, S.M., White, A.J., Jenkinson, W.E., and Anderson, G. (2024). Assembling the thymus medulla: Development and function of epithelial cell heterogeneity. *Bioessays* 46, e2300165. <https://doi.org/10.1002/bies.202300165>.
12. White, A.J., Parnell, S.M., Handel, A., Maio, S., Bacon, A., Cosway, E.J., Lucas, B., James, K.D., Cowan, J.E., Jenkinson, W.E., et al. (2022). Diversity in Cortical Thymic Epithelial Cells Occurs through Loss of a Foxn1-Dependent Gene Signature Driven by Stage-Specific Thymocyte Cross-Talk. *J. Immunol.* 210, 40–49. <https://doi.org/10.4049/jimmunol.2200609>.
13. Ashby, K.M., and Hogquist, K.A. (2024). A guide to thymic selection of T cells. *Nat. Rev. Immunol.* 24, 103–117. <https://doi.org/10.1038/s41577-023-00911-8>.
14. Anderson, M.S., Venanzi, E.S., Klein, L., Chen, Z., Berzins, S.P., Turley, S.J., von Boehmer, H., Bronson, R., Dierich, A., Benoist, C., and Mathis, D. (2002). Projection of an immunological self shadow within the thymus by the aire protein. *Science* 298, 1395–1401.
15. Kyewski, B., and Peterson, P. (2010). Aire, master of many trades. *Cell* 140, 24–26. <https://doi.org/10.1016/j.cell.2009.12.036>.
16. Yang, S., Fujikado, N., Kolodin, D., Benoist, C., and Mathis, D. (2015). Immune tolerance. Regulatory T cells generated early in life play a distinct role in maintaining self-tolerance. *Science* 348, 589–594. <https://doi.org/10.1126/science.aaa7017>.
17. Takaba, H., Morishita, Y., Tomofuji, Y., Danks, L., Nitta, T., Komatsu, N., Kodama, T., and Takayanagi, H. (2015). Fezf2 Orchestrates a Thymic Program of Self-Antigen Expression for Immune Tolerance. *Cell* 163, 975–987. <https://doi.org/10.1016/j.cell.2015.10.013>.
18. Anderson, M.S., and Su, M.A. (2016). AIRE expands: new roles in immune tolerance and beyond. *Nat. Rev. Immunol.* 16, 247–258. <https://doi.org/10.1038/nri.2016.9>.
19. Fujikado, N., Mann, A.O., Bansal, K., Romito, K.R., Ferre, E.M.N., Rosenzweig, S.D., Lionakis, M.S., Benoist, C., and Mathis, D. (2016). Aire Inhibits the Generation of a Perinatal Population of Interleukin-17A-Producing gammadelta T Cells to Promote Immunologic Tolerance. *Immunity* 45, 999–1012. <https://doi.org/10.1016/j.immuni.2016.10.023>.
20. Kondo, K., Ohigashi, I., and Takahama, Y. (2019). Thymus machinery for T-cell selection. *Int. Immunol.* 31, 119–125. <https://doi.org/10.1093/intimm/dxy081>.
21. Takada, K., Kondo, K., and Takahama, Y. (2017). Generation of Peptides That Promote Positive Selection in the Thymus. *J. Immunol.* 198, 2215–2222. <https://doi.org/10.4049/jimmunol.1601862>.
22. George, A.J., and Ritter, M.A. (1996). Thymic involution with ageing: obsolescence or good housekeeping? *Immunol. Today* 17, 267–272.
23. Palmer, S., Albergante, L., Blackburn, C.C., and Newman, T.J. (2018). Thymic involution and rising disease incidence with age. *Proc. Natl. Acad. Sci. USA* 115, 1883–1888. <https://doi.org/10.1073/pnas.1714478115>.

24. Kinsella, S., and Dudakov, J.A. (2020). When the Damage Is Done: Injury and Repair in Thymus Function. *Front. Immunol.* **11**, 1745. <https://doi.org/10.3389/fimmu.2020.01745>.
25. Davies, E.G., Cheung, M., Gilmour, K., Maimaris, J., Curry, J., Furmanski, A., Sebire, N., Halliday, N., Mengrelis, K., Adams, S., et al. (2017). Thymus transplantation for complete DiGeorge syndrome: European experience. *J. Allergy Clin. Immunol.* **140**, 1660–1670.e16. <https://doi.org/10.1016/j.jaci.2017.03.020>.
26. Hare, K.J., Jenkinson, E.J., and Anderson, G. (1999). In vitro models of T cell development. *Semin. Immunol.* **11**, 3–12.
27. Schmitt, T.M., and Zúñiga-Pflücker, J.C. (2002). Induction of T cell development from hematopoietic progenitor cells by delta-like-1 in vitro. *Immunity* **17**, 749–756.
28. Mohtashami, M., Shah, D.K., Nakase, H., Kianizad, K., Petrie, H.T., and Zúñiga-Pflücker, J.C. (2010). Direct comparison of Dll1- and Dll4-mediated Notch activation levels shows differential lymphomyeloid lineage commitment outcomes. *J. Immunol.* **185**, 867–876. <https://doi.org/10.4049/jimmunol.1000782>.
29. Seet, C.S., He, C., Bethune, M.T., Li, S., Chick, B., Gschweng, E.H., Zhu, Y., Kim, K., Kohn, D.B., Baltimore, D., et al. (2017). Generation of mature T cells from human hematopoietic stem and progenitor cells in artificial thymic organoids. *Nat. Methods* **14**, 521–530. <https://doi.org/10.1038/nmeth.4237>.
30. Montel-Hagen, A., Seet, C.S., Li, S., Chick, B., Zhu, Y., Chang, P., Tsai, S., Sun, V., Lopez, S., Chen, H.C., et al. (2019). Organoid-Induced Differentiation of Conventional T Cells from Human Pluripotent Stem Cells. *Cell Stem Cell* **24**, 376–389.e8. <https://doi.org/10.1016/j.stem.2018.12.011>.
31. Montel-Hagen, A., Tsai, S., Seet, C.S., and Crooks, G.M. (2022). Generation of Artificial Thymic Organoids from Human and Murine Hematopoietic Stem and Progenitor Cells. *Curr. Protoc.* **2**, e403. <https://doi.org/10.1002/cpz1.403>.
32. Bredenkamp, N., Ulyanchenko, S., O'Neill, K.E., Manley, N.R., Vaidya, H.J., and Blackburn, C.C. (2014). An organized and functional thymus generated from FOXP1-reprogrammed fibroblasts. *Nat. Cell Biol.* **16**, 902–908. <https://doi.org/10.1038/ncb3023>.
33. Parent, A.V., Russ, H.A., Khan, I.S., LaFlam, T.N., Metzger, T.C., Anderson, M.S., and Hebrok, M. (2013). Generation of functional thymic epithelium from human embryonic stem cells that supports host T cell development. *Cell Stem Cell* **13**, 219–229. <https://doi.org/10.1016/j.stem.2013.04.004>.
34. Sun, X., Xu, J., Lu, H., Liu, W., Miao, Z., Sui, X., Liu, H., Su, L., Du, W., He, Q., et al. (2013). Directed differentiation of human embryonic stem cells into thymic epithelial progenitor-like cells reconstitutes the thymic microenvironment in vivo. *Cell Stem Cell* **13**, 230–236. <https://doi.org/10.1016/j.stem.2013.06.014>.
35. Ramos, S.A., Armitage, L.H., Morton, J.J., Alzofon, N., Handler, D., Kelly, G., Homann, D., Jimeno, A., and Russ, H.A. (2023). Generation of functional thymic organoids from human pluripotent stem cells. *Stem Cell Rep.* **18**, 829–840. <https://doi.org/10.1016/j.stemcr.2023.02.013>.
36. Ramos, S.A., Morton, J.J., Yadav, P., Reed, B., Alizadeh, S.I., Shilleh, A.H., Perrenoud, L., Jagers, J., Kappler, J., Jimeno, A., and Russ, H.A. (2022). Generation of functional human thymic cells from induced pluripotent stem cells. *J. Allergy Clin. Immunol.* **149**, 767–781.e6. <https://doi.org/10.1016/j.jaci.2021.07.021>.
37. Ragazzini, R., Boeing, S., Zanieri, L., Green, M., D'Agostino, G., Bartolovic, K., Agua-Doce, A., Greco, M., Watson, S.A., Batsivari, A., et al. (2023). Defining the identity and the niches of epithelial stem cells with highly pleiotropic multilineage potency in the human thymus. *Dev. Cell* **58**, 2428–2446.e9. <https://doi.org/10.1016/j.devcel.2023.08.017>.
38. Hun, M., Barsanti, M., Wong, K., Ramshaw, J., Werkmeister, J., and Chidgey, A.P. (2017). Native thymic extracellular matrix improves in vivo thymic organoid T cell output, and drives in vitro thymic epithelial cell differentiation. *Biomaterials* **118**, 1–15. <https://doi.org/10.1016/j.biomaterials.2016.11.054>.
39. Lim, S., J F van Son, G., Wisma Eka Yanti, N.L., Andersson-Rolf, A., Willemssen, S., Korving, J., Lee, H.G., Begthel, H., and Clevers, H. (2024). Derivation of functional thymic epithelial organoid lines from adult murine thymus. *Cell Rep.* **43**, 114019. <https://doi.org/10.1016/j.celrep.2024.114019>.
40. Campinoti, S., Gjinovci, A., Ragazzini, R., Zanieri, L., Ariza-McNaughton, L., Catucci, M., Boeing, S., Park, J.E., Hutchinson, J.C., Muñoz-Ruiz, M., et al. (2020). Reconstitution of a functional human thymus by postnatal stromal progenitor cells and natural whole-organ scaffolds. *Nat. Commun.* **11**, 6372. <https://doi.org/10.1038/s41467-020-20082-7>.
41. Hubscher, T., Lorenzo-Martin, L.F., Barthlott, T., Tillard, L., Langer, J.J., Rouse, P., Blackburn, C.C., Hollander, G., and Lutolf, M.P. (2024). Thymic epithelial organoids mediate T-cell development. *Development* **151**, dev202853. <https://doi.org/10.1242/dev.202853>.
42. Koch, U., Fiorini, E., Benedito, R., Besseyrias, V., Schuster-Gossler, K., Pierres, M., Manley, N.R., Duarte, A., Macdonald, H.R., and Radtke, F. (2008). Delta-like 4 is the essential, nonredundant ligand for Notch1 during thymic T cell lineage commitment. *J. Exp. Med.* **205**, 2515–2523.
43. Hozumi, K., Mailhos, C., Negishi, N., Hirano, K.I., Yahata, T., Ando, K., Zuklys, S., Holländer, G.A., Shima, D.T., and Habu, S. (2008). Delta-like 4 is indispensable in thymic environment specific for T cell development. *J. Exp. Med.* **205**, 2507–2513. <https://doi.org/10.1084/jem.20080134>.
44. Janas, M.L., Varano, G., Gudmundsson, K., Noda, M., Nagasawa, T., and Turner, M. (2010). Thymic development beyond beta-selection requires phosphatidylinositol 3-kinase activation by CXCR4. *J. Exp. Med.* **207**, 247–261. <https://doi.org/10.1084/jem.20091430>.
45. Murata, S., Sasaki, K., Kishimoto, T., Niwa, S.I., Hayashi, H., Takahama, Y., and Tanaka, K. (2007). Regulation of CD8+ T cell development by thymus-specific proteasomes. *Science* **316**, 1349–1353. <https://doi.org/10.1126/science.1141915>.
46. Honey, K., Nakagawa, T., Peters, C., and Rudensky, A. (2002). Cathepsin L regulates CD4+ T cell selection independently of its effect on invariant chain: a role in the generation of positively selecting peptide ligands. *J. Exp. Med.* **195**, 1349–1358.
47. Nowell, C.S., Bredenkamp, N., Tetélin, S., Jin, X., Tischner, C., Vaidya, H., Sheridan, J.M., Stenhouse, F.H., Heussen, R., Smith, A.J.H., and Blackburn, C.C. (2011). Foxn1 regulates lineage progression in cortical and medullary thymic epithelial cells but is dispensable for medullary sublineage divergence. *PLoS Genet.* **7**, e1002348. <https://doi.org/10.1371/journal.pgen.1002348>.
48. Liu, D., Kousa, A.I., O'Neill, K.E., Rouse, P., Popis, M., Farley, A.M., Tomlinson, S.R., Ulyanchenko, S., Guillemot, F., Seymour, P.A., et al. (2020). Canonical Notch signaling controls the early thymic epithelial progenitor cell state and emergence of the medullary epithelial lineage in fetal thymus development. *Development* **147**, dev178582. <https://doi.org/10.1242/dev.178582>.
49. Rodewald, H.R., Paul, S., Haller, C., Bluethmann, H., and Blum, C. (2001). Thymus medulla consisting of epithelial islets each derived from a single progenitor. *Nature* **414**, 763–768.
50. O'Neill, K.E., Bredenkamp, N., Tischner, C., Vaidya, H.J., Stenhouse, F.H., Peddie, C.D., Nowell, C.S., Gaskell, T., and Blackburn, C.C. (2016). Foxn1 Is Dynamically Regulated in Thymic Epithelial Cells during Embryogenesis and at the Onset of Thymic Involution. *PLoS One* **11**, e0151666. <https://doi.org/10.1371/journal.pone.0151666>.
51. McCarthy, N.I., Cowan, J.E., Nakamura, K., Bacon, A., Baik, S., White, A.J., Parnell, S.M., Jenkinson, E.J., Jenkinson, W.E., and Anderson, G. (2015). Osteoprotegerin-Mediated Homeostasis of Rank+ Thymic Epithelial Cells Does Not Limit Foxp3+ Regulatory T Cell Development. *J. Immunol.* **195**, 2675–2682. <https://doi.org/10.4049/jimmunol.1501226>.
52. Lucas, B., White, A.J., Parnell, S.M., Henley, P.M., Jenkinson, W.E., and Anderson, G. (2017). Progressive Changes in CXCR4 Expression That Define Thymocyte Positive Selection Are Dispensable For Both Innate and Conventional alphabetaT-cell Development. *Sci. Rep.* **7**, 5068. <https://doi.org/10.1038/s41598-017-05182-7>.

53. Han, J., and Zúñiga-Pflücker, J.C. (2021). High-Oxygen Submersion Fetal Thymus Organ Cultures Enable FOXN1-Dependent and -Independent Support of T Lymphopoiesis. *Front. Immunol.* **12**, 652665. <https://doi.org/10.3389/fimmu.2021.652665>.
54. Kernfeld, E.M., Genga, R.M.J., Neherin, K., Magaletta, M.E., Xu, P., and Maehr, R. (2018). A Single-Cell Transcriptomic Atlas of Thymus Organogenesis Resolves Cell Types and Developmental Maturation. *Immunity* **48**, 1258–1270.e6. <https://doi.org/10.1016/j.immuni.2018.04.015>.
55. Magaletta, M.E., Lobo, M., Kernfeld, E.M., Aliee, H., Huey, J.D., Parsons, T.J., Theis, F.J., and Maehr, R. (2022). Integration of single-cell transcriptomes and chromatin landscapes reveals regulatory programs driving pharyngeal organ development. *Nat. Commun.* **13**, 457. <https://doi.org/10.1038/s41467-022-28067-4>.
56. Bornstein, C., Nevo, S., Giladi, A., Kadouri, N., Pouzolles, M., Gerbe, F., David, E., Machado, A., Chuprin, A., Tóth, B., et al. (2018). Single-cell mapping of the thymic stroma identifies IL-25-producing tuft epithelial cells. *Nature* **559**, 622–626. <https://doi.org/10.1038/s41586-018-0346-1>.
57. Baran-Gale, J., Morgan, M.D., Maio, S., Dhalla, F., Calvo-Asensio, I., Deadman, M.E., Handel, A.E., Maynard, A., Chen, S., Green, F., et al. (2020). Ageing compromises mouse thymus function and remodels epithelial cell differentiation. *Elife* **9**, e56221. <https://doi.org/10.7554/eLife.56221>.
58. Miragaia, R.J., Zhang, X., Gomes, T., Svensson, V., Illic, T., Henriksson, J., Kar, G., and Lönnberg, T. (2018). Single-cell RNA-sequencing resolves self-antigen expression during mTEC development. *Sci. Rep.* **8**, 685. <https://doi.org/10.1038/s41598-017-19100-4>.
59. Dhalla, F., Baran-Gale, J., Maio, S., Chappell, L., Holländer, G.A., and Ponting, C.P. (2020). Biologically indeterminate yet ordered promiscuous gene expression in single medullary thymic epithelial cells. *EMBO J.* **39**, e101828. <https://doi.org/10.15252/embj.2019101828>.
60. Hikosaka, Y., Nitta, T., Ohigashi, I., Yano, K., Ishimaru, N., Hayashi, Y., Matsumoto, M., Matsuo, K., Penninger, J.M., Takayanagi, H., et al. (2008). The cytokine RANKL produced by positively selected thymocytes fosters medullary thymic epithelial cells that express autoimmune regulator. *Immunity* **29**, 438–450. <https://doi.org/10.1016/j.immuni.2008.06.018>.
61. Givony, T., Leshkowitz, D., Del Castillo, D., Nevo, S., Kadouri, N., Dassa, B., Gruper, Y., Khalaila, R., Ben-Nun, O., Gome, T., et al. (2023). Thymic mimetic cells function beyond self-tolerance. *Nature* **622**, 164–172. <https://doi.org/10.1038/s41586-023-06512-8>.
62. Zuklys, S., Handel, A., Zhanybekova, S., Govani, F., Keller, M., Maio, S., Mayer, C.E., Teh, H.Y., Hafen, K., Gallone, G., et al. (2016). Foxn1 regulates key target genes essential for T cell development in postnatal thymic epithelial cells. *Nat. Immunol.* **17**, 1206–1215. <https://doi.org/10.1038/ni.3537>.
63. Ashby, K.M., Vobořil, M., Salgado, O.C., Lee, S.T., Martinez, R.J., O'Connor, C.H., Breed, E.R., Xuan, S., Roll, C.R., Bachigari, S., et al. (2024). Sterile production of interferons in the thymus affects T cell repertoire selection. *Sci. Immunol.* **9**, eadp1139. <https://doi.org/10.1126/sciimmunol.adp1139>.
64. Martinez, R.J., and Hogquist, K.A. (2023). The role of interferon in the thymus. *Curr. Opin. Immunol.* **84**, 102389. <https://doi.org/10.1016/j.coi.2023.102389>.
65. Benhammadi, M., Mathé, J., Dumont-Lagacé, M., Kobayashi, K.S., Gabor, L., Brochu, S., and Perreault, C. (2020). IFN-lambda Enhances Constitutive Expression of MHC Class I Molecules on Thymic Epithelial Cells. *J. Immunol.* **205**, 1268–1280. <https://doi.org/10.4049/jimmunol.2000225>.
66. Farley, A.M., Chengrui, A., Palmer, S., Liu, D., Kousa, A.I., Rouse, P., Major, V., Sweetman, J., Morys, J., Corsinotti, A., et al. (2023). Thymic epithelial cell fate and potency in early organogenesis assessed by single cell transcriptional and functional analysis. *Front. Immunol.* **14**, 1202163. <https://doi.org/10.3389/fimmu.2023.1202163>.
67. Lucas, B., White, A.J., Klein, F., Veiga-Villauriz, C., Handel, A., Bacon, A., Cosway, E.J., James, K.D., Parnell, S.M., Ohigashi, I., et al. (2023). Embryonic keratin19(+) progenitors generate multiple functionally distinct progeny to maintain epithelial diversity in the adult thymus medulla. *Nat. Commun.* **14**, 2066. <https://doi.org/10.1038/s41467-023-37589-4>.
68. Kang, M., Armenteros, J.J.A., Gulati, G.S., Gleyzer, R., Avagyan, S., Brown, E.L., Zhang, W., Usmani, A., Earland, N., Wu, Z., et al. (2024). Mapping single-cell developmental potential in health and disease with interpretable deep learning. Preprint at bioRxiv. <https://doi.org/10.1101/2024.03.19.585637>.
69. Rossi, S.W., Kim, M.Y., Leibbrandt, A., Parnell, S.M., Jenkinson, W.E., Glanville, S.H., McConnell, F.M., Scott, H.S., Penninger, J.M., Jenkinson, E.J., et al. (2007). RANK signals from CD4(+)3(-) inducer cells regulate development of Aire-expressing epithelial cells in the thymic medulla. *J. Exp. Med.* **204**, 1267–1272. <https://doi.org/10.1084/jem.20062497>.
70. Zhao, Z., Chen, X., Dowbaj, A.M., Sljukic, A., Bratlie, K., Lin, L., Fong, E.L.S., Balachander, G.M., Chen, Z., Soragni, A., et al. (2022). Organoids. *Nat. Rev. Methods Primers* **2**, 94. <https://doi.org/10.1038/s43586-022-00174-y>.
71. Revest, J.M., Suniara, R.K., Kerr, K., Owen, J.J., and Dickson, C. (2001). Development of the thymus requires signaling through the fibroblast growth factor receptor R2-IIIb. *J. Immunol.* **167**, 1954–1961.
72. Anderson, G., Anderson, K.L., Tchilian, E.Z., Owen, J.J., and Jenkinson, E.J. (1997). Fibroblast dependency during early thymocyte development maps to the CD25+ CD44+ stage and involves interactions with fibroblast matrix molecules. *Eur. J. Immunol.* **27**, 1200–1206.
73. Anderson, G., Jenkinson, E.J., Moore, N.C., and Owen, J.J. (1993). MHC class II positive epithelium and mesenchyme cells are both required for T-cell development in the thymus. *Nature* **362**, 70–73.
74. Jenkinson, W.E., Rossi, S.W., Parnell, S.M., Jenkinson, E.J., and Anderson, G. (2007). PDGFRalpha-expressing mesenchyme regulates thymus growth and the availability of intrathymic niches. *Blood* **109**, 954–960. <https://doi.org/10.1182/blood-2006-05-023143>.
75. Griffith, A.V., Cardenas, K., Carter, C., Gordon, J., Iberg, A., Engleka, K., Epstein, J.A., Manley, N.R., and Richie, E.R. (2009). Increased thymus- and decreased parathyroid-fated organ domains in *Sp1* mutant embryos. *Dev. Biol.* **327**, 216–227. <https://doi.org/10.1016/j.ydbio.2008.12.019>.
76. Gordon, J., Wilson, V.A., Blair, N.F., Sheridan, J., Farley, A., Wilson, L., Manley, N.R., and Blackburn, C.C. (2004). Functional evidence for a single endodermal origin for the thymic epithelium. *Nat. Immunol.* **5**, 546–553. <https://doi.org/10.1038/ni1064>.
77. Auerbach, R. (1960). Morphogenetic interactions in the development of the mouse thymus gland. *Dev. Biol.* **2**, 271–284.
78. Colantonio, A.D., Epeldegui, M., Jesiak, M., Jachimowski, L., Blom, B., and Uittenbogaart, C.H. (2011). IFN-alpha is constitutively expressed in the human thymus, but not in peripheral lymphoid organs. *PLoS One* **6**, e24252. <https://doi.org/10.1371/journal.pone.0024252>.
79. You, Y., Dunst, J., Ye, K., Sandoz, P.A., Reinhardt, A., Sandrock, I., Comet, N.R., Sarkar, R.D., Yang, E., Duprez, E., et al. (2024). Direct presentation of inflammation-associated self-antigens by thymic innate-like T cells induces elimination of autoreactive CD8(+) thymocytes. *Nat. Immunol.* **25**, 1367–1382. <https://doi.org/10.1038/s41590-024-01899-6>.
80. Wong, Y.F., Kumar, Y., Proks, M., Herrera, J.A.R., Rothová, M.M., Monteiro, R.S., Pozzi, S., Jennings, R.E., Hanley, N.A., Bickmore, W.A., and Brickman, J.M. (2023). Expansion of ventral foregut is linked to changes in the enhancer landscape for organ-specific differentiation. *Nat. Cell Biol.* **25**, 481–492. <https://doi.org/10.1038/s41556-022-01075-8>.
81. Perera, M., Nissen, S.B., Proks, M., Pozzi, S., Monteiro, R.S., Trusina, A., and Brickman, J.M. (2022). Transcriptional heterogeneity and cell cycle regulation as central determinants of Primitive Endoderm priming. *Elife* **11**, e78967. <https://doi.org/10.7554/eLife.78967>.
82. Lobov, I.B., Renard, R.A., Papadopoulos, N., Gale, N.W., Thurston, G., Yancopoulos, G.D., and Wiegand, S.J. (2007). Delta-like ligand 4 (Dll4) is induced by VEGF as a negative regulator of angiogenic sprouting. *Proc.*



- Natl. Acad. Sci. USA 104, 3219–3224. <https://doi.org/10.1073/pnas.0611206104>.
83. Wang, Z., McWilliams-Koeppen, H.P., Reza, H., Ostberg, J.R., Chen, W., Wang, X., Huynh, C., Vyas, V., Chang, W.C., Starr, R., et al. (2022). 3D-organoid culture supports differentiation of human CAR(+) iPSCs into highly functional CAR T cells. *Cell Stem Cell* 29, 651–653. <https://doi.org/10.1016/j.stem.2022.03.007>.
  84. Frenz-Wiessner, S., Fairley, S.D., Buser, M., Goek, I., Salewskij, K., Jonsson, G., Illig, D., Zu Putlitz, B., Petersheim, D., Li, Y., et al. (2024). Generation of complex bone marrow organoids from human induced pluripotent stem cells. *Nat. Methods* 21, 868–881. <https://doi.org/10.1038/s41592-024-02172-2>.
  85. Sheridan, J.M., Taoudi, S., Medvinsky, A., and Blackburn, C.C. (2009). A novel method for the generation of reaggregated organotypic cultures that permits juxtaposition of defined cell populations. *Genesis* 47, 346–351.
  86. Schneider, C.A., Rasband, W.S., and Eliceiri, K.W. (2012). NIH Image to ImageJ: 25 years of image analysis. *Nat. Methods* 9, 671–675. <https://doi.org/10.1038/nmeth.2089>.
  87. Zheng, G.X.Y., Terry, J.M., Belgrader, P., Ryvkin, P., Bent, Z.W., Wilson, R., Ziraldo, S.B., Wheeler, T.D., McDermott, G.P., Zhu, J., et al. (2017). Massively parallel digital transcriptional profiling of single cells. *Nat. Commun.* 8, 14049. <https://doi.org/10.1038/ncomms14049>.
  88. Hao, Y., Stuart, T., Kowalski, M.H., Choudhary, S., Hoffman, P., Hartman, A., Srivastava, A., Molla, G., Madad, S., Fernandez-Granda, C., and Satija, R. (2024). Dictionary learning for integrative, multimodal and scalable single-cell analysis. *Nat. Biotechnol.* 42, 293–304. <https://doi.org/10.1038/s41587-023-01767-y>.
  89. Li, J., Xue, F., and Blu, T. (2017). Fast and accurate three-dimensional point spread function computation for fluorescence microscopy. *J. Opt. Soc. Am. Opt Image Sci. Vis.* 34, 1029–1034. <https://doi.org/10.1364/JOSAA.34.001029>.
  90. Ronneberger, O., Fischer, P., and Brox, T. (2015). U-Net: Convolutional Networks for Biomedical Image Segmentation. In *Medical Image Computing and Computer-Assisted Intervention – MICCAI 2015*, J.H.N. Navab, W. Wells, and A. Frangi, eds. (Springer), Lecture Notes in Computer Science. [https://doi.org/10.1007/978-3-319-24574-4\\_28](https://doi.org/10.1007/978-3-319-24574-4_28).
  91. Shirshin, E.A., Shirmanova, M.V., Gayer, A.V., Lukina, M.M., Nikonova, E.E., Yakimov, B.P., Budylin, G.S., Dudenkova, V.V., Ignatova, N.I., Komarov, D.V., et al. (2022). Label-free sensing of cells with fluorescence lifetime imaging: The quest for metabolic heterogeneity. *Proc. Natl. Acad. Sci. USA* 119, e2118241119. <https://doi.org/10.1073/pnas.2118241119>.



## STAR★METHODS

### KEY RESOURCES TABLE

REAGENT or RESOURCE	SOURCE	IDENTIFIER
<b>Antibodies</b>		
HOECHST	Life Technologies	Cat#: 62249
b5t (rabbit)	MBL	Cat#: PD021; RRID:AB_2171885
PDGFR $\alpha$ APC	BioLegend	Cat#: 135908; RRID:AB_2043970
PDGFR $\beta$ APC	BioLegend	Cat#: 136007; RRID:AB_2043971
TER119 PE	BioLegend	Cat#: 116208; RRID:AB_313709
TER-119 FITC	Thermo Fisher	Cat#: 11-5921-85; RRID:AB_465312
CD3 $\epsilon$ BV785	BioLegend	Cat#: 100355; RRID:AB_2565969
CD4 PE	BioLegend	Cat#: 100512; RRID:AB_312715
CD5 FITC	BioLegend	Cat#: 100605; RRID:AB_312734
CD8 $\alpha$ (53-6.7) APC	eBioscience	Cat#: 17-0081-82
CD11b FITC	BioLegend	Cat#: 101205; RRID:AB_312788
CD11c FITC	BioLegend	Cat#: 117305; RRID:AB_313774
CD19 FITC	BioLegend	Cat#: 152403; RRID:AB_2629812
CD31 PE/Cy7	BioLegend	Cat#: 102523; RRID:AB_2572181
CD45 APC/eFluor780	eBioscience	Cat#: 47-0451-82; RRID:AB_1548781
CD45 (rat)	TONBO bioscience	Cat#: 70-0451-U100; RRID:AB_2621495
CD45R/B220 FITC	BioLegend	Cat#: 103206; RRID:AB_312991
CD69 BV421	BioLegend	Cat#: 104528; RRID:AB_2562328
CD117 (cKit) PE/Cy7	BioLegend	Cat#: 105813; RRID:AB_313222
CD135 (Flt3) APC	BioLegend	Cat#: 135310; RRID:AB_2107050
CD205 (mouse)	Bio-Rad	Cat#: MCA949; RRID:AB_322018
DAPI	Life Technologies	D1306
DLL4 (Armenian Hamster)	BioLegend	Cat#: 130802; RRID:AB_1227639
EpCAM FITC	BioLegend	Cat#: 118208; RRID:AB_1134107
F4/80 FITC	BioLegend	Cat#: 123108; RRID:AB_893502
Gr1 FITC	BioLegend	Cat#: 108405; RRID:AB_313370
K8 (rabbit)	Abcam	Cat#: ab53280; RRID:AB_869901
K14 (chicken)	BioLegend	Cat#: 906004; RRID:AB_2616962
MHC1 (H-2k) BV510	BioLegend	Cat#: 116523; RRID:AB_2800584
MHCI (mouse)	BD Bioscience	Cat#: 550550; RRID:AB_393744
MHCII (rat)	Abcam	Cat#: ab15630; RRID:AB_302007
NK1.1 FITC	BD Biosciences	Cat#: 553164; RRID:AB_394676
Sca-1 PE	BioLegend	Cat#: 108107; RRID:AB_313344
TCR $\beta$ chain PE/Cy7	BioLegend	Cat#: 109222; RRID:AB_893625
$\gamma/\delta$ TCR BV605	BioLegend	Cat#: 118124; RRID:AB_11204423
Vimentin (rabbit)	Abcam	Cat#: ab92547; RRID:AB_10562134
Alexa Fluor 488 (rabbit)	Molecular Probes	Cat#: A-11008; RRID:AB_143165
Alexa Fluor 568 (rabbit)	Molecular Probes	Cat#: A-11011; RRID:AB_143157
Alexa Fluor 568 (mouse)	Molecular Probes	Cat#: A11004; RRID:AB_2534072
Alexa Fluor 568 (chicken)	vWR	Cat#: 20104-1
Alexa Fluor 647 (rabbit)	Molecular Probes	Cat#: A-21245; RRID:AB_2535813
Alexa Fluor 647 (rat)	Molecular Probes	Cat#: A-21247; RRID:AB_141778
Alexa Fluor 647 (Armenian hamster)	Abcam	Cat#: ab173004; RRID:AB_2732023

(Continued on next page)

**Continued**

REAGENT or RESOURCE	SOURCE	IDENTIFIER
<b>Chemicals, peptides, and recombinant proteins</b>		
7AAD	BioLegend	Cat#: 420403
Recombinant Murine sRANK Ligand (CHO derived)	Peptotech	Cat#: 315-11C
<b>Critical commercial assays</b>		
Chromium Next GEM single cell reagent kit 3' V3.1 (dual index) with Feature Barcoding technology for Cell Multiplexing	10x Genomics	Cat#: CG000388
<b>Deposited data</b>		
Watchbreaker scRNAseq dataset	This paper	NCBI SRA: <a href="https://dataview.ncbi.nlm.nih.gov/object/PRJNA1078142?reviewer=o5lue3b36gm6d3vla92lp45s7q">https://dataview.ncbi.nlm.nih.gov/object/PRJNA1078142?reviewer=o5lue3b36gm6d3vla92lp45s7q</a>
Codes for analyses in <a href="#">Figures 4, 5, and 6</a> and <a href="#">Supplemental Information</a>	This paper	Zenodo: <a href="https://doi.org/10.5281/zenodo.14781551">https://doi.org/10.5281/zenodo.14781551</a> and <a href="https://doi.org/10.5281/zenodo.14779427">https://doi.org/10.5281/zenodo.14779427</a> .
<b>Experimental models: Organisms/strains</b>		
Mouse: B6J: Jax Mouse strain C57BL/6m	Charles River	Cat#642
Mouse: Foxn1 <sup>GFP</sup> : B6JCrI;129-Foxn1 <sup>GFP+/-</sup>	O'Neill et al. <sup>50</sup>	N/A
Mouse: Rank-Venus: B6;FVB-Tg(Tnfrsf11a-Venus)	McCarthy et al. <sup>51</sup>	N/A
Mouse: Cxcl12-dsRED: STOCK-Cxcl12tm2.1Sjm/J	The Jackson Laboratory	RRID:IMSR_JAX:022458
<b>Oligonucleotides</b>		
Primers used for genotyping transgenic mice, see <a href="#">Table S1</a>	This paper	N/A
<b>Software and algorithms</b>		
ImageJ v1.53c	Schneider et al. <sup>86</sup>	<a href="https://imagej.net/downloads">https://imagej.net/downloads</a>
Cell Ranger	10x Genomics	Zheng et al. <sup>87</sup>
SEURAT	Hao et al. <sup>88</sup>	<a href="https://satijalab.org/seurat/">https://satijalab.org/seurat/</a>
FCSEXPRESS	De Novo Software	<a href="https://denovosoftware.com">https://denovosoftware.com</a>
PRISM 10	Graphpad	<a href="http://www.graphpad.com">www.graphpad.com</a>
Python 3.11.5	python.org	<a href="https://www.python.org/downloads/">https://www.python.org/downloads/</a>
NumPy 1.25.0	numpy.org	<a href="https://pypi.org/project/numpy/1.25.0/">https://pypi.org/project/numpy/1.25.0/</a>
scikit-image 0.22.0	scikit-image.org	<a href="https://pypi.org/project/scikit-image/0.22.0/">https://pypi.org/project/scikit-image/0.22.0/</a>
Pytorch 2.2.0	pytorch.org	<a href="https://pytorch.org/">https://pytorch.org/</a>
Scipy 1.11.3	scipy.org	<a href="https://pypi.org/project/scipy/1.11.3/">https://pypi.org/project/scipy/1.11.3/</a>
Matplotlib 3.8.0	matplotlib.org	<a href="https://pypi.org/project/matplotlib/3.8.0/">https://pypi.org/project/matplotlib/3.8.0/</a>
H5py 3.9.0	h5py.org	<a href="https://pypi.org/project/h5py/3.9.0/">https://pypi.org/project/h5py/3.9.0/</a>
Numba 0.58.0	numba.pydata.org	<a href="https://pypi.org/project/numba/0.58.0/">https://pypi.org/project/numba/0.58.0/</a>
MicroscPSF-Py	N/A	<a href="https://github.com/MicroscPSF/MicroscPSF-Py">https://github.com/MicroscPSF/MicroscPSF-Py</a>
CUDA Toolkit 12.1	developer.nvidia.com	<a href="https://developer.nvidia.com/cuda-12-1-0-download-archive">https://developer.nvidia.com/cuda-12-1-0-download-archive</a>
cuDNN 8.8.1	developer.nvidia.com	<a href="https://developer.nvidia.com/rdp/cudnn-archive">https://developer.nvidia.com/rdp/cudnn-archive</a>

**EXPERIMENTAL MODEL AND STUDY PARTICIPANT DETAILS**

**Mice:** Foxn1<sup>GFP</sup><sup>50</sup>, Rank-Venus<sup>51</sup> and Cxcl12<sup>dsRed</sup><sup>12</sup> mice were as described. C57BL/6J(CrI) mice were used for isolation of fetal thymic cells except where otherwise specified. All animals were housed and bred in University of Edinburgh animal facilities. All experiments using animals were conformed to the regulatory standards set out in the Home Office Animals (Scientific Procedures) Act 1986, and conducted under project license PEEC9E359 to V. Wilson which was approved by the UK Home Office. Primers used for genotyping were as shown in [Table S1](#). For timed matings, noon of the day of the vaginal plug was taken as day 0.5. All controls were littermates unless otherwise stated.

## METHOD DETAILS

### Thymus dissociation

Microdissected fetal thymi were dissociated for 5 minutes in TrypLE Express Enzyme (Life Technologies 12604013) in an Eppendorf Thermomixer (1400 rpm, 37°C) followed by trituration with a 25G syringe ten times. Cell suspensions at 4°C were washed in 2% FCS FACS buffer, resuspended as required and filtered through a 70µm cell strainer (Corning) to remove clumps.

### Tissue culture

mTO, RTOC and FTOC were cultured in Advanced DMEM/F12 (Life Technologies, 12634010), 2% FCS (Life Technologies), 1% penicillin (10,000 units/ml)/streptomycin (10,000 µg/ml) (Invitrogen, 15140-122), 1% GlutaMax supplement (Life Technologies, 35050061), 1% non-essential amino acids (NEAA) (Invitrogen, 11140-036) (referred as 2% media herein). All cell manipulations were performed in a laminar flow sterile hood using sterile technique. Cell culture plastic ware was supplied by Iwaki. All solutions were tested for sterility and warmed to 37°C prior to use. Cells were examined using an inverted microscope (Olympus CK2).

### Generation of mTO

The required cell populations were obtained by dissociation of E14.5 fetal thymi followed by flow cytometric cell sorting if required (TEC, DAPI<sup>+</sup>TER119<sup>+</sup>CD45<sup>+</sup>EpCAM<sup>+</sup>; double negative thymocytes [DNs], DAPI<sup>+</sup>Lin<sup>+</sup>CD45<sup>+</sup>EpCAM<sup>+</sup>; FTM, DAPI<sup>+</sup>TER119<sup>+</sup>CD45<sup>+</sup>EpCAM<sup>+</sup>PDGFRαβ<sup>+</sup>; endothelial cells [ECs], DAPI<sup>+</sup>TER119<sup>+</sup>CD45<sup>+</sup>EpCAM<sup>+</sup>PDGFRαβ<sup>+</sup>CD31<sup>+</sup>; see [Figure S1](#)), pelleted, resuspended in 2% media and counted using the BioRad Cell Counter with the addition of Trypan Blue. Based on the cell counts, an appropriate volume from each population were pipetted into each well one-by-one or after prior mixing. Separate suspensions were created for each experimental condition. A maximum of 40µl per 96 well was gently dropped into the Gri3D® 96well plates (SunBioscience, Gri3D-96-S-8P) and left to reaggregate for 15 minutes, after which the wells were filled with medium to a total volume of 200µl. Medium was refreshed every other day using the reservoir well attached to each well. Recombinant Murine sRANK Ligand (CHO derived; Peprotech 315-11C) was added to the culture medium only when indicated. mTOs were cultured from 7 to 14 days depending on the experiment.

### FTOC and RFTOC

were generated as previously described.<sup>85</sup> The compacted cell pellets were extruded at the liquid-gas interface onto a polycarbonate filter paper raft floating on 1ml of medium in 24 well plates and cultured for 7 days. Medium was refreshed every other day. For FTOC, each whole intact lobe was placed on a filter membrane with the help of a microscope and cultured for 7 days as above.

### Flow cytometry

Cells were processed for flow cytometric sorting and analysis as previously described.<sup>32,47</sup> Compensation controls were performed using beads. Sorting and analysis gates were set using FMOs. Sorting was performed using a BD FACS Aria II running FACS Diva 4.1 (BD Biosciences). FACS analyses were performed on a FACSCalibur (BD Bioscience) or Novocyte running NovoExpress 1.3.0 (ACEA) at the CRM, University of Edinburgh. All post-acquisition analysis was performed with FCSexpress 7 (De Novo Software) software.

### Immunohistochemistry

All fixation and staining steps were carried out in the imaging bottom Gri3D® plates (Sun Bioscience, Gri3D-96IBI-S-8-800) such that the mTOs were kept intact. mTOs were washed (3x10 minutes) with PBS to remove excess medium, fixed in 4% PFA (Fisher Scientific UK Ltd, 15670799) for 20 minutes at room temperature (RT) while shaking slowly, and washed with 0.1% Triton (VWR, X100-100ML) in PBS/0.2% Sodium Azide (PBST). For the preparation of sections, mTOs were stained for HOECHST (1:1000) for 15 minutes at room temperature. mTOs were then embedded in 2% agarose, by incubating for 5 minutes at 65°C with the concentration gradually increasing from 0.125% to 2% in five incubation steps, then left to solidify and scooped out of the 96well in one piece. Further submersion in 2% agarose allowed preparation of 200µm Vibratome sections (Leica VT1000 S Vibrating blade microtome). mTOs (or sections) were then blocked in 10% goat serum in PBST for 4-6 hours at RT, incubated in primary antibody solution (optimized concentration in 1% goat serum in PBST) for up to 48h at RT, washed in PBST (3x15 minutes), incubated in secondary antibodies (optimized concentrations in 1% goat serum in PBS only) and HOECHST (1:1000) for 8-24h at RT, then washed in PBS (3x15 minutes). In the case of a dim HOECHST signal, another 1:1000 dilution was applied. 70µl RapiClear 1.49 ([www.sunjinlab.com](http://www.sunjinlab.com), RC149001) was then added to each well at least 15 minutes before imaging. For live imaging, mTOs were kept in the Gri3D® plates and imaged using the Opera Phenix® Plus High-Content Screening System in 5% CO<sub>2</sub> at 37°C. Fixed and stained mTOs were imaged similarly.

### Antibodies

The antibodies used for immunohistochemistry and flow cytometry were as listed in [Table S2](#).

### Image analysis

All post-acquisition analysis was performed using Image Artist software or ImageJ v1.53c.<sup>86</sup> For the segmented image in Figure 4C, the images presented were blind deconvolved using the Richardson-Lucy algorithm. Initial PSF guess was computed using Gibson–Lanni model (<https://github.com/MicroscPSF/MicroscPSF-Py>).<sup>89</sup> Cells were segmented using an automated algorithm based on U-Net neural network architecture.<sup>90</sup> This network predicted two channels, namely binary mask of nuclei and distance to the cell edge. The Watershed algorithm was used to segment the binary mask into individual nuclei using predicted distance as energy.<sup>91</sup> The images fed to the neural network were not deconvolved and were normalized to the range [0,1]. Deconvolved images were used for measurement of mean intensities for individual cells. Values were expressed as median values withing a segmented mask of each cell.

### Single cell RNA-seq

#### Processing of samples for library preparation, library preparation and sequencing

Cells from each condition were resuspended in 90μl FACS buffer (PBS without Ca<sup>2+</sup> and Mg<sup>2+</sup>, with 2% FCS), 0.45μl FC block was then added and incubated for 10 minutes on ice. Each condition was incubated with barcode tagged antibodies against MHCII, CD40, CD80 and EpCAM, with biotinylated UEA1, and with α-CD45-magnetic beads (Table S3) for 15 minutes on ice, then washed once with 1ml FACS buffer and centrifuged at 500rcf for 5 minutes. Each condition was hashed with 100μl lipid anchored Cell Multiplexing Oligos for sample multiplexing (CMOs, 10x Genomics)(see Figure S6). Samples were then passed through LS Columns to deplete CD45<sup>+</sup> cells according to the manufacturer's instructions. Cells eluted from the column were spun down and resuspended in 50μl FACS buffer, of which 10μl was taken for cell counting. Approximately 1-5000 cells were pooled from each condition, and were then filtered and loaded on a Chip G (10X Genomics). Cell-bead encapsulation was performed using the Chromium X (10x Genomics). Gene expression and multiplexing libraries were prepared following the manufacturer's instructions using the Chromium Next GEM single cell reagent kit 3' V3.1 (dual index) with Feature Barcoding technology for Cell Multiplexing (CG000388, 10x Genomics). Libraries were quantified using a Bioanalyzer DNA High-sensitivity Kit (Agilent Technologies), pooled at a molar ratio of 10:1 between gene expression and multiplexing libraries, and sequenced on an Illumina NextSeq 2000 P3 flow cell (100 cycles configuration) to obtain approximately 1.4B paired-end reads.

#### QC and analysis

FASTQ files were processed using Cell Ranger<sup>87</sup> (10x Genomics) and count matrices (for RNAseq, CITEseq and CMO multiplexing) were analyzed using the R package Seurat.<sup>88</sup> Deconvolution of the CMO tags revealed multiplets (318), where tags were shared between cells. These, plus unassigned (360) and blank (122) reads, were excluded from further analysis. The remaining captured cells were filtered such that only cells with >2000 RNA features were retained for downstream analysis. Normalisation was carried out using the Seurat function SCTransform with regression on mitochondrial gene transcript percentages. After initial clustering, a cluster with high levels of stress markers (*Ddit3* and *Herpud1*) was identified and excluded from further analysis. GO enrichment analysis was performed in R with the enrichR package, using the "GO\_Biological\_Process\_2021" database. The Seurat function *DEEnrichRPlot* was used with "max.genes=1000". DE gene analysis was carried out in R using the Seurat function *FindMarkers* with default settings.

## QUANTIFICATION AND STATISTICAL ANALYSIS

### Statistics and experimental design

For all analysis, statistical details can be found in the figure, the figure legend or the associated text, including the statistical tests used, exact value of n, what n represents (e.g., number of animals, number of cells, etc.), definition of centre, and dispersion and precision measures (e.g., mean, median, SD, SEM, confidence intervals). For all scRNAseq analyses, n represents the number of independent biological experiments. For all other experiments, n represents an independent biological replicate. At least three biologically independent replicates were performed for each condition with the exception of the antibody staining where n=1 in some cases. No statistical method was used to predetermine sample size, the experiments were not randomized, and the investigators were not blinded to allocation during experiments and outcome assessment. There were no limitations to repeatability of the experiments. No samples were excluded from the analysis.

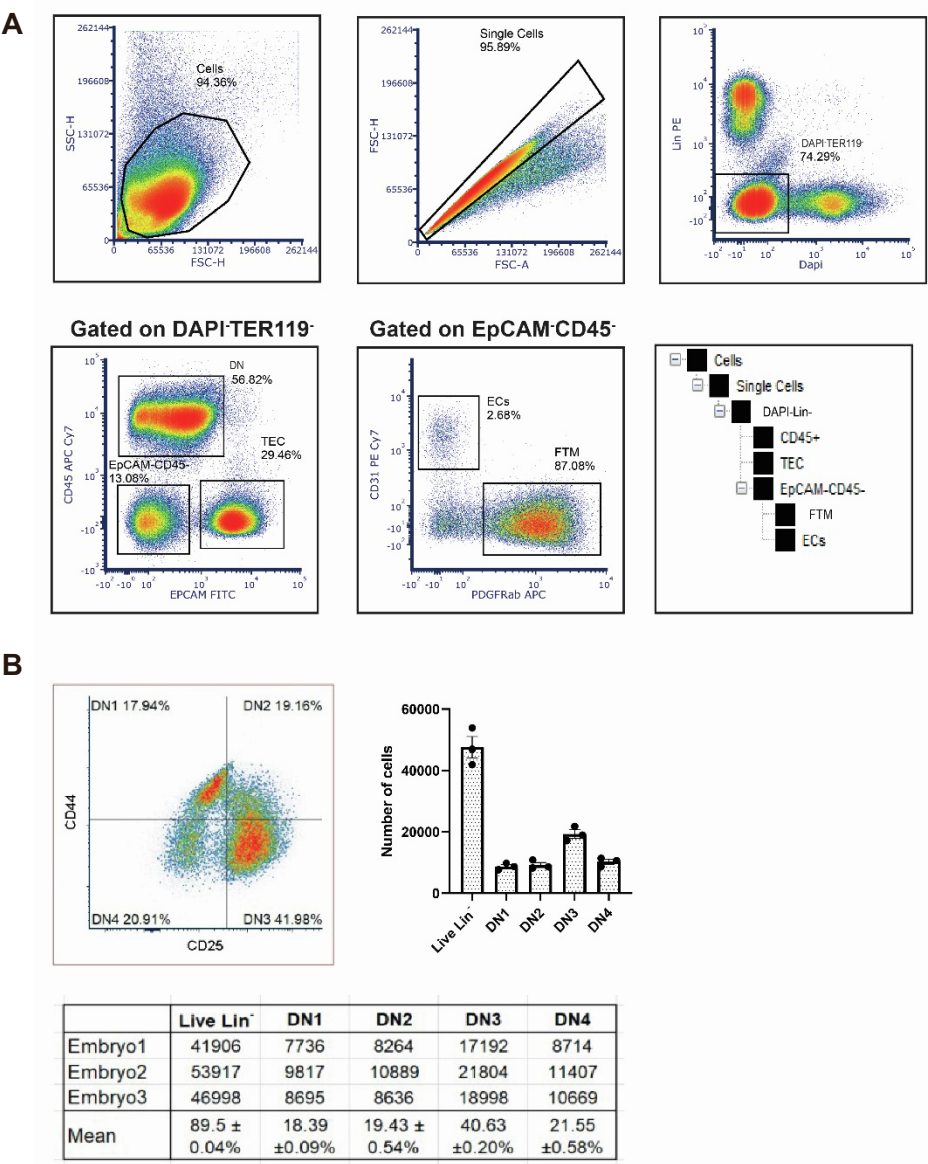
**Supplemental information**

**Establishment of a microwell-array-based  
miniaturized thymic organoid model  
suitable for high-throughput applications**

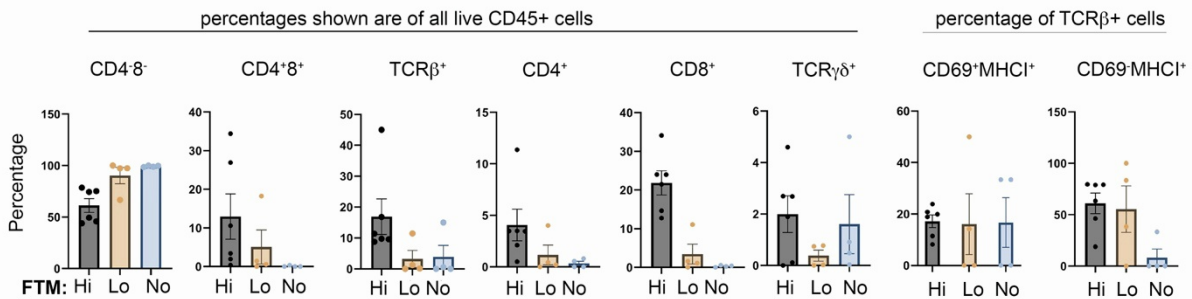
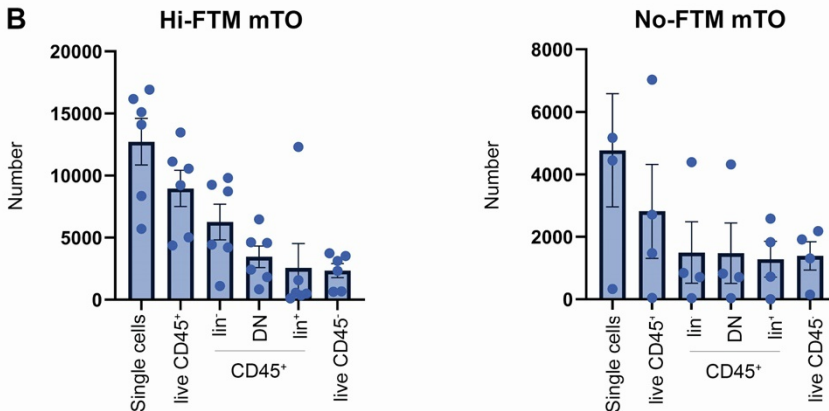
**Viktoria Major, Sam Palmer, Paul Rouse, Jan Morys, Timothy Henderson, Tania Hübscher, Joanna Sweetman, Andrea Bacon, Chengrui An, Qiu Guiyun, Yu Wang, Andrea Corsinotti, Justyna Cholewa-Waclaw, S. Jon Chapman, Matthias P. Lütolf, Graham Anderson, and C. Clare Blackburn**



Supplemental Figures

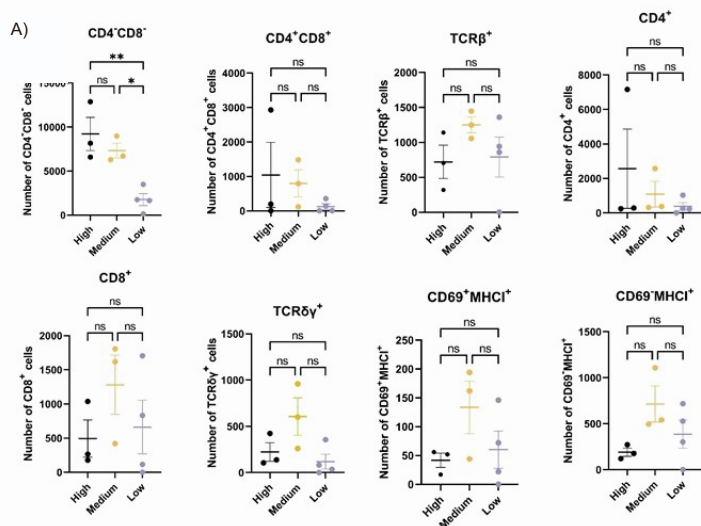


**Figure S1. Cellular composition of the E14.5 thymus.** A) Plots show gating strategy for isolating TEC, DN thymocytes, FTM and ECs from E14.5 thymic lobes. TEC were sorted from single cells as DAPI-TER119<sup>-</sup>CD45<sup>-</sup>EpCAM<sup>+</sup> cells, DNs as DAPI-Lin<sup>-</sup>CD45<sup>+</sup>EpCAM<sup>-</sup> cell, FTM as DAPI-TER119<sup>-</sup>CD45<sup>-</sup>EpCAM<sup>+</sup>PDGFRα<sup>+</sup> cells and ECs as DAPI-TER119<sup>-</sup>CD45<sup>-</sup>EpCAM<sup>+</sup>PDGFRα<sup>+</sup>CD31<sup>+</sup> cells. B) Representative plot showing the CD44 versus CD25 subset profile, absolute cell numbers and percentages for E14.5 DAPI-Lin<sup>-</sup>CD45<sup>+</sup> cells. Lin = α-CD4, α-CD8, α-CD11b, α-CD11c, Gr1, NK1.1, B220, TER-119, α-EpCAM.

**A**Input:  $1 \times 10^5$  TEC;  $5 \times 10^4$  DN; FTM as shown**B****C**

		Events							Cell percentages						
		Cells	Single cells	Live CD45 <sup>+</sup>	Lin <sup>-</sup>	DN	Lin <sup>+</sup>	Live CD45 <sup>-</sup>	Cells	Single cells	Live CD45 <sup>+</sup>	Lin <sup>-</sup>	DN	Lin <sup>+</sup>	Live CD45 <sup>-</sup>
No FTM	Rep 1.2020	618	328	44	39	37	5	148	7.89	53.07	13.41	88.64	94.87	11.36	45.12
	Rep 2.2020	12946	9155	7029	4397	4320	2581	1309	44.15	70.72	76.78	62.56	98.25	36.72	14.3
	Rep 4.2020	7711	4448	1476	710	709	723	2180	30.14	57.68	33.18	48.1	99.86	48.98	49.01
	Rep 5.2020	7658	5173	2713	843	824	1828	1916	9.36	67.55	52.45	31.07	97.75	67.38	37.04
Hi FTM	Rep 1.2020	6662	5700	4382	4203	1821	112	671	19.54	85.56	76.88	95.92	43.33	2.56	11.77
	Rep 2.2020	35629	16926	13476	1106	838	12305	645	60.88	47.51	79.62	8.21	75.77	91.31	3.81
	Rep 2.2020	16981	14111	9221	8731	6483	341	3119	30.99	83.1	65.35	94.69	74.25	3.7	22.1
	Rep 4.2020	18480	15106	10559	9812	4627	563	3524	44.31	81.74	69.9	92.93	47.16	5.33	23.33
	Rep 5.2020	10797	8359	5029	4441	2429	498	2330	10.8	77.42	60.16	88.31	54.69	9.9	27.87
	Rep 5.2020	21383	16177	11117	9262	4574	1570	3737	21.38	75.65	68.72	83.31	49.38	14.12	23.1

**Figure S2. Effect of FTM on mTO outputs.** mTO were established from E14.5 thymi using the following input conditions: Hi FTM ( $1 \times 10^5$  TEC,  $5 \times 10^4$  DN,  $4 \times 10^4$  FTM), Lo FTM ( $1 \times 10^5$  TEC,  $5 \times 10^4$  DN,  $1.5 \times 10^4$  FTM) and No FTM ( $1 \times 10^5$  TEC,  $5 \times 10^4$  DN, 0 FTM) and were cultured for 14 days before analysis of thymocyte populations shown. (A) Plots show mean  $\pm$  SEM of percentage for each subset. Each data point represents the cells harvested from one microwell. Percentages shown are after gating on the populations indicated. N = at least 4 independent biological replicates. DN (CD4<sup>-</sup>CD8<sup>-</sup>), DP (CD4<sup>+</sup>CD8<sup>+</sup>), (CD3 $\epsilon$ <sup>+</sup>TCR $\beta$ <sup>+</sup>), SP4 (CD4<sup>+</sup>), SP8 (CD8<sup>+</sup>), CD69<sup>+</sup>MHCII<sup>+</sup>, CD69-MHCII<sup>+</sup>,  $\gamma\delta$  T cells (CD3 $\epsilon$ <sup>+</sup>TCR $\gamma\delta$ <sup>+</sup>). (B, C) Plots (B) and Table (C) show number of cells in each of the populations shown. Lin = CD11b, CD11c, Gr-1, Nk1.1, B220, EpCAM and Ter119. In No-FTM mTO data, live CD45<sup>-</sup> cells are TEC; in Hi-FTM mTO data, live CD45<sup>-</sup> cells are TEC and FTM.



B)

	Single cells	Live CD45 <sup>+</sup> Lin <sup>-</sup>	TCRβ <sup>+</sup>	CD69 <sup>+</sup> MHCI <sup>+</sup>	CD69 <sup>+</sup> MHCI <sup>-</sup>	TCRγδ <sup>+</sup>	SP4 (CD4 <sup>+</sup> )	DP	SP8 (CD8 <sup>+</sup> )	DN
High number	73.7 ± 27%	76.4 ± 4.9%	5.3 ± 1%	5.9 ± 1%	32.2 ± 11.8%	1.6 ± 0.5%	17 ± 14.3%	6.1 ± 5.5%	3.4 ± 1.35%	73.6 ± 12%
Medium number	78.1 ± 5.2%	77.5 ± 3.15	12 ± 1.4%	10 ± 3.3%	54.2 ± 9%	5.8 ± 2.1%	11.3 ± 8.1%	7.1 ± 3.1%	12.1 ± 4.1%	70 ± 1.6%
Low number	73.8 ± 14.4%	68.2 ± 13.5%	21.6 ± 7.5%	5.4 ± 2.5%	36 ± 12.9%	2.5 ± 1.3%	12.2 ± 8.4%	2.8 ± 1.6%	15.4 ± 7.8%	69.71 ± 10%

**Figure S3. Effect of total cell number on mTO outputs.** mTO were established using the same ratio but different absolute numbers of input cells per well (1.5, 1 or 0.5 x the Hi FTM condition numbers) and were cultured for 14 days before analysis of thymocyte development for the subsets shown. A) Graphs show mean ± SEM of absolute cell numbers recovered per well for the input populations. N=3 independent biological replicates, one with two technical replicates for the Low proportion condition. B) Table shows cell mean ± SEM of percentages of parent gates of defined thymocyte subsets present in High, Medium, Low input number mTOs. All data shown cell numbers after gating on live CD45<sup>+</sup> cells except the CD69<sup>+</sup>MHCI<sup>+</sup> and CD69<sup>+</sup>MHCI<sup>-</sup> populations which are gated on TCRβ<sup>+</sup> cells. Statistical analysis was one-way ANOVA or Kruskal-Wallis rank test based on Shapiro-Wilk normality test. ns not significant; p > 0.05. DN (CD4<sup>+</sup>CD8<sup>-</sup>), DP (CD4<sup>+</sup>CD8<sup>+</sup>), (CD3ε<sup>+</sup>TCRβ<sup>+</sup>), SP4 (CD4<sup>+</sup>), SP8 (CD8<sup>+</sup>), CD69<sup>+</sup>MHCI<sup>+</sup>, CD69<sup>+</sup>MHCI<sup>-</sup>, γδ T cells (CD3ε<sup>+</sup>TCRγδ<sup>+</sup>).

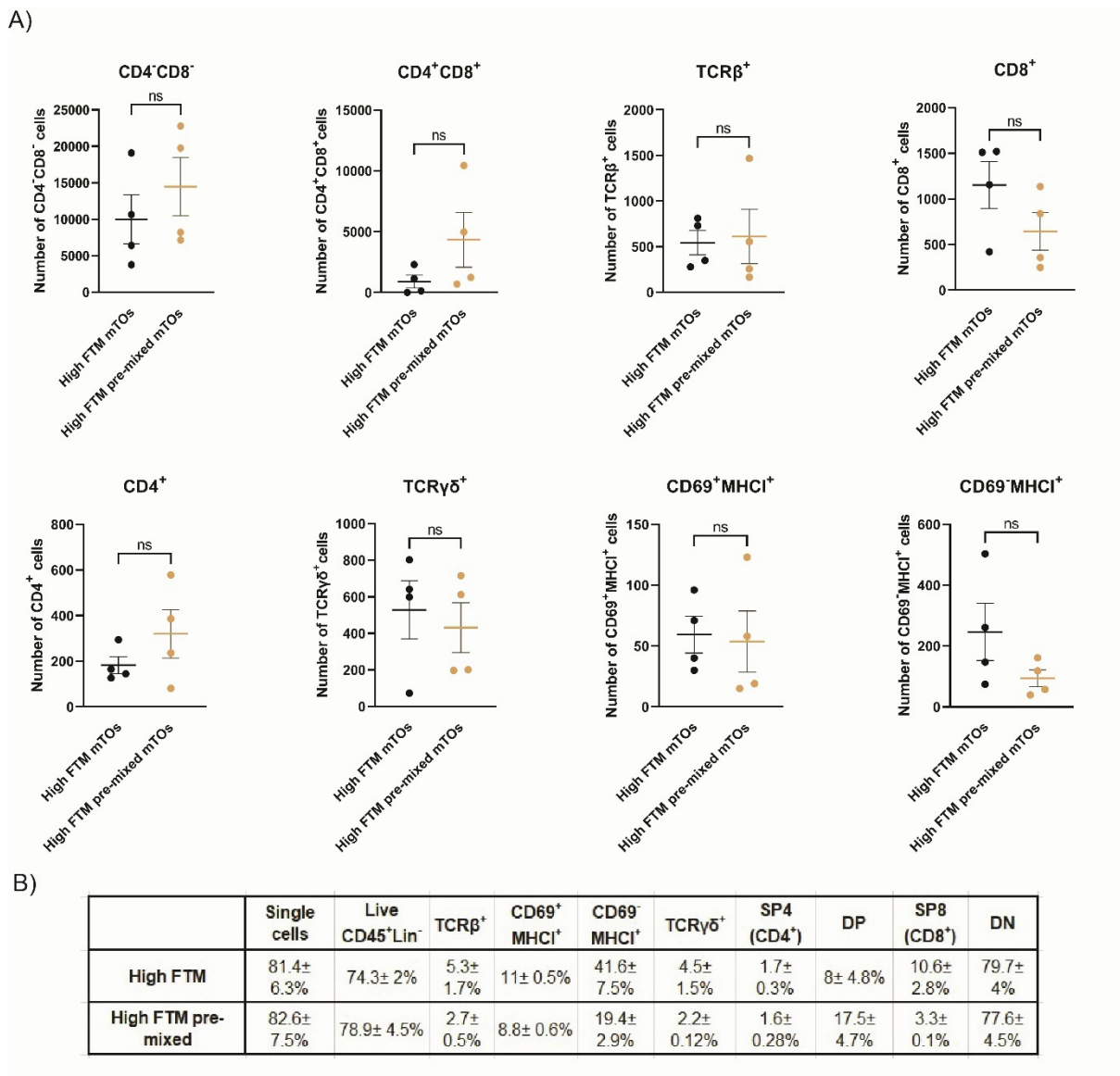


**Figure S4. Effect of pre-mixing input cells on mTO outputs.** mTO were established from E14.5 thymi using High FTM conditions with or without pre-mixing of input populations (in the without pre-mixing condition the input cell types were added sequentially) as indicated and were cultured for 14 days before analysis of thymocyte development for the subsets shown. (A) Graphs show mean±SEM. High FTM and High FTM pre-mixed had the same cellular composition ( $1 \times 10^5$  TEC,  $5 \times 10^4$  DN,  $4 \times 10^4$  FTM). Each data point represents the cells harvested from one microwell. (B) Table shows mean±SEM for percentages of parent gates of the thymocyte subsets shown in High FTM and High FTM pre-mixed mTOs. N=4 independent biological replicates. Statistical analysis was by unpaired t-test or Mann-Whitney rank test based on Shapiro-Wilk normality test. ns, not significant;  $p > 0.05$ . DN (CD4<sup>+</sup>CD8<sup>-</sup>), DP (CD4<sup>+</sup>CD8<sup>+</sup>), (CD3ε<sup>+</sup>TCRβ<sup>+</sup>), SP4 (CD4<sup>+</sup>), SP8 (CD8<sup>+</sup>), CD69<sup>+</sup>MHCi<sup>+</sup>, CD69<sup>+</sup>MHCii<sup>+</sup>, γδ T cells (CD3ε<sup>+</sup>TCRγδ<sup>+</sup>).

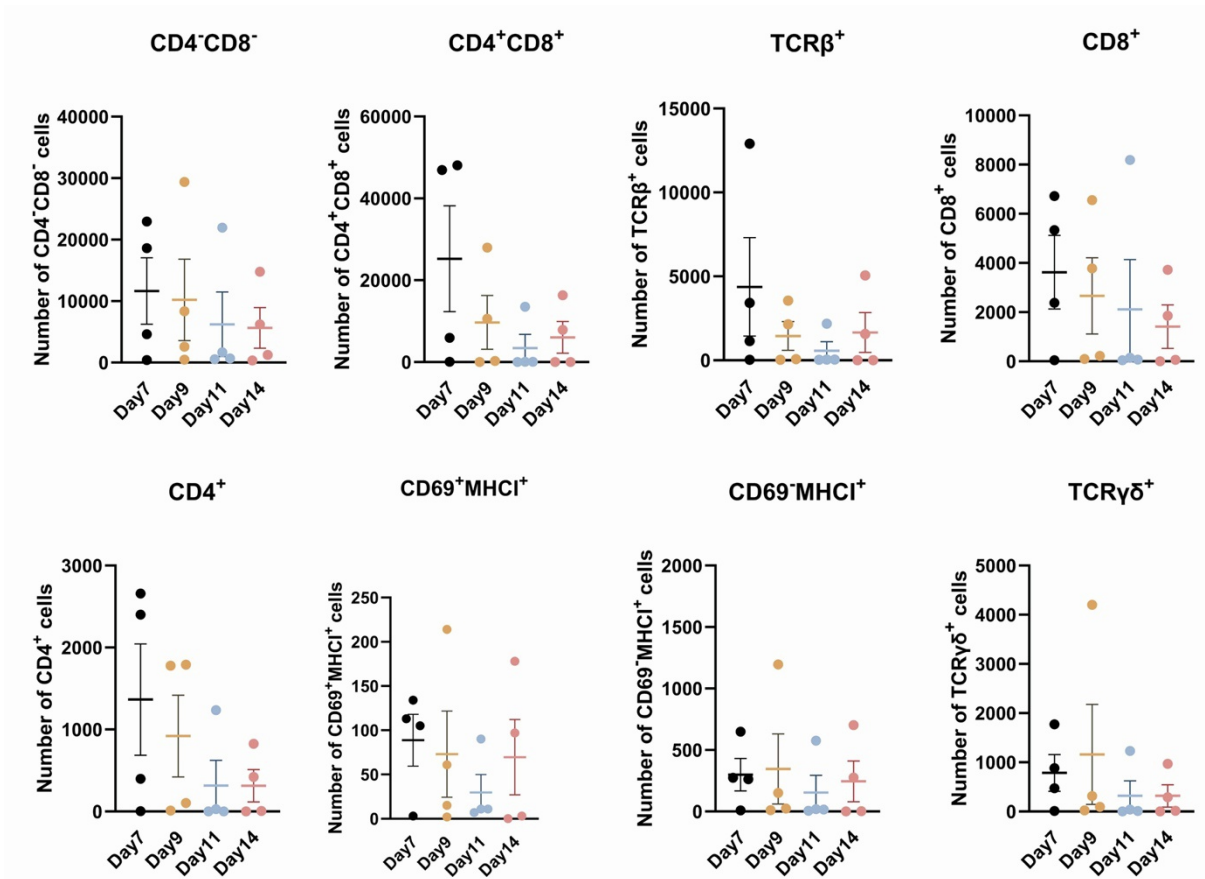
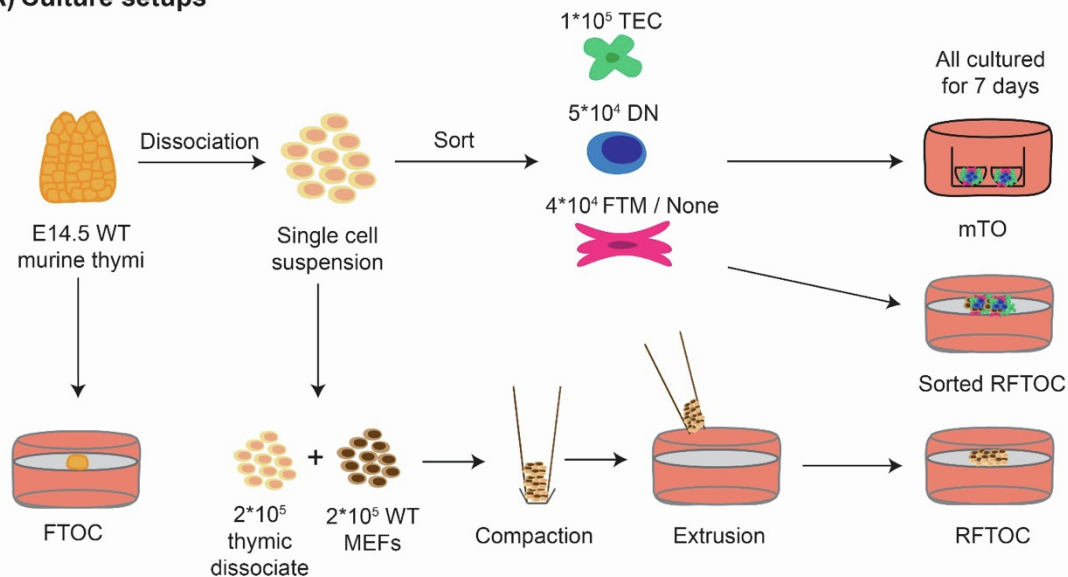


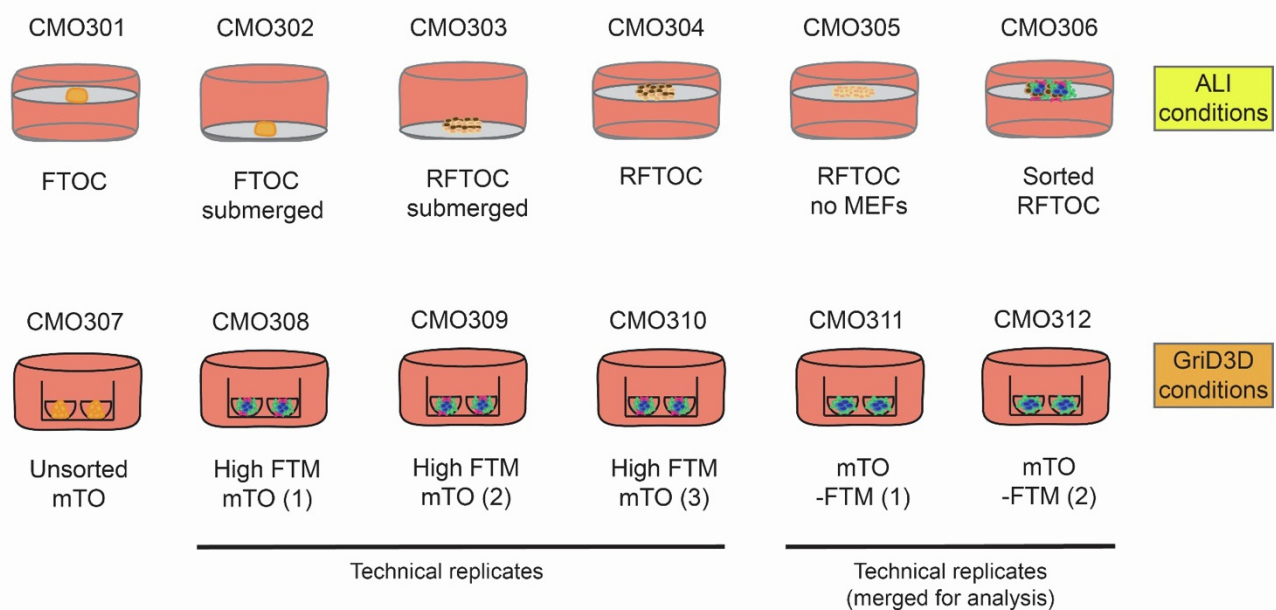
**Figure S5. Effect of culture period on mTO outputs.** mTO were established from E14.5 thymi using Hi FTM conditions and cultured for the time-periods indicated before analysis of thymocyte development for the subsets shown. (A) Graphs show mean±SEM. Each data point represents the cells harvested from one microwell. N=4 independent biological replicates. DN (CD4<sup>+</sup>CD8<sup>-</sup>), DP (CD4<sup>+</sup>CD8<sup>+</sup>), (CD3ε<sup>+</sup>TCRβ<sup>+</sup>), SP4 (CD4<sup>+</sup>), SP8 (CD8<sup>+</sup>), CD69<sup>+</sup>MHCII<sup>+</sup>, CD69<sup>+</sup>MHCI<sup>+</sup>, γδ T cells (CD3ε<sup>+</sup>TCRγδ<sup>+</sup>).



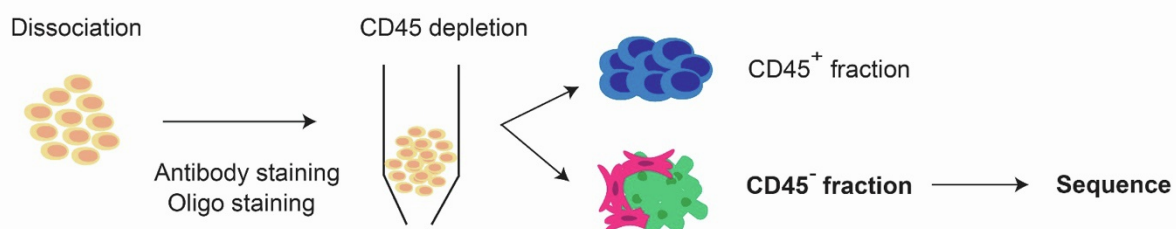
## A) Culture setups



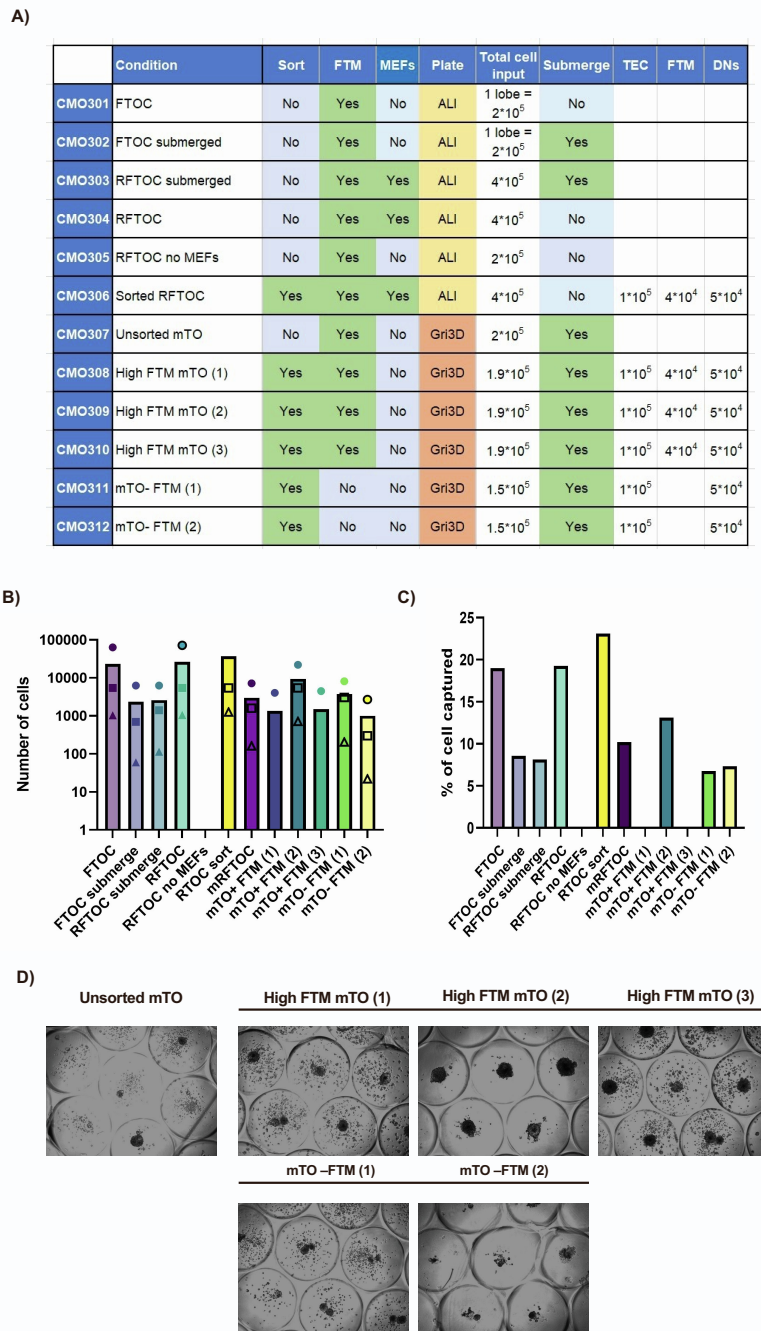
## B) CMO assignments



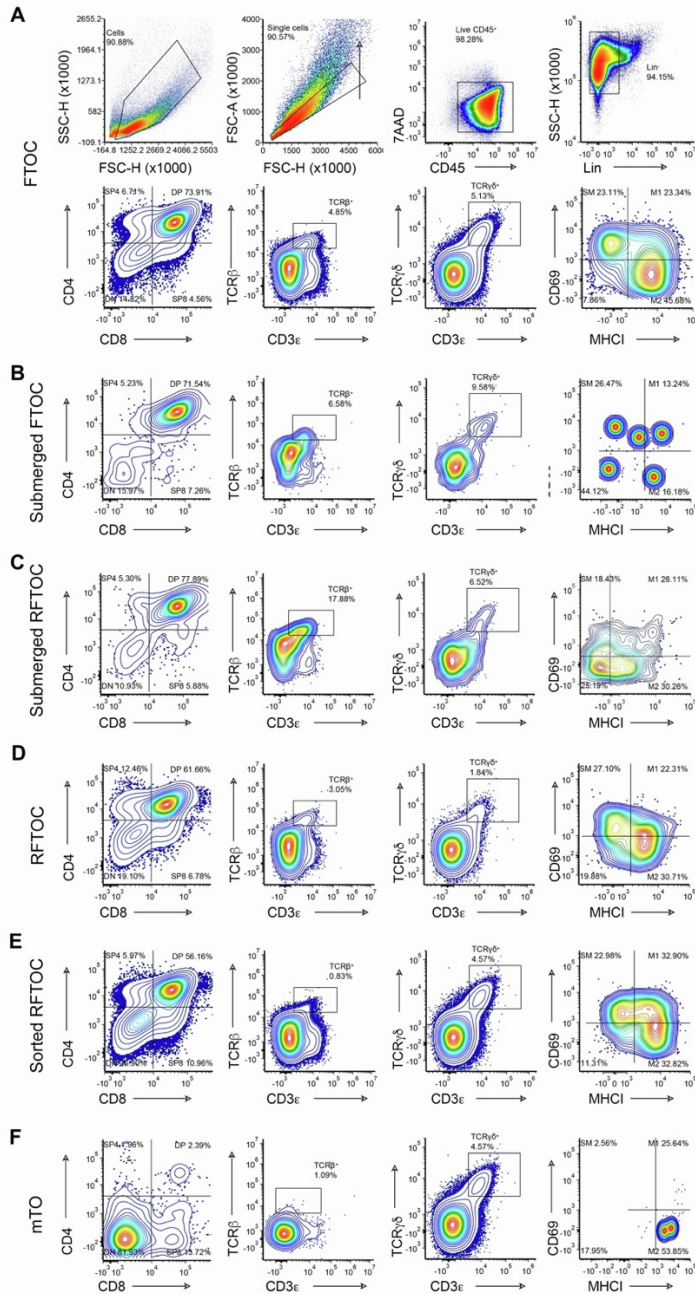
## C) Sample preparation



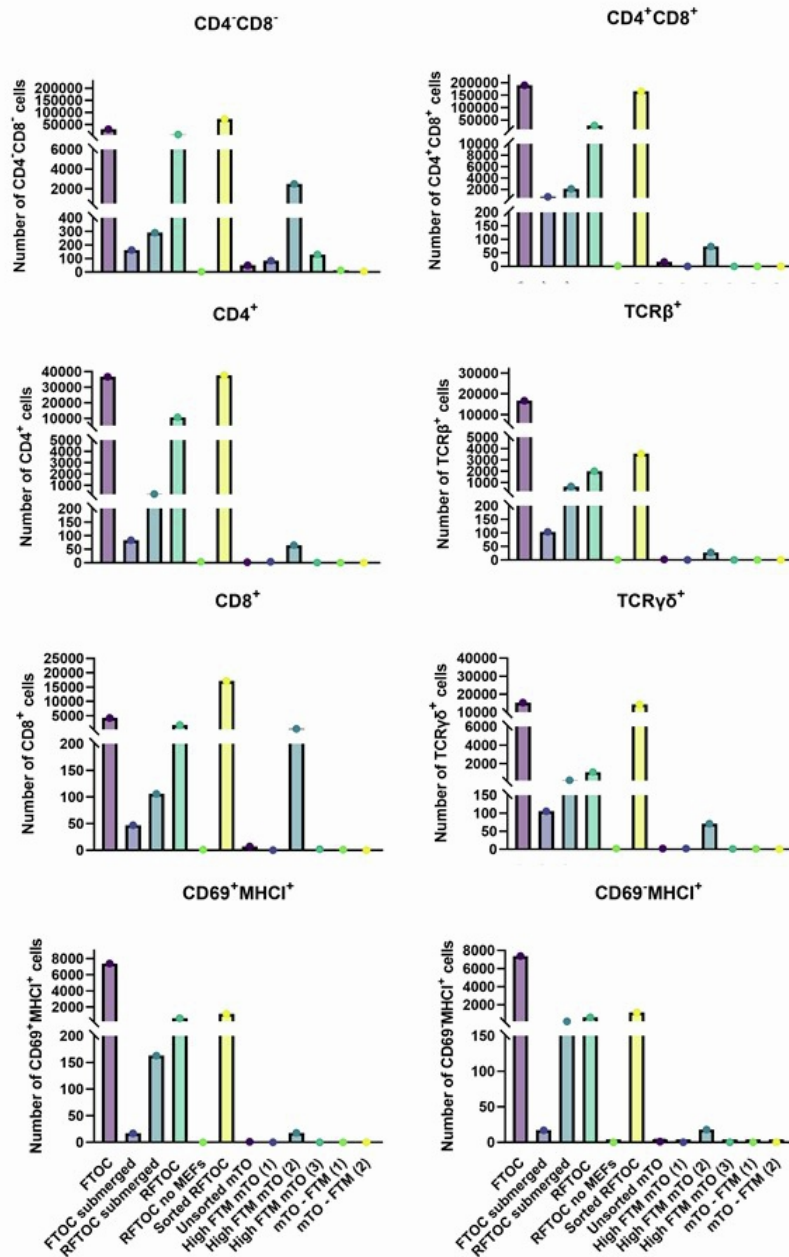
**Figure S6. Experimental design for scRNAseq analysis.**



**Figure S7. Cell inputs and outputs from ‘Watchbreaker’ scRNAseq experiment.** (A) Table showing details of each experimental condition set up for the 10x experiment. (B, C) Graphs show (B) total number of cells counted (circle), loaded on the chip (square) and sequenced (triangle) for each condition and (C) percentage of cells captured by sequencing for each of the experimental conditions; capture efficiency calculated by the ratio of cells sequenced/ cells counted. Note that due to clumping during sample preparation the proportion of cells captured by sequencing is relatively low; this explains the lack of recovery of cells from the mTO (1) and mTO (3) conditions. (D) Images show representative microwells for each of the mTO conditions.

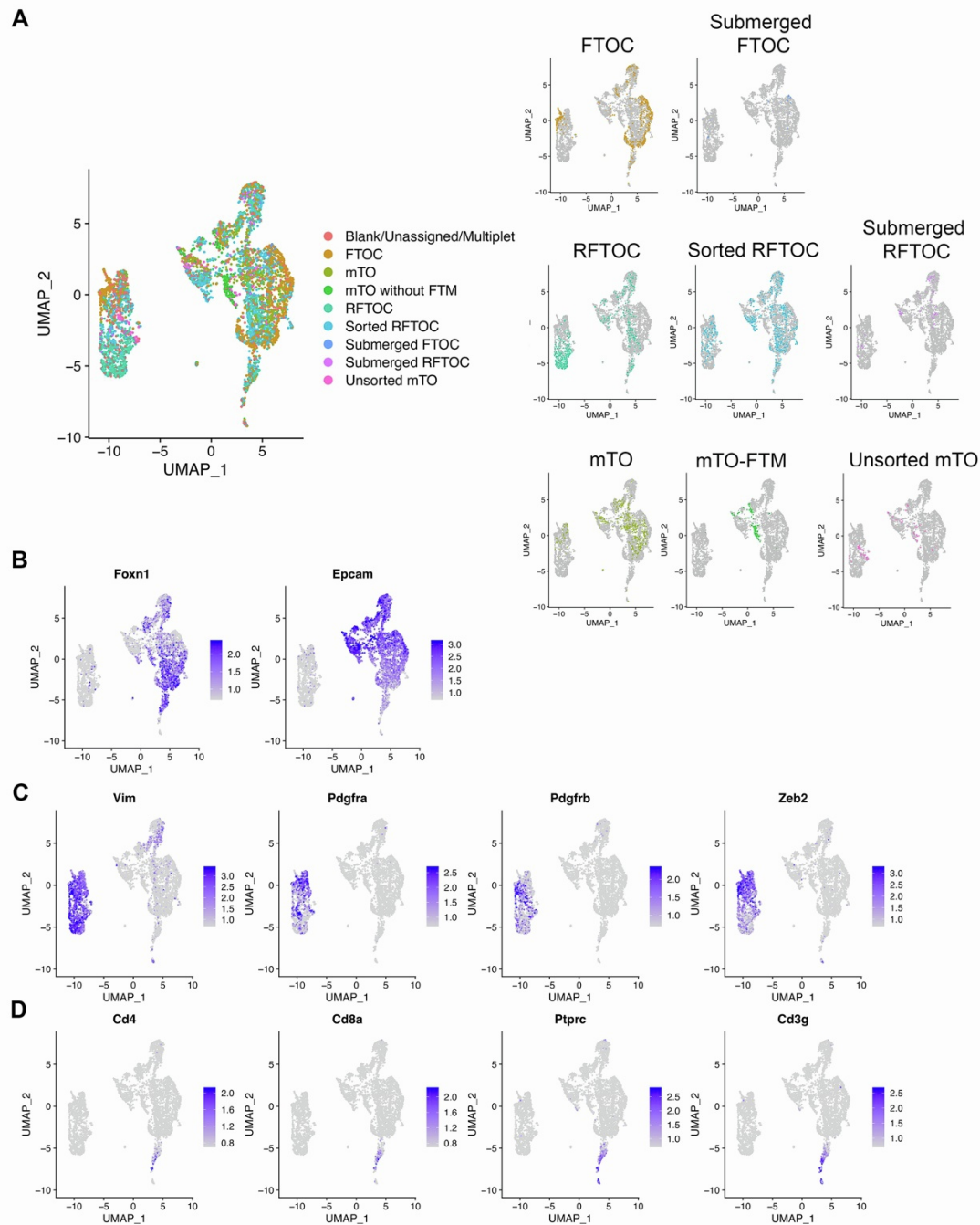


**Figure S8. Thymocyte development in different conditions in the 'Watchbreaker' 10x experiment.** Plots show thymocyte subset analysis of CD45<sup>+</sup> cells from the conditions shown after seven days of culture. Markers are as shown. (A) Plots show data from FTOC condition (CMO301), including gating strategy. (B-F) Plots show data from the conditions shown; Submerged FTOC (CMO302), Submerged RFTOC (CMO303), RFTOC (CMO304), Sorted RFTOC (CMO306), mTO replicate 2 (CMO309). Note that no DN to DP progression was observed in the following conditions, and therefore those data are not shown: RFTOC without MEFs (CMO305), mTO replicate 1 (CMO308), mTO replicate 3 (CMO310), mTO without FTM replicates 1 and 2 (CMO311 and CMO312). Among these, a DN population was present in all of these conditions except RFTOC without MEFs (CMO305) and the two mTO without FTM replicates. Very few cells were recovered from the unsorted mTO condition (CMO307) those data are also not shown.



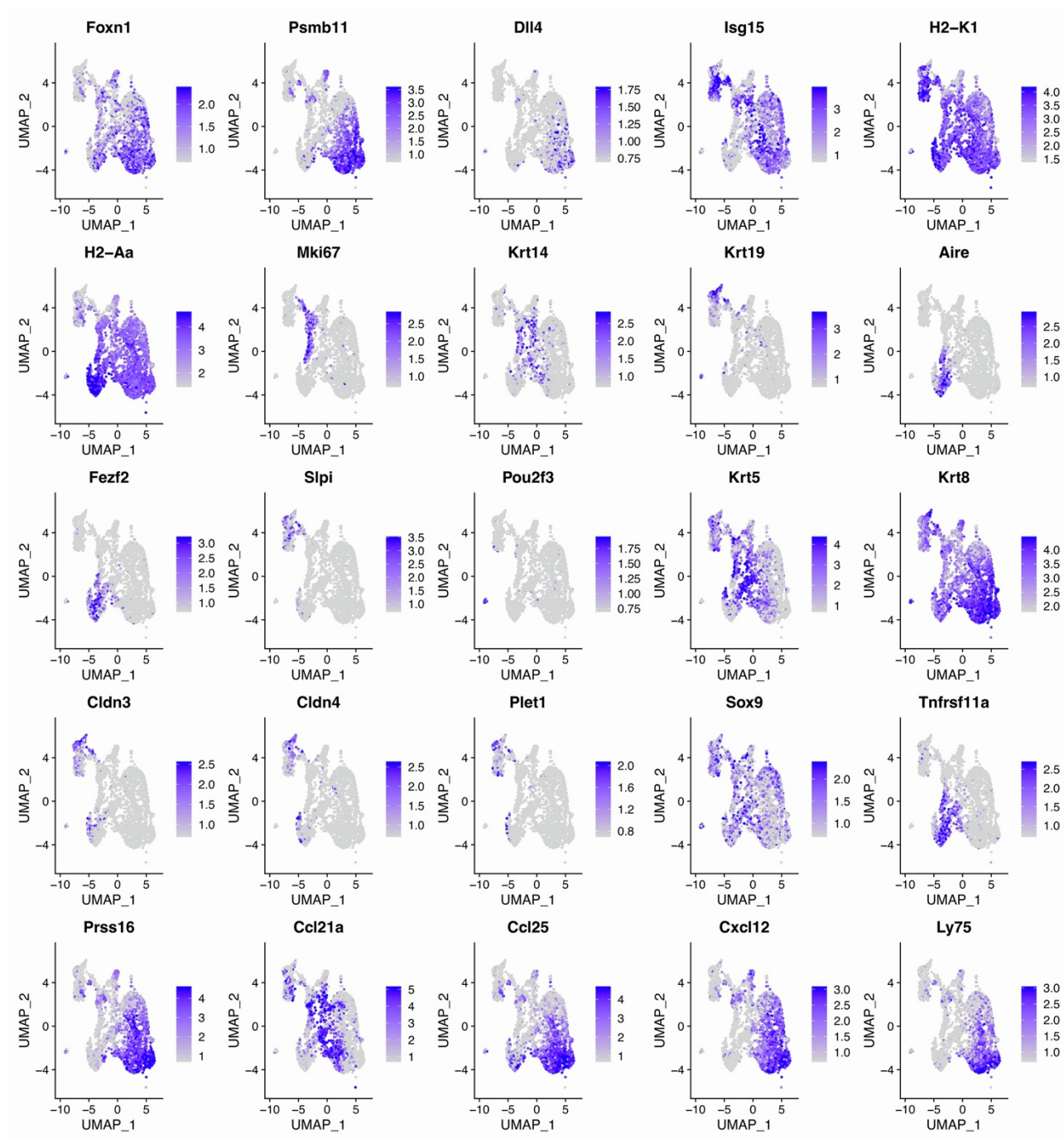
**Figure S9. Thymocyte subset numbers in each Watch-breaker condition in the ‘Watchbreaker’ 10x experiment.** FTOC, RFTOC and mTO were established as described in Figure S6 and were cultured for 7 days, after which thymocyte development was assessed by analysing the CD45<sup>+</sup> population for the following subsets (see Figure S8 for flow cytometry plots): DN (CD4<sup>-</sup>CD8<sup>-</sup>), DP (CD4<sup>+</sup>CD8<sup>+</sup>), (CD3ε<sup>+</sup>TCRβ<sup>+</sup>), SP4 (CD4<sup>+</sup>), SP8 (CD8<sup>+</sup>), CD69<sup>+</sup>MHCII<sup>+</sup>, CD69<sup>+</sup>MHCII<sup>-</sup>, γδ T cells (CD3ε<sup>+</sup>TCRγδ<sup>+</sup>). A) Graphs show cell numbers recovered for each subset, for each condition. N=1. B) Graphs show percentages of parent gates present in each condition, for the subsets shown.



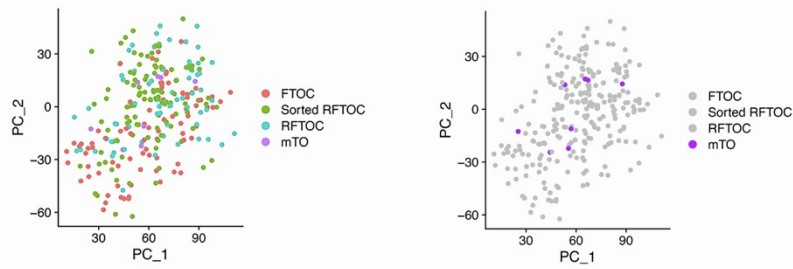
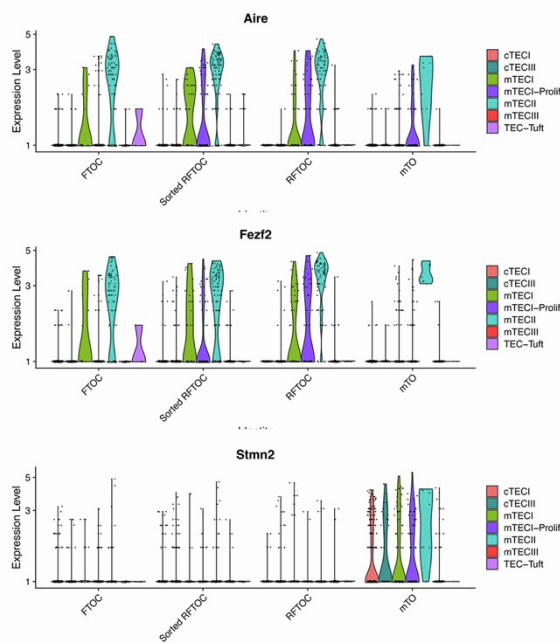


**Figure S10. Dimensional reduction showing scRNAseq data from all cells captured from all conditions.** (A) UMAP shows distribution of cells from each condition across the combined dataset. Data shown are the 4919 cells remaining after initial quality control. (B-D) Plots show distribution across combined dataset of markers for TEC (B; *Foxn1*, *Epcam*), mesenchymal cells (C; *Pdgfra*, *Pdgfrb*, *Vim*, *Zeb2*) and thymocytes (D; *Cd3g*, *Cd4*, *Cd8a*, *Prprc*).

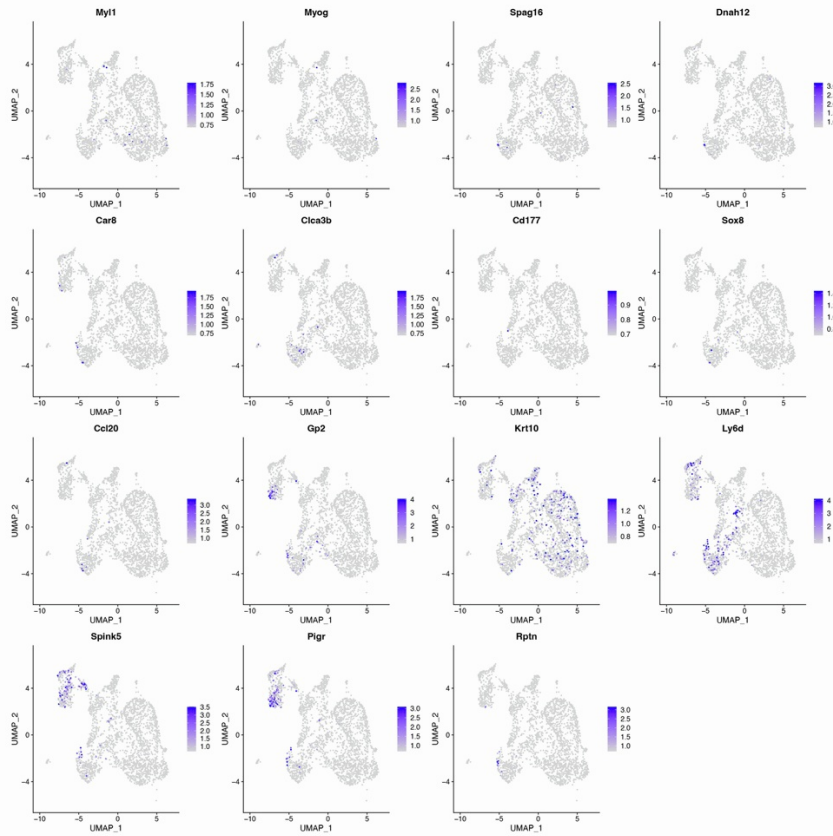
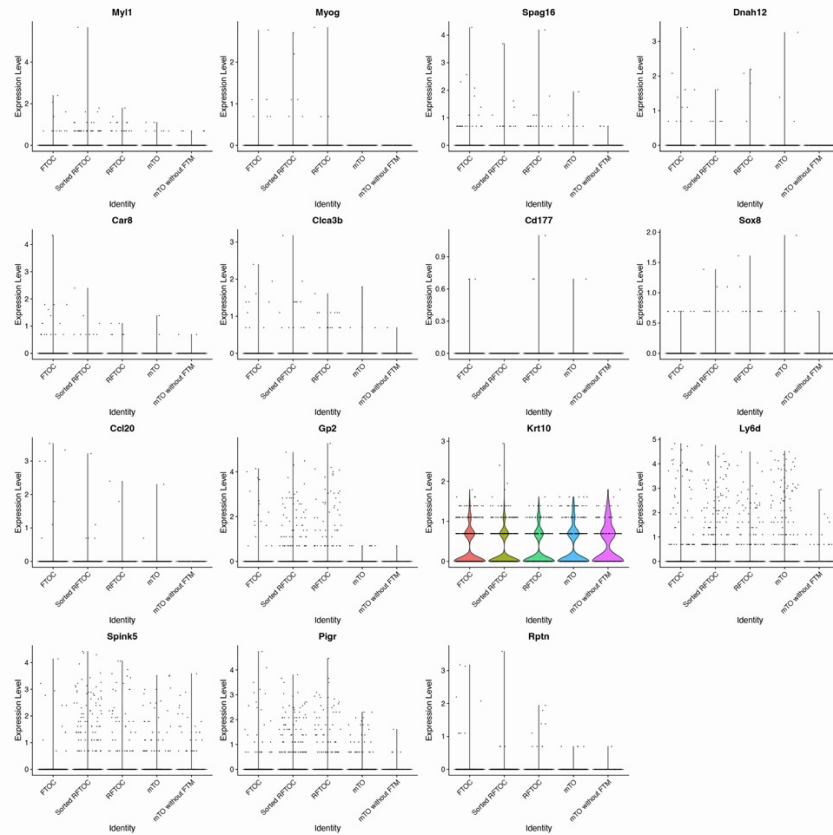




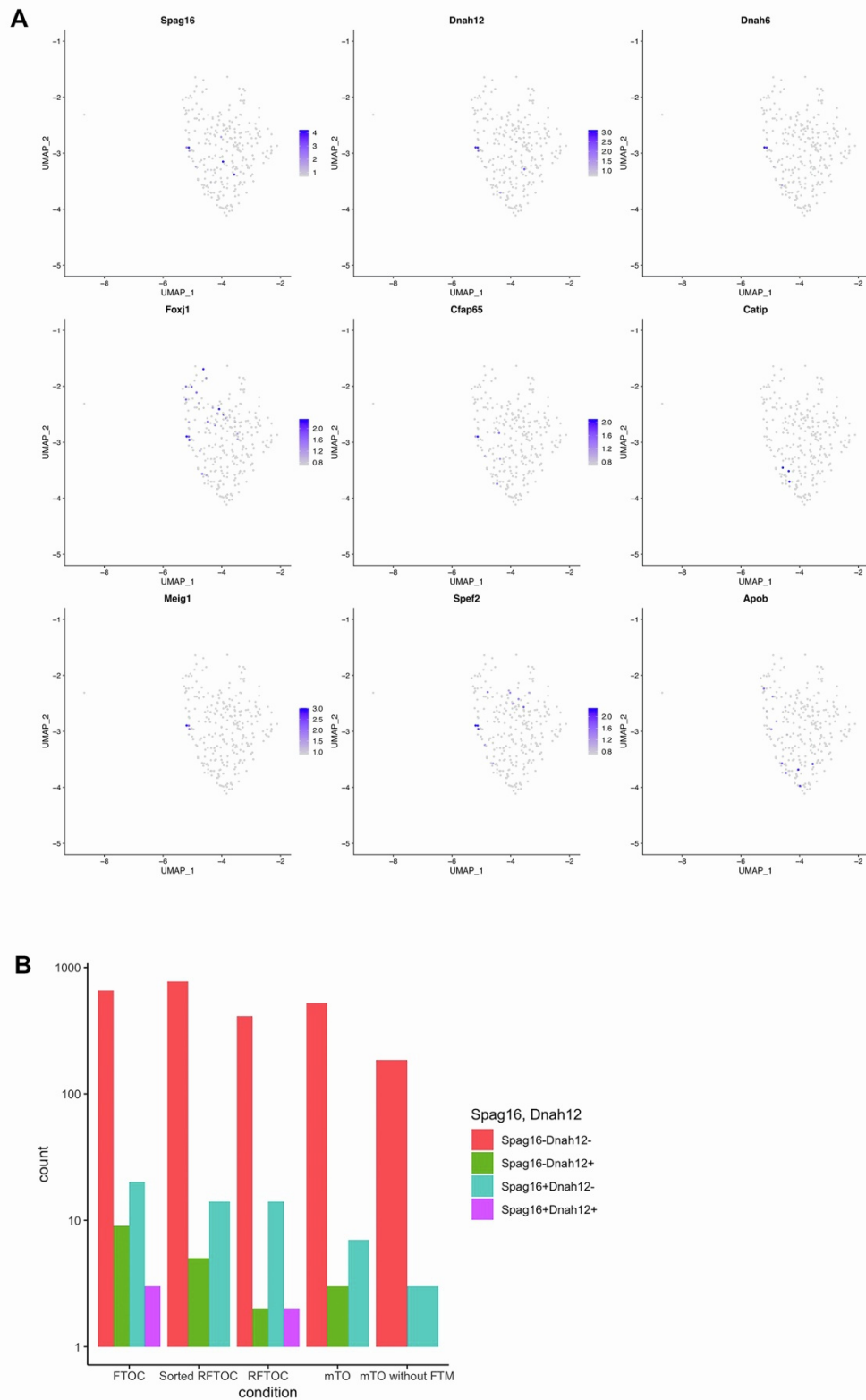
**Figure S11. Distribution of markers across TEC.** UMAPs show distribution of the markers shown across all TEC in the FTOC, RFTOC, sorted RFTOC, mTO and no-FTM mTO conditions.

**A****B**

**Figure S12. Analysis of mTECII subset across four Watchbreaker conditions. (A)** PCA shows distribution of mTECII cells in FTOC, RFTOC, Sorted RFTOC and mTO. **(B)** Violin plots showing expression profiles of Aire, Fezf2 and Stmn2 in the different TEC subsets, for each of the above four conditions.

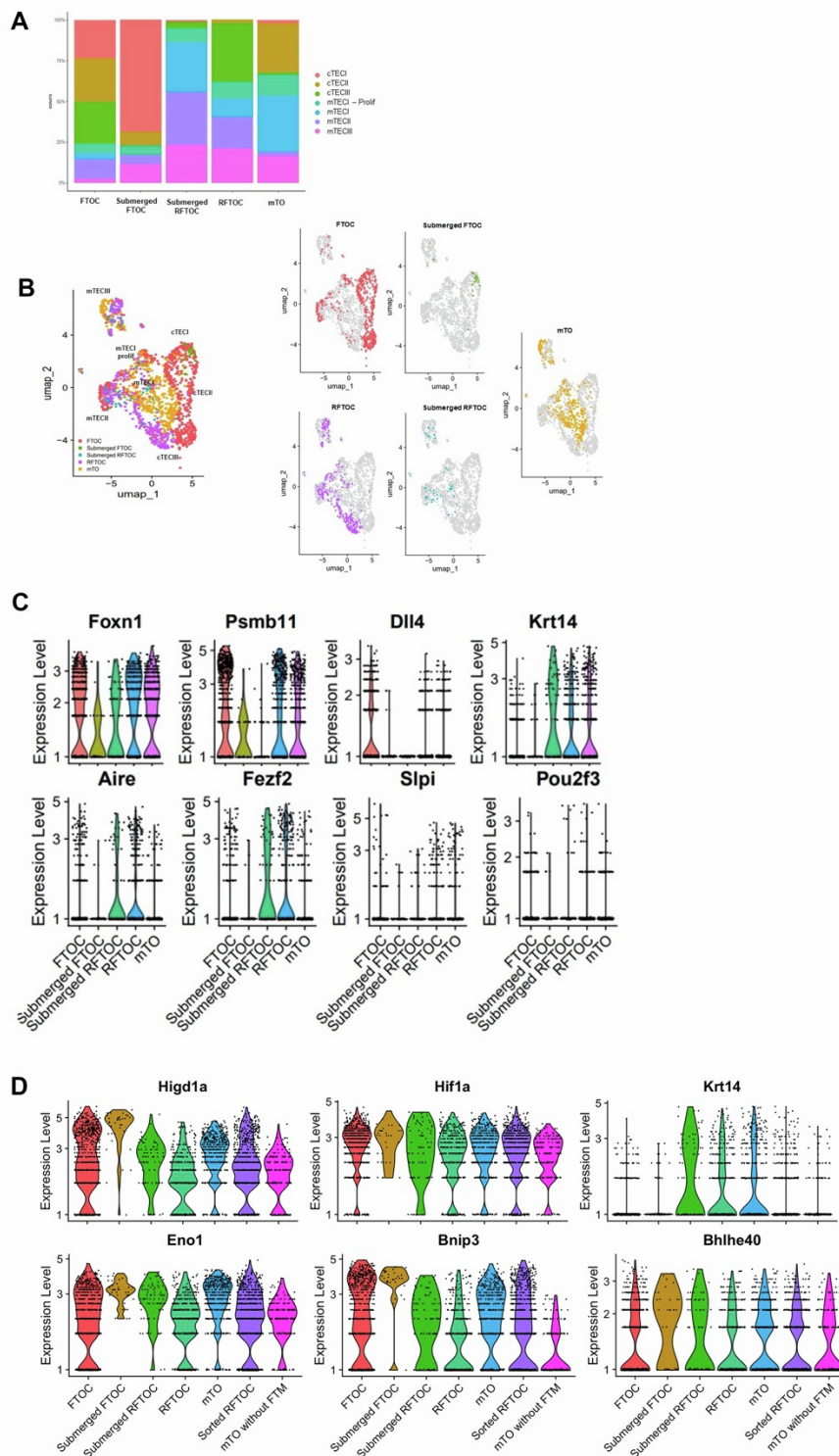
**A****B**

**Figure S13. Analysis of mimetic TEC markers across five Watchbreaker conditions. (A)** UMAPs and **(B)** Violin plots showing expression profiles of the markers shown, across the FTOC, sorted RFTOC, RFTOC, mTO and no-FTM mTO conditions.

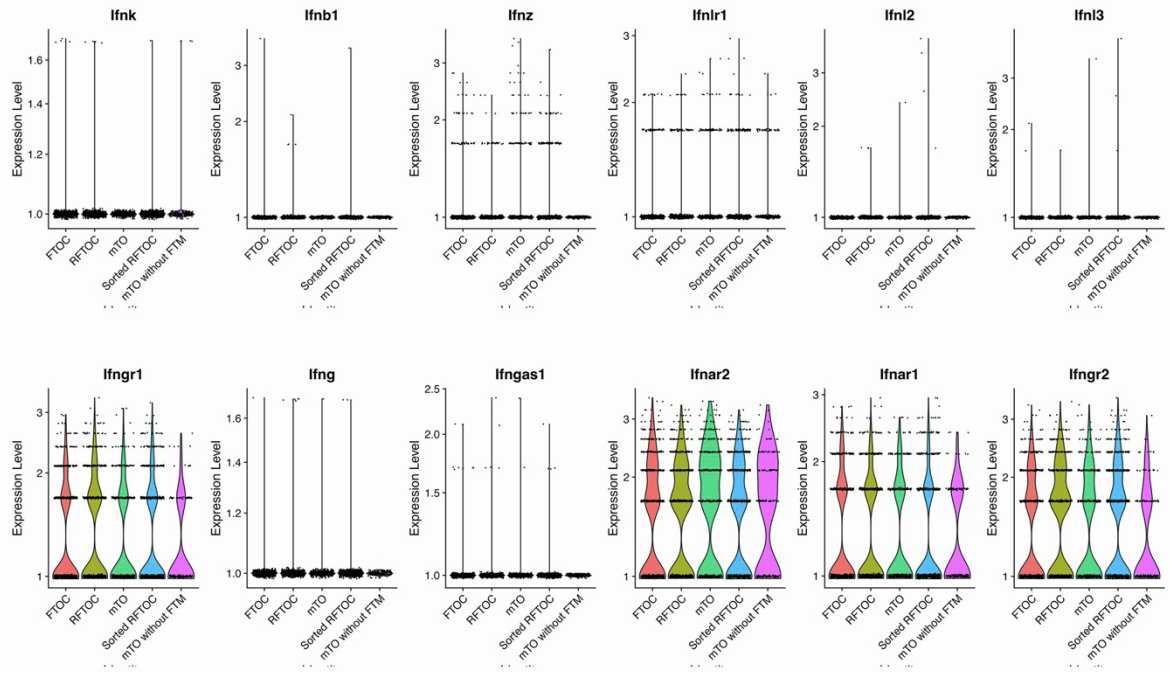
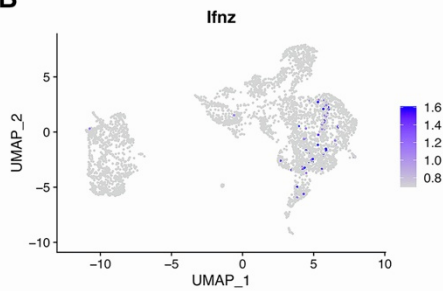


**Figure S14. Analysis of CilTEC markers among mTECII, across all Watchbreaker conditions. (A)** UMAPs show distribution of CilTEC markers within the mTECII cluster, **(B)** plot shows number of cells with each phenotype in each of five Watchbreaker conditions.





**Figure S15. Effect of submersion on cell distribution and gene expression in FTOC and RTOC.** **A, B)** Distribution of cell types in the FTOC, Submerged FTOC, Submerged RFTOC, RFTOC, and mTO conditions. UMAPs in (B) show combined data from the conditions shown (left panel) and distributions of TEC in individual conditions (middle and right panels). **C, D)** Violin plots show the expression profiles of the genes shown in the FTOC, Submerged FTOC, Submerged RFTOC, RFTOC, and mTO conditions. Plots in (C) show TEC markers; plots in (D) show hypoxia response genes.

**A****B**

**Figure S16. Expression of IFN family and IFN receptor genes in selected ‘Watch-breaker’ conditions. (A)** Violin plots show the expression profiles of the genes shown in the FTOC, Sorted RFTOC, RFTOC, mTO and mTO-FTM conditions. Analyses show gene expression across all cells in the dataset, including mesenchymal cells. IFN $\alpha$  and IFN $\gamma$  receptors were expressed, but expression of the IFN family genes analysed was not detected, or was detected in only very few cells in each condition (*Ifnz*). *Ifna* was not detected. **(B)** UMAP shows distribution of *Ifnz*+ cells.

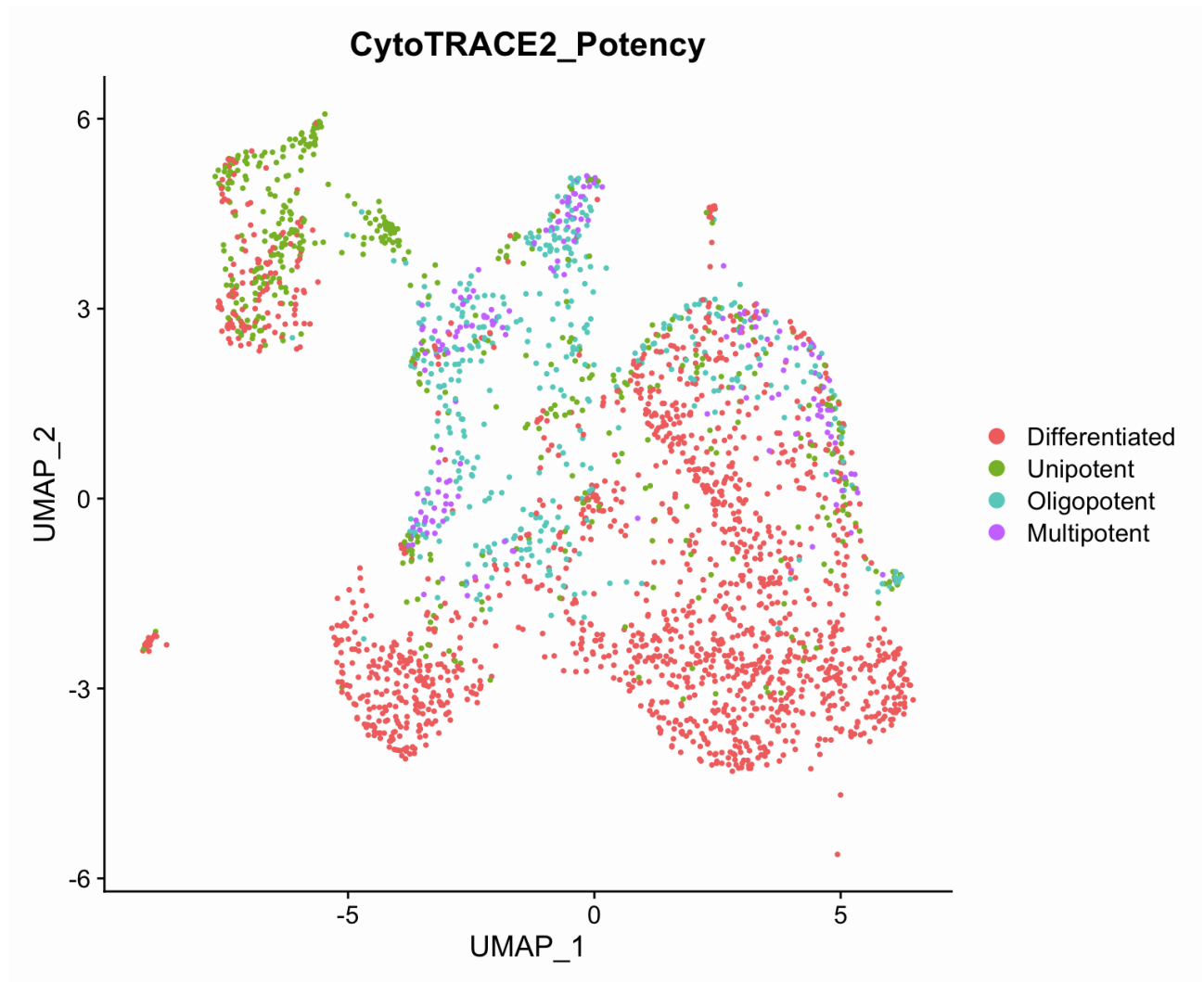


**Figure S17. CytoTRACE2 analysis across all 'Watch-breaker' conditions.** The UMAP projection is as in Figure 6. Colours indicate cell potency as predicted by the CytoTRACE2 algorithm. The mTECIII cluster is predicted to contain both unipotent progenitors and differentiated cells.

## Supplemental Tables

<i>Transgene</i>	<i>Orientation</i>	<i>Sequence</i>
Cxcl12 WT	Forward	5' CTG GTT TTC GCC TCT AAA GC
Cxcl12 Tg	Forward	5' TCG GCA AAA TCC CTT ATA AAT C
Cxcl12	Reverse	5' CAG AGC TGC GAG CCT TTC
Rank Venus WT	Forward	5' CTGCGTGCTGCTCGTTCCAC
Rank Venus Tg	Forward	5' GAAGAACGGCATCAAGGCCAACTTC
Rank Venus	Reverse	5' CTGTACATACAATCTTACTGAGGGTCGC
GFP	Forward	5' TAT ATC ATG GCC GAC AAG CA
GFP	Reverse	5' GAA CTC CAG CAG GAC CAT GT

**Table S1. Primers used to genotype transgenic lines.**



	Antigen	Fluorophore	Dilution	Supplier	Cat. Number	Clone
Flow cytometric isolation of TEC, DN thymocytes, FTM and EC from E14.5 thymic lobes	EpCAM	FITC	1:1000	BioLegend	118208	G8.8
	PDGFR $\alpha$	APC	1:2000	BioLegend	35908	APA5
	PDGFR $\beta$	APC	1:2000	BioLegend	136007	APB5
	TER119	PE	1:3000	BioLegend	116208	TER-119
	CD31	Pe/Cy7	1:1600	BioLegend	102523	MEC13.3
	CD45	APC-eFLuor780	1:1000	eBioscience	47-0451-82	30-F11
	DAPI	-	0.5 $\mu$ g/ml	Life Technologies	D1306	-
Flow cytometric isolation of LMPPs from E14.5 fetal liver	DAPI	-	0.5 $\mu$ g/ml	Life Technologies	D1306	-
	CD5	FITC	1:1000	BioLegend	100605	53-7.3
	CD19	FITC	1:500	BioLegend	152403	1D2
	Gr1	FITC	1:800	BioLegend	108405	RB6-8C5
	NK1.1	FITC	1:800	BD Biosciences	553164	PK136
	CD45R/B220	FITC	1:800	BioLegend	103206	RA3-6B2
	TER-119	FITC	1:800	eBioscience	11-5921-85	TER-119
	F4/80	FITC	1:1600	BioLegend	2BM8	123108
	CD135 (Flt3)	APC	1:50	BioLegend	135310	A2F10
	Sca-1	PE	1:2000	BioLegend	108107	D7
	CD117 (cKit)	PE/Cy7	1:1600	BioLegened	105813	2B8
Flow cytometric analysis of T cell subsets from mTOs	7AAD	-	1:200	BioLegend	420403	-
	CD11b	FITC	1:800	BioLegend	101205	M1/70
	CD11c	FITC	1:800	BioLegend	117305	N418
	Gr1	FITC	1:800	BioLegend	108405	RB6-8C5
	NK1.1	FITC	1:800	BD Biosciences	553164	PK136
	CD45R/B220	FITC	1:800	BioLegend	103206	RA3-6B2

	TER-119	FITC	1:800	eBioscience	11-5921-85	TER-119
	EpCAM	FITC	1:800	BioLegend	118208	G8.8
	CD4	PE	1:800	BioLegend	100512	RM4-5
	CD8 $\alpha$	APC	1:400	eBioscience	17-0081-82	53-6.7
	CD3 $\epsilon$	BV785	1:100	BioLegened	100355	145-2C11
	TCR $\beta$ chain	PE/Cy7	1:100	BioLegend	109222	H57-597
	CD45	APC/eFluor 780	1:800	eBioscience	47-0451-82	30-F11
	$\gamma/\delta$ TCR	BV605	1:400	BioLegend	118124	GL3
	MHC1 (H-2k)	BV510	1:400	BioLegend	116523	AF6-88.5
	CD69	BV421	1:100	BioLegend	104528	H1.2F3
IHC of in vitro cultures	Vimentin	-	1:250	Abcam	ab92547	Abcam (rabbit)
	MHCII	-	1:200	Abcam	ab15630	ER-TR3
	$\beta$ 5t	-	1:100	MBL	PD021	Polyclonal
	DLL4	-	1:50	BioLegend	130802	HMD4-1
	MHCI	-	1:200	BDBioscience	550550	AF6-88.5
	HOECHST	-	1:1000	Life Technologies	62249	
	Anti-Rabbit secondary	Alexa Fluor 568	1:1000	Invitrogen	A-11011	
	Anti-Rat secondary	Alexa Fluor 647	1:1000	Invitrogen	A-21247	

**Table S2. Antibodies used in panels for flow cytometry and immunohistochemistry.** Table shows the name, associated fluorophore where appropriate, supplier and clone number. DAPI, (4',6-Diamidino-2-Phenylindole, Dihydrochloride); IHC, immunohistochemistry.

Antibody	Barcoded Reagent	Dilution	Supplier	Cat. Number
UEA1-Biotin	TotalSeq™-SAV-Pe-B0952	1:1500	Vector Laboratories	B-1065
MHCII (α-mouse I-A/I-E)	TotalSeq™ - B0117	1:10000	BioLegend	107657
CD40	TotalSeq™ - B0903	1:3200	BioLegend	124639
CD80	TotalSeq™ - B0849	1:3200	BioLegend	104757
EpCAM	TotalSeq™ - B0449	1:800	BioLegend	118247
CD45	Beads	1:10	Miltenyi Biotec Inc.	130-052-301

**Table S3. Cell staining reagents used in 10x sequencing experiment.**

TEC subset	Markers	Reference
<b>cTECneg, cTECI and cTECIII</b>	<i>Psmb11, Cxcl12, Prss16</i>	Kernfeld et al 2018 <sup>1</sup> , Baran-Gale et al. 2020 <sup>2</sup>
<b>mTECI</b>	<i>Krt5, Ccl21a</i>	Kernfeld et al 2018 <sup>1</sup> , Baran-Gale et al. 2020 <sup>2</sup>
<b>mTECI prolifer</b>	<i>Mki67, Ccna2, Pbk</i>	Yayon et al. 2024 <sup>3</sup> , Baran-Gale et al. 2020 <sup>2</sup>
<b>mTECII</b>	<i>Aire, H2-Aa</i>	Bornstein et al. 2018 <sup>4</sup>
<b>mTECIII</b>	<i>Pigr, Ly6d</i>	Bornstein et al. 2018 <sup>4</sup> , Givony et al 2023 <sup>5</sup>
<b>TEC-Tuft</b>	<i>Avil, Spink5</i>	Baran-Gale et al. 2020 <sup>2</sup>
<b>CiITEC</b>	<i>Spag16, Dnah12</i>	Givony et al 2023 <sup>5</sup>

**Table S4: List of genes used to identify TEC subpopulations** annotated in Figures 5, 6 and S10-17.

## References

1. Kernfeld, E.M., Genga, R.M.J., Neherin, K., Magaletta, M.E., Xu, P., and Maehr, R. (2018). A Single-Cell Transcriptomic Atlas of Thymus Organogenesis Resolves Cell Types and Developmental Maturation. *Immunity* 48, 1258-1270 e1256. 10.1016/j.immuni.2018.04.015.
2. Baran-Gale, J., Morgan, M.D., Maio, S., Dhalla, F., Calvo-Asensio, I., Deadman, M.E., Handel, A.E., Maynard, A., Chen, S., Green, F., et al. (2020). Ageing compromises mouse thymus function and remodels epithelial cell differentiation. *Elife* 9. 10.7554/eLife.56221.
3. Yayon, N., Kedlian, V.R., Boehme, L., Suo, C., Wachter, B.T., Beuschel, R.T., Amsalem, O., Polanski, K., Koplev, S., Tuck, E., et al. (2024). A spatial human thymus cell atlas mapped to a continuous tissue axis. *Nature* 635, 708-718. 10.1038/s41586-024-07944-6.
4. Bornstein, C., Nevo, S., Giladi, A., Kadouri, N., Pouzolles, M., Gerbe, F., David, E., Machado, A., Chuprin, A., Toth, B., et al. (2018). Single-cell mapping of the thymic stroma identifies IL-25-producing tuft epithelial cells. *Nature* 559, 622-626. 10.1038/s41586-018-0346-1.
5. Givony, T., Leshkowitz, D., Del Castillo, D., Nevo, S., Kadouri, N., Dassa, B., Gruper, Y., Khalaila, R., Ben-Nun, O., Gome, T., et al. (2023). Thymic mimetic cells function beyond self-tolerance. *Nature* 622, 164-172. 10.1038/s41586-023-06512-8.